

ABSTRACT

Compliant Knee Exoskeletons and Their Effects on Gait Biomechanics

Kamran Shamaei Ghahfarokhi

2014

The human knee joint exhibits a spring-type behavior during the stance phase of walking at the preferred speed, which is both subject-specific and gait-specific. This observation led us to hypothesize that the human knee joint could partially adapt to an externally-applied tuned mechanical stiffness during the stance phase leading to reduced muscle involvement and energy expenditure. We also hypothesized that a spring, which is tuned to the body size and gait speed, in parallel with an impaired knee joint during the stance phase can partially restore the natural spring-type behavior of the knee joint. Three experimental and theoretical steps were taken to test these hypotheses.

First, a series of statistical models were developed that can closely characterize the moment-angle behavior of the knee joint using a set of measurable parameters including body weight and height, gait speed, and joint excursion. It is explained that these models can be used to tune the components of knee exoskeletons/orthoses and prostheses to the body size and gait speed of users, as well as general applications in understanding gait biomechanics. The statistical models of the knee joint were used in the next steps of this research to tune the stiffness of the experimental exoskeletal devices throughout the experimental sessions.

To experimentally test the first main hypothesis, a pair of quasi-passive knee exoskeletons was developed. When worn on a healthy subject, each exoskeleton implements an interchangeable spring in parallel with the knee joint during the stance and allows free rotation during the swing phase. The exoskeletons with a range of stiffness were used in a series of experiments on healthy individuals to study the mechanics and energetics of human gait in interaction with exoskeletal impedances in parallel with the knee joint. Healthy lower extremity joints showed substantial

adaptation to the exoskeleton stiffness/assistance suggesting that replicating the natural behavior of a joint could be a viable method for the design of lower extremity exoskeletons to reduce muscle involvement and energy expenditure. It was also observed that a healthy knee joint can fully accommodate external assistance only to a certain level, above which the knee joint adaptation saturates and biarticular effects emerge.

To test the second hypothesis, a compliant stance control orthosis was developed that implements a spring in parallel with an impaired knee joint during the stance and allows free rotation during the swing phase. It was found that a compliant stance control orthosis can restore the natural spring-type behavior of an impaired knee joint during the stance phase. The compliant stance control orthosis showed higher gait speed and more natural kinematic patterns when compared with the state-of-the-art stance control orthoses that rigidly lock the knee during the stance phase. The findings of this research also showed that a friction-based latching mechanism can be a viable option in the design of lower extremity assistive devices that require engagement and disengagement of passive components.

Compliant Knee Exoskeletons and Their Effects on Gait Biomechanics

A Dissertation

Presented to the Faculty of the Graduate School

of

Yale University

in Candidacy for the Degree of

Doctor of Philosophy

by

Kamran Shamaei Ghahfarokhi

Dissertation Director: Professor Aaron M. Dollar

December 2014

UMI Number: 3582223

All rights reserved

INFORMATION TO ALL USERS

The quality of this reproduction is dependent upon the quality of the copy submitted.

In the unlikely event that the author did not send a complete manuscript and there are missing pages, these will be noted. Also, if material had to be removed, a note will indicate the deletion.

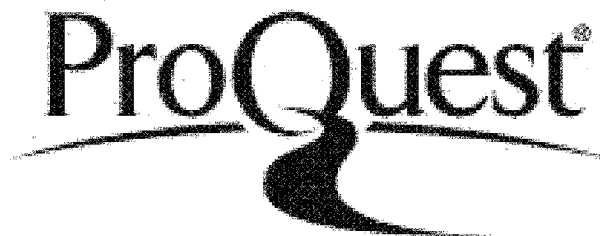


UMI 3582223

Published by ProQuest LLC 2015. Copyright in the Dissertation held by the Author.

Microform Edition © ProQuest LLC.

All rights reserved. This work is protected against unauthorized copying under Title 17, United States Code.



ProQuest LLC
789 East Eisenhower Parkway
P.O. Box 1346
Ann Arbor, MI 48106-1346

Compliant Knee Exoskeletons and Their Effects on Gait Biomechanics

A Dissertation

Presented to the Faculty of the Graduate School

of

Yale University

in Candidacy for the Degree of

Doctor of Philosophy

by

Kamran Shamaei Ghahfarokhi

Dissertation Director: Professor Aaron M. Dollar

December 2014

© 2015 by Kamran Shamaei Ghahfarokhi
All rights reserved

**To my mother and father who made utmost sacrifices to
make it possible for me to fulfill my goals and
contribute to the human society and science**

ABSTRACT

Compliant Knee Exoskeletons and Their Effects on Gait Biomechanics

Kamran Shamaei Ghahfarokhi

2014

The human knee joint exhibits a spring-type behavior during the stance phase of walking at the preferred speed, which is both subject-specific and gait-specific. This observation led us to hypothesize that the human knee joint could partially adapt to an externally-applied tuned mechanical stiffness during the stance phase leading to reduced muscle involvement and energy expenditure. We also hypothesized that a spring, which is tuned to the body size and gait speed, in parallel with an impaired knee joint during the stance phase can partially restore the natural spring-type behavior of the knee joint. Three experimental and theoretical steps were taken to test these hypotheses.

First, a series of statistical models were developed that can closely characterize the moment-angle behavior of the knee joint using a set of measurable parameters including body weight and height, gait speed, and joint excursion. It is explained that these models can be used to tune the components of knee exoskeletons/orthoses and prostheses to the body size and gait speed of users, as well as general applications in understanding gait biomechanics. The statistical models of the knee joint were used in the next steps of this research to tune the stiffness of the experimental exoskeletal devices throughout the experimental sessions.

To experimentally test the first main hypothesis, a pair of quasi-passive knee exoskeletons was developed. When worn on a healthy subject, each exoskeleton implements an interchangeable spring in parallel with the knee joint during the stance and allows free rotation during the swing phase. The exoskeletons with a range of stiffness were used in a series of experiments on healthy individuals to study the mechanics and energetics of human gait in interaction with exoskeletal impedances in parallel with the knee joint. Healthy lower extremity joints showed substantial

adaptation to the exoskeleton stiffness/assistance suggesting that replicating the natural behavior of a joint could be a viable method for the design of lower extremity exoskeletons to reduce muscle involvement and energy expenditure. It was also observed that a healthy knee joint can fully accommodate external assistance only to a certain level, above which the knee joint adaptation saturates and biarticular effects emerge.

To test the second hypothesis, a compliant stance control orthosis was developed that implements a spring in parallel with an impaired knee joint during the stance and allows free rotation during the swing phase. It was found that a compliant stance control orthosis can restore the natural spring-type behavior of an impaired knee joint during the stance phase. The compliant stance control orthosis showed higher gait speed and more natural kinematic patterns when compared with the state-of-the-art stance control orthoses that rigidly lock the knee during the stance phase. The findings of this research also showed that a friction-based latching mechanism can be a viable option in the design of lower extremity assistive devices that require engagement and disengagement of passive components.

ACKNOWLEDGMENTS

I would like to thank Prof. Aaron Dollar who advised my dissertation research with extensive support, guidance, insight, and friendship. I would also like to thank my former and current committee members, Prof. Gregory Sawicki, Prof. Brian Scassellati, Prof. Paul Ivancic, and Dr. John Morrell for their insight and guidance throughout my dissertation research.

I would like to acknowledge our collaborators Dr. Jeffrey Schiffman, Ms. Karen Gregorczyk, and Mr. Albert Adams at U.S. Army Natick Soldier Research, Development, and Engineering Center who led the efforts on recruitment of healthy participants and gait laboratory experimentation.

I would like to acknowledge our collaborators Prof. Linda Resnik, Dr. Susan D'Andrea, Prof. Alber Lo, and Ms. Melany Westwell from Brown University and Providence VA Medical Center, who led the efforts on recruitment of affected participants and gait laboratory experimentation.

I would also like to thank all the members of Prof. Dollar's group at Yale University, Department of Mechanical Engineering and Materials Science for their insightful inputs on the design and fabrication of the developed systems and analysis of my dissertation research.

Finally, I would like to thank all American tax payers and agencies who provided the funding for this research through US Defense Medical Research and Development Program contract # W81XWH-11-2-0054, and US Army Natick Soldier Research, Development, and Engineering Center contract #W911NF-07-D-0001.

TABLE OF CONTENTS

LIST OF FIGURES	vi
LIST OF TABLES	viii
CHAPTER 1 INTRODUCTION.....	1
CHAPTER 2 STATE OF THE ART OF ASSISTIVE DEVICES AND HYPOTHESIS FORMULATION.....	7
2.1 Introduction.....	7
2.2 State of the Art of Assistive Devices.....	7
2.3 Spring-Type Behavior of the Knee Joint.....	10
2.4 Formulation of Dissertation Hypotheses	16
2.5 Dissertation Approach	17
CHAPTER 3 CHARACTERIZATION OF MOMENT-ANGLE BEHAVIOR OF THE KNEE JOINT.....	25
3.1 Introduction	25
3.2 Moment-Angle Behavior of the Knee Joint during Walking.....	28
3.3 Inverse Dynamics Analysis.....	30
3.4 Identifying the Model Parameters and Form of Fits.....	37
3.5 Experimental Protocols.....	40
3.6 Data Extraction and Statistical Analysis.....	41
3.7 General-Form Statistical Models.....	43
3.8 Simplification of Models for Preferred Gait Speed.....	47
3.9 Conclusions and Future Work.....	50
CHAPTER 4 MECHANICS AND ENERGETICS OF HUMAN BODY IN INTERACTION WITH EXOSKELETAL IMPEDANCES IN PARALLEL WITH THE KNEE JOINT DURING WALKING.....	62
4.1 Introduction.....	62
4.2 Design and Evaluation of the Exoskeletons.....	69
4.2.1 Design Overview.....	69
4.2.2 Friction-Based Latching Mechanism.....	73
4.2.3 Control Scheme.....	74
4.2.4 Moment-Angle Characterization.....	76
4.2.5 Mechanical Evaluation.....	79
4.3 Experimental Conditions and Protocols.....	81
4.3.1 Subjects.....	81
4.3.2 Data Collection Instrumentation.....	82
4.3.3 Experimental Conditions.....	84
4.3.4 Experimental Protocols.....	84
4.3.5 Kinematic and Kinetic Analysis.....	86
4.3.6 Profile Comparison Measures.....	94
4.3.7 Knee Complex Moment-Angle Analysis.....	94
4.3.8 Locomotor Adaptation to Parallel Stiffness.....	95
4.3.9 Calculation of Mechanical and Metabolic Power.....	97
4.4 Kinematic and Kinetic Profiles.....	100
4.4.1 Effects of Exoskeleton Mass.....	100
4.4.2 Effects of Exoskeleton Articulations.....	105
4.4.3 Effects of Exoskeleton Stiffness.....	106
4.5 Effects of Exoskeleton Impedance on Moment-Angle Behavior of the Knee Joint.....	106
4.5.1 Moment-Angle Performance of the Knee Complex.....	106
4.5.2 Adaptation of Knee Moment and Quasi-Stiffness.....	108

4.6	Effects of Exoskeleton Impedance on Gait Energetics.....	109
4.6.1	Metabolic Power.....	109
4.6.2	Determinants of Metabolic Power.....	109
4.7	Conclusions and Future Work.....	110
 CHAPTER 5 DESIGN AND FUNCTIONAL EVALUATION OF A COMPLIANT STANCE CONTROL KNEE-ANKLE-FOOT ORTHOSIS.....		123
5.1	Introduction.....	123
5.2	Device Design.....	125
5.2.1	Moment-Angle Behavior of Knee.....	125
5.2.2	Design Objectives.....	128
5.2.3	Description of the Quasi-Passive Compliant Stance Control Orthosis..	130
5.2.4	Compliance Control Module.....	130
5.2.5	Control Algorithm.....	133
5.2.6	Design Analyses and Characterization.....	135
5.3	Mechanical and Functional Evaluation.....	141
5.4	Conclusions and Future Work.....	154
 CHAPTER 6 SUMMARY AND CONCLUSIONS.....		161

LIST OF FIGURES

Figure 2-1	Schematic arcs of motion for the knee joint during a gait cycle.....	12
Figure 2-2	A sample moment-angle graph for the knee joint during a gait cycle.....	12
Figure 2-3	The quasi-stiffness of the knee in flexion and extension modes, and the weight acceptance stage of the gait plotted against the load weight.....	15
Figure 3-1	Knee moment vs. relative angle curve for a representative subject during walking..	29
Figure 3-2	A schematic model of the support thigh, shank, and foot.....	32
Figure 3-3	Knee quasi-stiffness in flexion and extension stages, and weight acceptance phase plotted against the gait speed for a sample subject.....	46
Figure 3-4	Knee quasi-stiffness in the weight acceptance phase for a speed closest to the preferred gait speed.....	48
Figure 4-1	A volunteer walking with the quasi-passive knee exoskeletons.....	65
Figure 4-2	Knee complex is defined as the combination of the knee joint and exoskeleton.....	66
Figure 4-3	Schematic function of the exoskeletons that implement a high-stiffness spring in the weight acceptance phase of the gait and a low-stiffness spring.....	66
Figure 4-4	A volunteer walking with a pair of joint-less replica devices that have mass distribution similar to that of the exoskeletons.....	70
Figure 4-5	Detailed view of the exoskeleton design.....	70
Figure 4-6	Moment-angle characterization of the exoskeleton.....	75
Figure 4-7	Timing of the control signals and engagement of the exoskeleton spring	75
Figure 4-8	The diagram of the finite state machine that the exoskeleton controller uses to engage/disengage the assistance spring.....	78
Figure 4-9	A schematic model of the knee complex.....	78
Figure 4-10	The stiffness control module mechanically tested on a knee simulator.....	80
Figure 4-11	Inter-subject mean \pm SD angle profiles.....	88
Figure 4-12	Inter-subject mean \pm SD moment profiles.....	89
Figure 4-13	Inter-subject mean \pm SD power profiles.....	90
Figure 4-14	Inter-subject mean \pm SD profile of the travel of the body center of mass.....	91
Figure 4-15	Inter-subject mean \pm SD trajectory of the body center of mass.....	92
Figure 4-16	Inter-subject mean \pm SD velocity trajectory of the body center of mass.....	93
Figure 4-17	A sample moment-angle graph for one of the subjects.....	93
Figure 4-18	Inter-subject moment-angle analysis of the knee complex, joint, and exoskeleton in the sagittal plane.....	96
Figure 4-19	Normalized quasi-stiffness and loading effort of the knee complex and joint with respect to the normalized parallel stiffness and assistance, respectively.....	99
Figure 4-20	Mean \pm SD of metabolic power, efficiency of positive work, and cost of transport across the conditions.....	101
Figure 4-21	Mean \pm SD of average positive rate of moment generation across conditions.....	102
Figure 4-22	Mean \pm SD of average positive power across conditions.....	103
Figure 4-23	Average positive rate of moment generation and average positive power with respect to the metabolic power.....	104
Figure 5-1	Quasi-passive compliant stance control orthosis.....	124
Figure 5-2	Moment-angle behavior of the knee during a gait cycle.....	127
Figure 5-3	Detailed view of the compliant stance control module.....	131
Figure 5-4	Detailed view of the engagement mechanism function.....	134
Figure 5-5	The configuration of heel and toe sensors in the instrumented shoe insoles.....	134
Figure 5-6	Timing of the control signals and the friction lever engagement.....	136
Figure 5-7	The finite state machine used to control the stiffness of the compliance stance control module.....	136
Figure 5-8	The schematic configuration of the return and support spring and theoretical moment-angle behavior of the compliant stance control orthosis.....	140
Figure 5-9	Free body diagram of the friction lever of the compliant stance control orthosis....	140
Figure 5-10	Moment-angle characterization of the compliant stance control module.....	142
Figure 5-11	Knee simulator used to evaluate the mechanical function of the compliance control	142

	module.....	
Figure 5-12	Inter-subject mean angle profiles of the ankle, knee, and hip joints for three healthy volunteers walking at the preferred gait speed across conditions.....	145
Figure 5-13	High-speed image captures of the compliant stance control orthosis in a gait cycle of a healthy subject walking on a treadmill.....	145
Figure 5-14	Preclinical experiments including a patient walking with the compliant stance control orthosis.....	149
Figure 5-15	Intra-subject mean angle profiles of the lower extremity joints.....	151
Figure 5-16	Intra-subject mean angle profiles of the trunk across the conditions.....	152
Figure 5-17	Intra-subject mean EMG signals for five target muscles across the conditions.....	153

LIST OF TABLES

Table 2-1	Demographic properties and mechanical parameters for the knee joint of the subject sets.....	14
Table 2-2	Definition of the mathematical terms of chapter 2.....	14
Table 3-1	Description of the mathematical expressions of chapter 3.....	34
Table 3-2	Details on subjects and experimental trials used for regression fits.....	42
Table 3-3	Knee quasi-stiffnesses in the weight acceptance phase.....	44
Table 3-4	Statistical models to predict the quasi-stiffnesses of the knee joint and estimation errors.....	49
Table 4-1	Definition of mathematical parameters of chapter 4.....	71
Table 4-2	Demographic data of the participants and the stiffnesses of exoskeleton	83
Table 4-3	Mass properties of the exoskeleton.....	83
Table 5-1	Target and realized values for the design parameters.....	147
Table 5-2	Models to size the support spring of the compliant stance control orthosis.....	147
Table 5-3	Demographic data of the participants and trials information.....	147

Chapter 1

Introduction

Researchers have substantially studied the human gait biomechanics at a muscle, joint, and leg level, and the level of the entire body [1-4]. Researchers have also explored numerous engineered actuation and control techniques for the design of lower extremity assistive devices [5-10]. However, there is a lack of knowledge about the interaction between the human lower extremities and engineered devices during locomotion tasks [11-13]. Therefore, several fields benefit from a better understanding of the human body behavior in interaction with external engineered devices, including the fields of lower extremity exoskeletons/orthoses [13-15], prostheses [16-18], and general physiology [13,19].

Research on design of lower extremity exoskeletons started decades ago aiming to improve human gait energetics, and centered mostly on development of technologies and assistive methods [15]. Despite impressive improvement in designs and technologies, lower extremity exoskeletons showed limited success in reducing the gait energy expenditure [12,13,15]. The lack of success in the design of lower extremity exoskeletons prompted basic research on the interaction between human lower extremities and exoskeletal devices aiming to reduce the metabolic cost and muscle involvement [11,12,20].

Research on assistive devices over the last few decades revolutionized lower extremity orthoses and prostheses from simple passive devices to advanced active and quasi-passive devices [17,18,21-24]. Despite substantial improvement in the design technologies and science, lower extremity orthoses and prostheses showed limited success in exhibiting adaptability to the user's size and gait condition [17,25]. This prompted basic research on the behavior of lower extremity joints during walking and also in interaction with these engineered devices [11,24,26-31].

Despite numerous undertakings that led to substantial progress in the mechanical design and control schemes, research on the lower extremity assistive devices still aims to answer several open problems. How does the human body interact with exoskeletal systems at a leg level and a joint level, and what are the effects of exoskeleton mass and kinematic constraints imposed by the exoskeleton articulations on the kinematics and kinetics of human gait? What control schemes can exoskeletons viably employ to energetically augment gait and what is the optimal level/method of exoskeletal assistance? This dissertation reports our efforts to approach a number of open problems in lower extremity orthotics and prosthetics and to expand basic research on the physiology of the human body during walking and also in interaction with lower extremity exoskeletal systems.

Chapter 2 starts with a brief discussion on the state of the art in the field of assistive devices including orthoses/exoskeletons and prostheses and explanation of the open problems in these fields. It continues with an investigation of the moment-angle behavior of the knee joint revealing that the knee joint exhibits linear moment-angle behavior during the stance phase of walking at all speeds, which particularly approaches a spring-type behavior at the preferred walking speed. The chapter finishes with formulation of the main hypotheses of this dissertation. It is also explained that Chapter 3, 4 and 5 report our efforts in experimentally and theoretically testing the hypotheses.

Chapter 3 includes analysis of moment and angle behavior of the normal knee joint centering on development of a series of statistical models that can relatively accurately characterize the moment-angle behavior of this joint during normal walking. The chapter starts with an inverse dynamics analysis of the lower extremities that leads to a generic equation for the moment of the knee joint. The chapter continues with simplification of the generic equation and statistical analyses that lead to development of the statistical models for the knee joint. The chapter ends with a discussion on the orthotic and prosthetic applications and biomechanical implications of the models.

Chapter 4 starts with the mechanical and control design of a pair of quasi-passive knee exoskeletons whose design was inspired by the spring-type behavior of the knee joint in the stance phase in that each exoskeleton implements a spring in parallel with the knee joint in the stance phase and allows free motion throughout the rest of the gait cycle. Using the exoskeletons in a series of experiments on healthy and adult volunteers, we investigated the human body interaction with exoskeletal impedances in parallel with the knee joint. The chapter reports a comprehensive study on the effects of the exoskeletal impedances in parallel with the knee joint on the kinematic and kinetic performance of the ankle, knee, and hip joints, as well as the motion of the human body center of mass, metabolic cost of walking, and gait energetics. The chapter concludes with a discussion on how the findings of the study influence the design of lower extremity exoskeletons and prostheses as well as general gait biomechanics and physiology.

Chapter 5 explains the design and functional evaluation of a compliant stance control orthosis (CSCO) as an advancement over current stance control orthoses. The CSCO intends to restore the spring-type behavior of a knee joint that is impaired by musculoskeletal disorders including spinal cord injury and stroke. Inspired by the spring-type behavior of the knee joint, the CSCO compliantly supports an impaired knee during the stance phase and allows free motion during the swing phase of gait. The chapter explains that the orthosis allows for higher gait speed and more natural kinematic patterns when compared to a stance control orthosis that rigidly lock the knee during the stance phase.

Chapter 6 summarizes the results and findings of this dissertation and draws conclusions accordingly. It also explains the challenges we experienced, limitations of our research, and the potential future steps as possible continuation to the current research.

Putting together, this dissertation reports my research on the mechanics and energetics of healthy and affected human knee joints during normal walking as well as in interaction with exoskeletal impedances.

REFERENCES

1. Winter D (2005) *Biomechanics and Motor Control of Human Movement*. Hoboken, New Jersey: John Wiley & Sons. 325 p.
2. Perry J (1992) *Gait Analysis : Normal and Pathological Function*. Thorofare, NJ: SLACK. 524 p. p.
3. Farris D, Sawicki G (2011) The mechanics and energetics of human walking and running: A joint level perspective. *Journal of The Royal Society Interface* 9: 110-118.
4. Endo K, Herr H (2009) A model of muscle-tendon function in human walking. *Proceedings of 2009 IEEE International Conference on Robotics and Automation (ICRA)*. Kobe, Japan. pp. 2790-2796.
5. Chu A, Kazerooni H, Zoss A (2005) On the biomimetic design of the berkeley lower extremity exoskeleton (BLEEX). *Proceedings of the IEEE International Conference on Robotics and Automation (ICRA)*. Barcelona, Spain. pp. 4345-4352.
6. Walsh C, Endo K, Herr H (2007) A quasi-passive leg exoskeleton for load-carrying augmentation. *International Journal of Humanoid Robotics* 4: 487-506.
7. Sawicki G, Ferris D (2009) A pneumatically powered knee-ankle-foot orthosis (KAFO) with myoelectric activation and inhibition. *Journal of Neuroengineering and Rehabilitation* 6.
8. Ferris D, Czerniecki J, Hannaford B (2005) An ankle-foot orthosis powered by artificial pneumatic muscles. *Journal of Applied Biomechanics* 21: 189-197.
9. Dollar A, Herr H, Chatila R, Kelly A, Merlet J (2008) Design of a quasi-passive knee exoskeleton to assist running. *Proceedings of the 2008 IEEE/RSJ International Conference on Robots and Intelligent Systems (IROS)*: 747-754.
10. Sulzer J, Roiz R, Peshkin M, Patton J (2009) A highly backdrivable, lightweight knee actuator for investigating gait in stroke. *IEEE Transactions on Robotics* 25: 539-548.
11. Elliott G, Sawicki G, Marecki A, Herr H (2013) The biomechanics and energetics of human running using an elastic knee exoskeleton. *Proceedings of IEEE Conference on Rehabilitation Robotics (ICORR)*. Seattle, USA.

12. Grabowski A, Herr H (2009) Leg exoskeleton reduces the metabolic cost of human hopping. *Journal of Applied Physiology* 107: 670-678.
13. Shamaei K, Cenciarini M, Adams A, Gregorczyk K, Schiffman J, et al. (2014) Design and Evaluation of a Quasi-Passive Knee Exoskeleton for Investigation of Motor Adaptation in Lower Extremity Joints. *Biomedical Engineering, IEEE Transactions on PP*: 1-1.
14. Shamaei K, Napolitano PC, Dollar AM (2014) Design and Functional Evaluation of a Quasi-Passive Compliant Stance Control Knee-Ankle-Foot Orthosis. *Neural Systems and Rehabilitation Engineering, IEEE Transactions on* 22: 258-268.
15. Dollar A, Herr H (2008) Lower extremity exoskeletons and active orthoses: challenges and state-of-the-art. *IEEE Transactions on Robotics* 24: 144-158.
16. Bregman D, van der Krogt M, de Groot V, Harlaar J, Wisse M, et al. (2011) The effect of ankle foot orthosis stiffness on the energy cost of walking: A simulation study. *Clinical Biomechanics* 26: 955-961.
17. Martinez-Vilalpando E, Herr H (2009) Agonist-antagonist active knee prosthesis: A preliminary Study in level-ground walking. *Journal of Rehabilitation Research and Development* 46: 361-373.
18. Sup F, Bohara A, Goldfarb M (2008) Design and control of a powered transfemoral prosthesis. *International Journal of Robotics Research* 27: 263-273.
19. Kao P, Lewis C, Ferris D (2010) Invariant ankle moment patterns when walking with and without a robotic ankle exoskeleton. *Journal of Biomechanics* 43: 203-209.
20. Farris D, Sawicki G (2012) Linking the mechanics and energetics of hopping with elastic ankle exoskeletons. *J Appl Physiol* 113: 1862-1872.
21. Zissimopoulos A, Fatone S, Gard S (2007) Biomechanical and energetic effects of a stance-control orthotic knee joint. *Journal of Rehabilitation Research and Development* 44: 503-513.
22. Yakimovich T, Lemaire E, Kofman J (2009) Engineering design review of stance-control knee-ankle-foot orthoses. *Journal of Rehabilitation Research and Development* 46: 257-267.
23. Kaufman K, Irby S, Mathewson J, Wirta R, Sutherland D (1996) Energy-efficient knee-ankle-foot orthosis: A case study. *JPO: Journal of Prosthetics and Orthotics* 8: 79-85.

24. Collins S, Kuo A (2010) Recycling energy to restore impaired ankle function during human walking. Plos One 5.
25. Geyer H, Herr H (2010) A muscle-reflex model that encodes principles of legged mechanics produces human walking dynamics and muscle activities. IEEE Transactions on Neural Systems and Rehabilitation Engineering 18: 263-273.
26. Grabowski A, D'Andrea S (2013) Effects of a powered ankle-foot prosthesis on kinetic loading of the unaffected leg during level-ground walking. Journal of Neuroengineering and Rehabilitation 10.
27. Ferris D, Sawicki G, Domingo A (2005) Powered lower limb orthoses for gait rehabilitation. Topics in spinal cord injury rehabilitation 11: 34.
28. Sawicki G, Lewis C, Ferris D (2009) It pays to have a spring in your step. Exercise and Sport Sciences Reviews 37: 130-138.
29. Shamaei K, Sawicki G, Dollar A (2013) Estimation of quasi-stiffness and propulsive work of the human ankle in the stance phase of walking. PLoS ONE 8: e59935.
30. Shamaei K, Sawicki GS, Dollar AM (2013) Estimation of quasi-stiffness of the human hip in the stance phase of walking. PLoS ONE 8: e81841.
31. Shamaei K, Sawicki G, Dollar A (2013) Estimation of quasi-stiffness of the human knee in the stance phase of walking. PLoS ONE 8: e59993.

Chapter 2

State of the Art of Assistive Devices and Hypothesis Formulation

2.1 Introduction

In this chapter, we introduce the dissertation terminology and discuss the state of the art in the design of assistive devices and explain a number of open problems in this field. It is explained that the design of an assistive device requires better knowledge of the interaction between human body and an exoskeleton at the level of a joint, a leg, and the entire body. This dissertation reports our study of the interaction between an impaired and unimpaired human knee joint with an externally-applied mechanical impedance. We explain that the knee joint behaves similarly to a linear torsional spring during the stance phase and accordingly hypothesize that a spring in parallel with an unimpaired knee joint during the stance phase can partially/fully replace the function of the knee joint and accordingly reduce muscle involvement. We also hypothesize that a spring in parallel with an impaired knee joint during the stance phase can restore the natural function of the knee joint.

2.2 State of the Art of Assistive Devices

Lower extremity assistive devices have been developed to enhance the gait performance of healthy humans or enable patients with musculoskeletal disorders or lost limbs to walk. In terms of functionality and morphology, assistive devices can be categorized as orthoses/exoskeletons and prostheses. An orthosis is defined as a device that is mounted on an existing impaired/dysfunctional limb and intends to restore the natural function of that limb; whereas, an exoskeleton is defined as a device that is mounted on an unimpaired limb and intends to augment the performance of that limb [4]. A prosthesis is defined as a device that replaces a missing limb and is intended to mimic the function of the missing limb [4]. Lower extremity assistive devices

emerged centuries ago, but it was mostly the undertakings of the last four decades that led to substantial advances in design and associated technologies. Despite technological advances in computing, power sources, actuation, and sensing, prosthetics and orthotics (including exoskeletons) have many challenges to overcome.

Orthoses are prescribed for millions of people suffering from musculoskeletal disorders following injury, stroke, post-polio, multiple sclerosis, spina bifida, SCI, and others [6-8]. Many of these disorders could lead to an impaired knee joint and quadriceps weakness that would collapse under the weight of the body and without external orthotic support. Traditional approaches (as described elsewhere [10]) involve stabilizing an impaired knee joint using a Knee-Ankle-Foot Orthosis (KAFO) which locks the knee throughout the entire gait cycle (i.e. the period confined between two consecutive heel strikes with the ground). Since these traditional devices often prevent the knee from flexing, they result in unnatural and energetically expensive compensatory movements including vaulting over the rigidly locked leg and lateral circumducting.

Stance control orthoses, as an advancement over traditional KAFOs, lock the knee during the stance phase (i.e. the period when the foot is on the ground) and allow free movement during the swing phase (i.e. the period when the foot is off the ground) [11-16]. Stance control orthoses proved effective in increasing the walking speed and cadence for novice users ([18] and [20]), and knee range of motion, stride, step lengths, and user satisfaction for both experienced and novice users ([14]- [20]). Moreover, users demonstrated reduced energy expenditure and a reduction in gait asymmetry [14]. However, rigid support of the knee during the stance phase obscures the shock absorption functionality of the knee joint and can lead to unnatural gait requiring compensatory movements, which causes increased metabolic cost, user pain and discomfort. Therefore, an orthosis that mimics the natural compliant behavior of the support limb during stance can be highly beneficial.

Lower extremity exoskeletons constitute a younger and rapidly growing family of assistive devices. Several research groups center on development of lower extremity exoskeletons with a wide spectrum of sophistication [4]. At one end of this spectrum, researchers developed fully actuated exoskeletons that include high-power actuators intended to directly provide assistance to the target lower extremity joints [25-29]. At the other end of the spectrum, researcher developed purely passive devices, which do not include actuators [30]. In the middle of this spectrum, researchers developed quasi-passive exoskeletons using low-power actuators that do not directly provide assistance to the limbs rather modify the performance of the device through engagement/disengagement of passive component [31-33].

Despite numerous undertakings that led to substantial progress in the mechanical design and control schemes, lower extremity exoskeletons showed limited success in achieving the envisioned goal of energetic/metabolic augmentation of gait [4,32,34], which prompted basic research on human physiology in interaction with exoskeletal systems [29,32-38]. The basic research in this field aims to answer several open problems that can be briefly formulated as:

1. How does the human body interact with exoskeletal systems at the level of the leg and a joint?
2. What control schemes can exoskeletons viably employ to energetically augment gait?
3. What are the effects of exoskeleton mass and kinematic constraints imposed by the exoskeleton articulations on the kinematics and kinetics of human gait?
4. What is the trade-off between the burden imposed by the exoskeleton mass and articulation and the assistance provided by the exoskeleton?
5. What is optimal level/method of exoskeletal assistance for the human body?

Lower limb prostheses emerged centuries ago and remained crude until 70s when researchers started developing more sophisticated mechanical and electromechanical prosthetic mechanisms [39,40]. Since then, numerous passive, quasi-passive, and active prostheses emerged [39,40]. Despite the wide range of sophistication in control scheme and mechanical mechanism, lower

limb prostheses showed limited success in gait energetics as well as adaptability to the gait conditions and users characteristics including weight and height [39,40]. To this end, researchers recently have focused on development of lower extremity prostheses that can exhibit gait adaptability using impedance control schemes that are founded on bio-inspired models of the musculoskeletal system and lower extremity joints [41-43]. Therefore, models that can characterize the behavior of musculoskeletal system, lower extremity joints, and overall behavior of the human movement can be extensively used in the design of bipedal robots, lower extremity orthoses, exoskeleton, and prostheses, and in therapeutic and biomechanical evaluation of gait [16,32,40,42,44-52].

2.3 Spring-Type Behavior of the Knee Joint

Researchers have explored the biomechanics of the lower extremities [53-55]. These works extract the impedance of the joints (passive/active elastic, inertia, and viscous parameters) at different angles and muscle activation levels, using system identification techniques. Since the joints experience complex loading conditions and movement pattern in walking, the findings of these researchers could not be directly used in the design of orthoses and prostheses. As a solution, researchers study the moment-angle behavior of the lower extremity joints at different instants of gait to gain insight about the design of assistive devices and to evaluate gait impairments [15,16,32,47-49,56-59]. The moment-angle behavior of a lower extremity joint during a particular phase of gait is characterized using the slope of a linear fit to the moment-angle data points of that joint during that particular phase, which is referred to as the *quasi-stiffness* of the joint in the corresponding phase.

The knee has a wide range of roles during gait, including supporting the body weight and decelerating and absorbing the shock resulted from the heel strike during the stance phase [60]. The stance phase can be divided into two stages including a weight acceptance stage (consisting of the initial contact, loading response, and mid-stance phases [61]) and a stance termination

stage (consisting of the terminal stance and pre-swing phases [61]). The knee undergoes a resistive flexion and a propulsive extension mode during the weight acceptance stage. Exhibiting a shock damping mechanism [62,63], the knee applies considerable moment in the weight acceptance stage [60]. Accordingly, the knee is highly prone to collapse at this stage without proper function of the musculature system or external assistance. Contrary to the stance phase, the knee approximately undergoes a ballistic movement in the swing phase [64], which does not demand considerable external assistance.

An example knee moment-angle graph and a schematic view of lower extremities are shown in Fig. 2-1 and 2 (data from [2]), with the instant of the onset and end of the flexion and extension modes displayed. The letters in Fig. 2-2 correspond to those displayed in Fig. 2-1. In a similar fashion, we obtained knee joint moment-angle profiles of several subject groups from open literature [1,2,22,65-71]. The demographic properties of subjects and subject groups whose kinetic and kinematic data are employed are listed in Table 2-1. These parameters include the mean weight (\bar{W}), mean gait speed/cadence (\bar{V}), mean age (\overline{Age}), mean height (\bar{H}), gender, and number of subjects in each group (n). The *Control* parameter defines the corresponding parameter studied in the original text that allows the readers to identify the subject groups.

The quasi-stiffness of the knee in flexion (K_f) and extension (K_e) modes are defined as the slopes of the corresponding regression lines shown in Fig. 2-2. The quasi-stiffness of the entire weight acceptance stage (\bar{K}_K) is defined as the mean of the quasi-stiffness of the flexion and extension modes. Table 2-1 includes the demographic and gait properties of the individual subjects and sets of subjects for whom the moment-angle relationships are extracted (with terms defined in Table 2-2).

The units of the parameters of the original texts are left intact. The reason is twofold: first, using the same units allows for comparison and avoids inconsistency. Second, in order to use identical units, the physical characteristics as well as the moment and angle time profiles of the

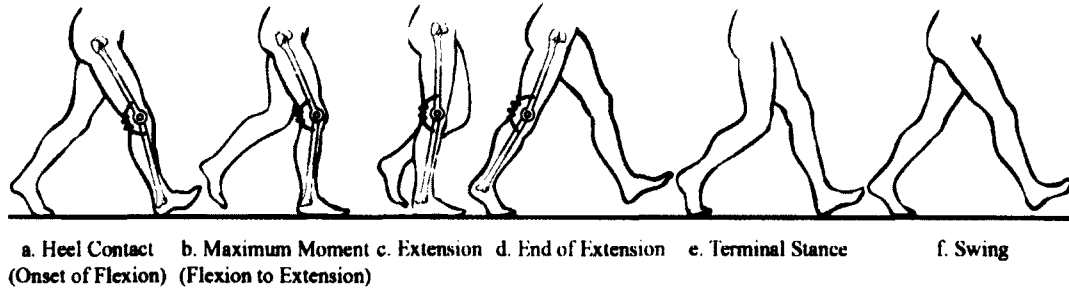


Figure 2-1. The knee flexes and extends under the weight of the body and then it prepares for the swing phase.

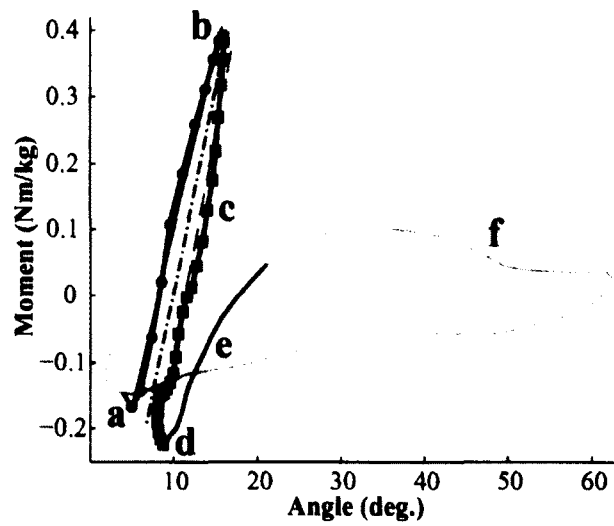


Figure 2-2. The knee moment-angle graph of one gait cycle for a set of subjects walking with slow cadences (85steps/min) [2].

individual subjects are required, which is usually not the case. Indeed, the mean and standard deviation of the parameters and physical properties of the groups (rather than individuals) are often provided in the original texts.

High values of coefficients of determination (R^2) for the linear regressions both in flexion and extension modes, as shown in Table 2-1, indicate that a linear fit to the moment-angle graphs of the knee joint explains most of the variability in the data. In fact, 22 of 24 subject groups have R^2 greater than 90% in flexion mode, as shown in Table 2-1. Furthermore, 19 of 24 subjects have R^2 greater than 90% in the extension mode, similarly, shown in Table 2-1. We further studied the effect of gait speed on the knee joint quasi-stiffness, as shown in Fig. 2-3. The data are primarily extracted from other sources [65]. The subjects' gait speeds are adjusted to be a function of the height of the subject ($0.785 \text{ Stature/sec.}$). The quasi-stiffness of the flexion and extension modes and the overall quasi-stiffness of the weight acceptance stage are shown with black solid, dark gray dashed, and light gray dashed lines, respectively. The speed of $25\%Ref.$ is removed from the original data showing inconsistency with other speeds (the original source highlights this inconsistency [65]).

Linear regression shows that the quasi-stiffness of the knee changes linearly as the gait speed changes ($R^2 = 98.7, p = 0.007$ for both flexion and extension modes) [49,57]. It is noticeable that the changes in stiffness are in two different fashions for the flexion mode and the extension mode; namely, the quasi-stiffness of the knee in flexion mode linearly increases as the gait speed increases; whereas the quasi-stiffness of the knee in the extension mode decreases as the gait increases.

TABLE 2-1. Demographic Properties of the Subject Sets and Mechanical Parameters of the Knee

	Properties of Subject Groups						Mechanical Parameters					Ref.	
	\bar{W}	$\bar{V}^{\ddagger\dagger}$	\bar{Age}	\bar{H}	Gen.	n	CTRL	K_f	K_e	\bar{K}_K	R_f^2		R_e^2
1†	76.8	99.8C	30.3	1.81	M	16	6kg	351	222	286.5	98	97	[1]
2†		100.6C					20kg	406	260	333	98	98	
3†		100.0C					33kg	532	286	409	98	98	
4†		102.4C					47kg	553	322	437.5	96	98	
5•	69.7	25NS	28.8	1.72	M/F	18	25%	11.1	16.7	19.4	90	80	[3]
6•		50NS					50%	14.8	23.8	19.3	95	94	
7•		75NS					75%	17.8	22.7	20.3	99	98	
8•		100NS					100%	23.0	20.8	21.9	99	99	
9•		125NS					125%	28.0	19.1	23.5	99	94	
10‡	*	*	64.4	*	M/F	37	Normal	3.02	3.02	3.02	99	99	[5]
11‡	70.8	120C	27.9	1.71	M/F	12	Level	14.89	6.25	5.98	80	98	[9]
12‡							Downhill	6.21	9.55	7.88	96	91	
13‡	64.7	1.34S	28.3	1.73	M/F	20	Healthy	4.90	3.7	4.3	90	90	[17]
14†	82	*	28	1.76	M	26	EE	253	100	176.5	90	86	[19]
15†	67.2	96C	23	1.75	M	1	A	90	146	98	75	91	[21]
16†		104C	26	1.8	M	1	B	181	264	222.5	99	94	
17†		109C	29	1.81	M	1	C	745	259	502	85	89	
18†		1.21S	21	1.82	M	1	A	157	223	190	96	88	
19†	56	1.18S	26	1.76	M	1	B	147	250	198.5	98	98	[22]
20†		1.40S	21	1.62	F	1	C	122	122	122	97	99	
21‡		71.5	85C	22.2	1.77	*	14	Slow	3.05	3.79	3.42	98	
22‡	69.1	105C	25.6	1.75	*	16	Normal	2.92	2.92	2.92	99	97	[23]
23‡		125C	22.2	1.77	*	14	Fast	5.12	3.39	4.25	98	88	
24‡	76.4	111.8C	68.9	1.71	*	18	Elderly	3.62	3.27	3.44	99	95	[24]

†: Stiffness (*N.m rad.*), Moment (*N.m*), and Work (*J*)
 •: Stiffness (*%BW.Ht. rad.*) and Moment (*%BW.Ht.*), work (*%BW.Ht.*)
 *: Not specified
 Notice that the subject groups are divided by the lines.

‡: Stiffness (*N.m kg.rad.*), Moment (*N.m kg*), and Work (*J kg.*)
 ††: Cadence (*steps min*), Speed (*m sec.*), and Normalized Speed (*%0.785Stature sec.*)

TABLE 2-2. Definition of the Mathematical Terms

K_f	Quasi-stiffness of the knee in flexion mode
K_e	Quasi-stiffness of the knee in extension mode
\bar{K}_K	Quasi-stiffness of the knee in weight acceptance stage
R_f^2	Coefficient of determination of flexion mode for the knee
R_e^2	Coefficient of determination of flexion mode for the knee
\bar{W}	Mean body weight (<i>kg</i>)
\bar{v}	Mean speed/cadence
\bar{Age}	Mean age
\bar{H}	Mean height (<i>m</i>)
Control	Control parameter in the original text
n	Number of the subjects

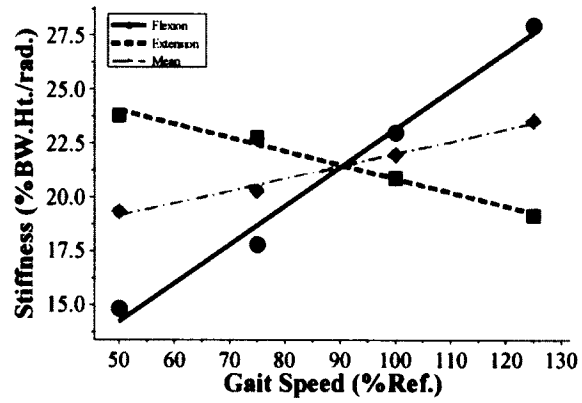


Figure 2-3. The quasi-stiffness of the knee in the flexion ($K_f = 5.276 + 0.178\bar{V}$, $R^2 = 98.7\%$, $p = \{0.059, 0.007\}$) and extension ($K_e = 27.230 - 0.064\bar{V}$, $R^2 = 98.7\%$, $p = \{0.000, 0.007\}$) modes, and in the weight acceptance stage ($K_K = 16.250 + 0.057\bar{V}$) of the gait plotted against the gait speed, (Ref. = 0.785 Stature/sec.).

The stiffnesses of these two modes are perceived to be identical for a gait speed around $90\%Ref.$ (the intersection of the regression lines of the flexion and extension modes shown in Fig. 2-3), which is close to the preferred walking speed. In other words, *the quasi-stiffnesses of the knee in flexion and extension modes are nearly identical at the preferred walking speed and differ as the gait speed deviates from the natural value implying that the human knee joint behaves similarly to a linear torsional spring at the preferred gait speed [49,57].* Consequently, a device (including orthoses, exoskeletons, prostheses, and biped robots) can mimic the behavior of the human knee by implementing a spring with a suitable stiffness during the stance phase and allowing free motion during the swing phase.

2.4 Formulation of Dissertation Hypotheses

We found that the human knee joint exhibits a linear moment-angle behavior during the stance phase of walking at all speeds and a spring-type behavior during the stance phase of walking at the preferred speed, which are both subject-specific and gait-specific [49,57]. Therefore, we formulate the following hypotheses:

1. The significant dependence of the moment-angle behavior of the knee joint on the body size and gait speed [49,57] leads us to hypothesize that, from a design point of view, the moment-angle behavior of the knee joint can be sufficiently accurately characterized using a set of measurable parameters including body weight, height, gait speed, and joint excursion. Characterization of the moment-angle behavior of the knee joint paves the way for the design of knee orthoses/exoskeletons and prostheses.

2. The spring-type behavior of the knee joint during the stance phase at the preferred gait speed leads us to hypothesize that the behavior of unaffected human lower extremity joints during normal walking adapts to externally-applied mechanical stiffnesses in parallel with the knee joint such that the overall kinematic and kinetic patterns remain invariant. Particularly, the knee joint stiffness and moment during the stance phase adapt to an externally-applied stiffness and moment

implying that a knee exoskeleton can provide assistance to the knee joint and reduce muscle involvement and metabolic cost by implementing a spring in parallel with the knee joint during the stance phase and allowing free rotation during the rest. We also anticipate that the mass and articulations of an exoskeleton would perturb gait patterns.

3. We hypothesize that a knee orthosis can restore the natural spring-type behavior of an impaired knee joint during the stance phase, provided it implemented a spring tuned to the gait requirements of the user during the stance phase. This implies that a stance control orthosis can compliantly support (as opposed to the oftentimes rigidly supporting) the knee joint during the stance phase to restore the natural gait of users with impaired knee joints.

2.5 Dissertation Approach

This dissertation reports our efforts in approaching some of the open problems in the area of assistive lower extremity devices by experimentally testing the formulated hypotheses. We experimentally study the behavior of lower extremity joints (particularly the knee joint) during normal walking as well as in interaction with mechanical exoskeletal impedances in parallel with the knee joint. We investigate the formulated hypotheses in the next three chapters. Chapter 3 reports a theoretical and empirical study through which we established a series of statistical models that relatively accurately characterize the moment-angle behavior of the knee joint during the stance phase of gait using a set of measurable parameters. Chapter 4 reports a comprehensive experimental study on the interaction between unimpaired lower extremities and mechanical impedances externally-applied in parallel with the knee joint using a robotic knee exoskeleton. Chapter 5 explains the design and evaluation of a compliant stance control orthosis on a set of healthy subjects and one impaired subject, and investigates the effects of compliant stabilization of the knee joint during stance phase through comparison with a state-of-the-art stance control orthosis that rigidly locks the knee during the stance phase.

REFERENCES

1. Harman E, Hoon K, Frykman P, Pandorf C (2000) The effects of backpack weight on the biomechanics of load carriage. Natick, USA: Military Performance DivisionUS Army Research Institute of Environmental Medicine.
2. Winter D (1983) Biomechanical motor patterns in normal walking. *Journal of Motor Behavior* 15: 302-330.
3. Holden JP, Chou G, Stanhope SJ (1997) Changes in Knee Joint Function Over a Wide Range of Walking Speeds. *Clinical Biomechanics*: 375-382.
4. Dollar A, Herr H (2008) Lower extremity exoskeletons and active orthoses: challenges and state-of-the-art. *IEEE Transactions on Robotics* 24: 144-158.
5. Deluzio KJ, Wyss UP, Zee B, Costigan PA, Sorbie C (1997) Principal Component Models of Knee Kinematics and Kinetics: Normal vs. Pathological Gait Patterns. *Human Movement Science*: 201-217.
6. Waters R, Campbell J, Thomas L, Hugos L, Davis P (1982) Energy costs of walking in lower-extremity plaster casts. *Journal of Bone and Joint Surgery-American* 64: 896-899.
7. Hurley E (2006) Use of KAFOs for patients with cerebral vascular accident, traumatic brain injury, and spinal cord injury. *Journal of Prosthetics and Orthotics* 18: 199-201.
8. Taylor M (2006) KAFOs for patients with neuromuscular deficiencies. *Journal of Prosthetics & Orthotics* 18: 202-203.
9. Kuster M, Sakurai S, Wood GA (1995) Kinematic and Kinetic Comparison of Downhill and Level Walking. *Clinical Biomechanics*: 79-84.
10. Redford J, Basmajian J, Trautman P (1995) *Orthotics: Clinical Practice and Rehabilitation Technology*. New York: Churchill Livingstone. 337 p. p.
11. Yakimovich T, Lemaire ED, Kofman J (2009) Engineering Design Review of Stance-Control Knee-Ankle-Foot Orthoses. *Journal of Rehabilitation Research and Development*: 257-267.

12. Herr H (2009) Exoskeletons and Orthoses: Classification, Design Challenges and Future Directions. *Journal of Neuroengineering and Rehabilitation*: -.
13. Kaufman K, Irby S, Mathewson J, Wirta R, Sutherland D (1996) Energy-efficient knee-ankle-foot orthosis: A case study. *JPO: Journal of Prosthetics and Orthotics* 8: 79-85.
14. McMillan AG, Kendrick K, Michael JW, Aronson J, Horton GW (2004) Preliminary Evidence for Effectiveness of a Stance Control Orthosis. *JPO: Journal of Prosthetics and Orthotics* 16: 6-13.
15. Shamaei K, Napolitano P, Dollar A (2013) A quasi-passive compliant stance control knee-ankle-foot orthosis. *Proceedings of the IEEE International Conference on Rehabilitation Robotics (ICORR)*. Seattle, USA.
16. Shamaei K, Napolitano PC, Dollar AM (2014) Design and Functional Evaluation of a Quasi-Passive Compliant Stance Control Knee-Ankle-Foot Orthosis. *Neural Systems and Rehabilitation Engineering, IEEE Transactions on* 22: 258-268.
17. Houck J, Yack HJ (2003) Associations of Knee Angles, Moments and Function Among Subjects that are Healthy and Anterior Cruciate Ligament Deficient (ACL) During Straight Ahead and Crossover Cutting Activities. *Gait & Posture*: 126-138.
18. Irby SE, Bernhardt KA, Kaufman KR (2007) Gait Changes Over Time in Stance Control Orthosis Users. *Prosthetics and Orthotics International*: 353-361.
19. Smidt GL (1973) Biomechanical Analysis of Knee Flexion and Extension. *Journal of Biomechanics*: 79-&.
20. Irby SE, Bernhardt KA, Kaufman KR (2005) Gait of Stance Control Orthosis Users: The Dynamic Knee Brace System. *Prosthetics and Orthotics International*: 269-282.
21. Pedotti A (1977) Study of Motor Coordination and Neuromuscular Activities in Human Locomotion. *Biological Cybernetics*: 53-62.
22. Apkarian J, Naumann S, Cairns B (1989) A 3-dimensional kinematic and dynamic-model of the lower-limb. *Journal of Biomechanics*: 143-155.
23. Winter DA (1983) Biomechanical Motor Patterns in Normal Walking. *Journal of Motor Behavior*: 302-330.

24. Winter DA (1991) *The Biomechanics and Motor Control of Human Gait : Normal, Elderly and Pathological*. Waterloo, Ont.: University of Waterloo Press. x, 143 p. p.
25. Zoss A, Kazerooni H, Chu A (2006) Biomechanical design of the Berkeley lower extremity exoskeleton (BLEEX). *IEEE/ASME Transactions on Mechatronics* 11: 128-138.
26. Aguirre-Ollinger G, Colgate J, Peshkin M, Goswami A (2011) Design of an active one-degree-of-freedom lower-limb exoskeleton with inertia compensation. *International Journal of Robotics Research* 30: 486-499.
27. Farris R, Quintero H, Goldfarb M (2011) Preliminary evaluation of a powered lower limb orthosis to aid walking in paraplegic individuals. *IEEE Transactions on Neural Systems and Rehabilitation Engineering* 19: 652-659.
28. Gregorczyk K, Hasselquist L, Schiffman J, Bensek C, Obusek J, et al. (2010) Effects of a lower-body exoskeleton device on metabolic cost and gait biomechanics during load carriage. *Ergonomics* 53: 1263-1275.
29. Lenzi T, Carrozza M, Agrawal S (2013) Powered hip exoskeletons can reduce the user's hip and ankle muscle activations during walking. *IEEE Transactions on Neural Systems and Rehabilitation Engineering*.
30. Agrawal S, Banala S, Fattah A, Sangwan V, Krishnamoorthy V, et al. (2007) Assessment of motion of a swing leg and gait rehabilitation with a gravity balancing exoskeleton. *IEEE Transactions on Neural Systems and Rehabilitation Engineering* 15: 410-420.
31. Walsh C, Endo K, Herr H (2007) A quasi-passive leg exoskeleton for load-carrying augmentation. *International Journal of Humanoid Robotics* 4: 487-506.
32. Shamaei K, Cenciarini M, Adams A, Gregorczyk K, Schiffman J, et al. (2014) Design and Evaluation of a Quasi-Passive Knee Exoskeleton for Investigation of Motor Adaptation in Lower Extremity Joints. *Biomedical Engineering, IEEE Transactions on PP*: 1-1.
33. Elliott G, Sawicki G, Marecki A, Herr H (2013) The biomechanics and energetics of human running using an elastic knee exoskeleton. *Proceedings of IEEE Conference on Rehabilitation Robotics (ICORR)*. Seattle, USA.
34. Grabowski A, Herr H (2009) Leg exoskeleton reduces the metabolic cost of human hopping. *Journal of Applied Physiology* 107: 670-678.

35. Ferris D, Bohra Z, Lukos J, Kinnaird C (2006) Neuromechanical adaptation to hopping with an elastic ankle-foot orthosis. *Journal of Applied Physiology* 100: 163-170.
36. Farris D, Sawicki G (2012) Linking the mechanics and energetics of hopping with elastic ankle exoskeletons. *J Appl Physiol* 113: 1862-1872.
37. Wiggin M, Sawicki G, Collins S (2011) An exoskeleton using controlled energy storage and release to aid ankle propulsion. *Proceedings of IEEE International Conference on Rehabilitation Robotics (ICORR)*. Zurich, Switzerland.
38. Sawicki G, Ferris D (2009) A pneumatically powered knee-ankle-foot orthosis (KAFO) with myoelectric activation and inhibition. *Journal of Neuroengineering and Rehabilitation* 6.
39. Herr H, Wilkenfeld A (2003) User-adaptive control of a magnetorheological prosthetic knee. *Industrial Robot: an International Journal* 30: 42-55.
40. Martinez-Vilialpando E, Herr H (2009) Agonist-antagonist active knee prosthesis: A preliminary Study in level-ground walking. *Journal of Rehabilitation Research and Development* 46: 361-373.
41. Endo K, Herr H (2009) A model of muscle-tendon function in human walking. *Proceedings of 2009 IEEE International Conference on Robotics and Automation (ICRA)*. Kobe, Japan. pp. 2790-2796.
42. Eilenberg M, Geyer H, Herr H (2010) Control of a powered ankle-foot prosthesis based on a neuromuscular model. *IEEE Transactions on Neural Systems and Rehabilitation Engineering* 18: 164-173.
43. Sup F, Varol H, Mitchell J, Withrow T, Goldfarb M (2008) Design and control of an active electrical knee and ankle prosthesis. *Proceedings of 2nd IEEE/RAS & EMBS International Conference on Biomedical Robotics and Biomechanics (Biorob)*. Scottsdale, USA.
44. Geyer H, Seyfarth A, Blickhan R (2006) Compliant leg behaviour explains basic dynamics of walking and running. *Proceedings of the Royal Society B-Biological Sciences* 273: 2861-2867.
45. Alexander R (1992) A model of bipedal locomotion on compliant legs. *Philosophical Transactions of the Royal Society of London Series B-Biological Sciences* 338: 189-198.

46. Taga G (1995) A model of the neuro-musculo-skeletal system for human locomotion.1. emergence of basic gait. *Biological Cybernetics* 73: 97-111.
47. Shamaei K, Sawicki G, Dollar A (2013) Estimation of quasi-stiffness and propulsive work of the human ankle in the stance phase of walking. *PLoS ONE* 8: e59935.
48. Shamaei K, Sawicki GS, Dollar AM (2013) Estimation of quasi-stiffness of the human hip in the stance phase of walking. *PLoS ONE* 8: e81841.
49. Shamaei K, Sawicki G, Dollar A (2013) Estimation of quasi-stiffness of the human knee in the stance phase of walking. *PLoS ONE* 8: e59993.
50. Hitt J, Sugar T, Holgate M, Bellman R (2010) An active foot-ankle prosthesis with biomechanical energy regeneration. *Transactions of the ASME Journal of Medical Devices* 4.
51. Lemaire E, Goudreau L, Yakimovich T, Kofman J (2009) Angular-velocity control approach for stance-control orthoses. *IEEE Transactions on Neural Systems and Rehabilitation Engineering* 17: 497-503.
52. Collins S, Kuo A (2010) Recycling energy to restore impaired ankle function during human walking. *Plos One* 5.
53. Weiss P, Kearney R, Hunter I (1986) Position dependence of ankle joint dynamics: 1. passive mechanics. *Journal of Biomechanics* 19: 727-735.
54. Weiss P, Kearney R, Hunter I (1986) Position dependence of ankle joint dynamics: 2. active mechanics. *Journal of Biomechanics* 19: 737-751.
55. Salsich G, Mueller M (2000) Effect of plantar flexor muscle stiffness on selected gait characteristics. *Gait & Posture* 11: 207-216.
56. Frigo C, Crenna P, Jensen L (1996) Moment-angle relationship at lower limb joints during human walking at different velocities. *Journal of Electromyography and Kinesiology* 6: 177-190.
57. Shamaei K, Dollar A (2011) On the mechanics of the knee during the stance phase of the gait. *Proceedings of IEEE International Conference on Rehabilitation Robotics (ICORR)*. Zurich, Switzerland.

58. Shamaei K, Cenciarini M, Dollar A (2011) On the mechanics of the ankle in the stance phase of the gait. Proceedings of the IEEE Annual International Conference of Engineering in Medicine and Biology Society (EMBC). Boston, USA. pp. 8135-8140.
59. Davis R, DeLuca P (1996) Gait characterization via dynamic joint stiffness. *Gait & Posture* 4: 224-231.
60. Winter D, Robertson D (1978) Joint torque and energy patterns in normal gait. *Biological Cybernetics* 29: 137-142.
61. Perry J (1992) *Gait Analysis : Normal and Pathological Function*. Thorofare, NJ: SLACK. 524 p. p.
62. Gard S, Childress D (2001) What determines the vertical displacement of the body during normal walking? *Journal of Prosthetics and Orthotics* 13: 64-67.
63. Ratcliffe R, Holt K (1997) Low frequency shock absorption in human walking. *Gait & Posture* 5: 93-100.
64. Mochon S, McMahon T (1980) Ballistic walking - an improved model. *Mathematical Biosciences* 52: 241-260.
65. Holden J, Chou G, Stanhope S (1997) Changes in knee joint function over a wide range of walking speeds. *Clinical Biomechanics* 12: 375-382.
66. Deluzio K, Wyss U, Zee B, Costigan P, Sorbie C (1997) Principal component models of knee kinematics and kinetics: normal vs. pathological gait patterns. *Human Movement Science* 16: 201-217.
67. Kuster M, Sakurai S, Wood G (1995) Kinematic and kinetic comparison of downhill and level walking. *Clinical Biomechanics* 10: 79-84.
68. Houck J, Yack HJ (2003) Associations of knee angles, moments and function among subjects that are healthy and anterior cruciate ligament deficient (ACLD) during straight ahead and crossover cutting activities. *Gait & Posture* 18: 126-138.
69. Smidt G (1973) Biomechanical analysis of knee flexion and extension. *Journal of Biomechanics* 6: 79-92.

70. Pedotti A (1977) Study of motor coordination and neuromuscular activities in human locomotion. *Biological Cybernetics* 26: 53-62.

71. Winter D (1991) *The Biomechanics and Motor Control of Human Gait : Normal, Elderly and Pathological*. Waterloo, Ont.: University of Waterloo Press. 143 p.

Chapter 3

Characterization of Moment-Angle Behavior of the Knee Joint

3.1 Introduction

A number of engineered locomotion systems aim to emulate the biomechanical behavior of humans including anthropomorphic bipedal robots [1,2], lower-limb wearable exoskeletons [3-10], and biologically-inspired prosthetic limbs [11-14]. Robust performance of these systems can be achieved using mechanisms that function similar to the biological joints. These mechanisms should ideally be built upon a foundation of simple models (theoretical or empirical) that can accurately characterize the normal mechanical behavior of the human joints during the locomotion tasks [15-17]. Therefore, design of these locomotion systems requires knowledge of how individual joints behave during locomotion tasks. To this end, researchers have used both empirical and theoretical approaches to characterize human locomotion. Experiments have been performed to measure the kinetics and kinematics of the human joints in locomotion tasks using gait laboratory equipment [19-21], and whole-leg models have been implemented with a range of complexity that can generate human locomotion patterns [1,17,22-30]. Researchers have also investigated the torque generation capabilities of the joints in terms of the passive and active stiffness using system identification techniques that employ statistical analyses and experimental data [31-33]. Most of these studies examined the joint and leg stiffness under controlled conditions and in specific tasks such as hopping or lateral balance; making it difficult to extend results to the behavior of joints during walking/running [26,31,32,36-38]. However, a common finding from all of these approaches is that compliance (i.e. springy limb behavior) plays a central role in shaping human motion.

Previous studies show that the lower extremity joints have moment-angle patterns with highly linear phases during gait, especially during periods of high loading [35,39-42]. These findings have motivated incorporation of passive elastic components in the design of lower extremity orthoses/exoskeletons and prostheses to unload/mimic the musculature system function [43-45]. Moreover, the loading/unloading behavior of the lower extremity joints has been investigated using the concept of quasi-stiffness or “dynamic stiffness” [35,39-42,46-51]. The term quasi-stiffness is usually reserved for lower extremity joints (e.g. ankle, knee, and hip) and can be distinguished from the passive and active stiffness of a joint typically used to describe the ‘local’ tangent to the moment-angle curve exhibited for a given joint at a specific angle and for a certain level of muscle activation as described in the literature; hence, it should be distinguished from the passive and active stiffness of a joint defined as a specific function of angle and time [31,32,52].

The concept of quasi-stiffness applies well to major loading phases of the lower extremity joints, mainly the ankle joint during stance phase, knee during the weight acceptance phase, and hip joint during the late stance and early swing phase of walking [35,39-42,47,53]. From a design standpoint, a spring with a rotational stiffness equal to the joint quasi-stiffness can closely mimic the function of that joint in that specific task. Accordingly, many researchers develop and size prostheses according to the *average* joint quasi-stiffness (and additional tuning on the user) [13,35,39,40,46-51]. Our previous research shows that the quasi-stiffness of lower limb joints can significantly change according to the gait conditions and subject size [35,40-42]. Moreover, a simple and fast measurement of the joint quasi-stiffness for patients in a gait laboratory is very difficult. Therefore, the design of prostheses and orthoses could benefit from subject and gait specific model estimates for the quasi-stiffness of lower extremity joints in the key loading/unloading phases of gait.

The concept of quasi-stiffness applies particularly well to the knee joint during stance phase of walking, where a substantial moment is applied to compliantly support the body weight. This compliance was originally considered a determinant factor in reducing the vertical travel of center

of gravity of the body [54], and later shown to play a major role in shock absorption [55-57]. Applying a preliminary quasi-stiffness analysis revealed a nearly linear spring-like behavior that changes with both gait speed and load carriage [40]. Indeed, a simple spring-like approximation of knee performance leads to much simpler mechanical designs of assistive devices, leading to greater robustness, lower cost, lighter weight, and higher shock tolerance. The overall goal of this chapter is to establish statistical models that can closely characterize quasi-stiffnesses of the knee joint in the weight acceptance phase of walking for adult humans spanning body size (height and weight) across a wide range of walking speeds. The results of this chapter promise to aid in the development of biologically-inspired assistive devices (e.g. exoskeletons, orthoses, and prostheses) for the knee joint [4,35,40-44,58].

We begin with a description of the moment-angle behavior of the knee joint, modeling approach and data collection methods used in the study. To extract the models, we obtain generic equations of the knee joint moment through an inverse dynamics analysis and identify subsets of factors that can explain the quasi-stiffnesses of this joint. We then employ a data set including the moment-angle information for 136 gait trials across 14 human adult subjects for the knee joint spanning a substantial range of body sizes and gait speeds to extract the coefficients of each factor and obtain *general-form* statistical models. We show that the models can closely estimate the quasi-stiffnesses across the gait trials examined.

The general-form models estimate the quasi-stiffnesses using the magnitude of lower extremity joints excursion, gait speed, and body size. For design occasions where it would be undesirably time-consuming or expensive or where joint kinematics cannot be easily and repeatedly characterized (e.g. in an orthosis for a spinal cord injury patient), we develop more simplified models that only include the body size. These models favor the design of compliant assistive devices that are versatile enough to perform well over a range of speeds around the preferred gait speed. These simplified equations are termed *stature-based* models, and are only functions of body weight and height. There are many applications where a priori knowledge of

the joints excursion is not available and only one stiffness is required, such as “sizing” compliant knee prostheses or orthoses that are versatile enough to perform around the optimal gait speed, without needing time-consuming ‘on-board’ measurements. For these cases, the stature-based models can be used that only include height and weight, at the expense of reduced accuracy.

3.2 Moment-Angle Behavior of the Knee Joint during Walking

To evaluate the knee joint quasi-stiffness, we first divide the gait cycle into stance and swing phases (schematically shown in Fig. 3-1, top). The stance phase can be further divided into two sub-phases including a weight acceptance phase (consisting of the initial contact, loading response, and mid-stance phases) and a stance termination phase (consisting of the terminal stance and pre-swing phases) [59]. This study centers on the weight acceptance sub-phase (Fig. 3-1, top a-c). During this phase, the knee undergoes a flexion stage (a-b) and an extension stage (b-c) while supporting body weight. Exhibiting a shock damping mechanism [55,57], the knee applies a large moment in the weight acceptance phase [60]. Accordingly, the knee is highly prone to collapse at this stage without proper action of the musculoskeletal system or external assistance (a problem that exists in patients with musculoskeletal disorders such as spinal cord injury and stroke). Contrary to the stance leg, the swing leg approximately undergoes a ballistic movement [29] that does not demand considerable muscular effort.

We define the quasi-stiffness of the flexion stage (K_{kf}) and extension stage (K_{ke}) as the slopes of the lines fit on the moment-angle graph of the knee in the corresponding stage (see Fig. 3-1, bottom). We also introduce the quasi-stiffness of the entire weight acceptance phase (K_k) as the average of K_{kf} and K_{ke} . Alternatively, K_k can be introduced as the slope of a line fit on the moment-angle graph of the weight acceptance phase. However, since the extension stage is more prolonged in time, the slope of the fit is highly affected by the behavior of the knee in that stage.

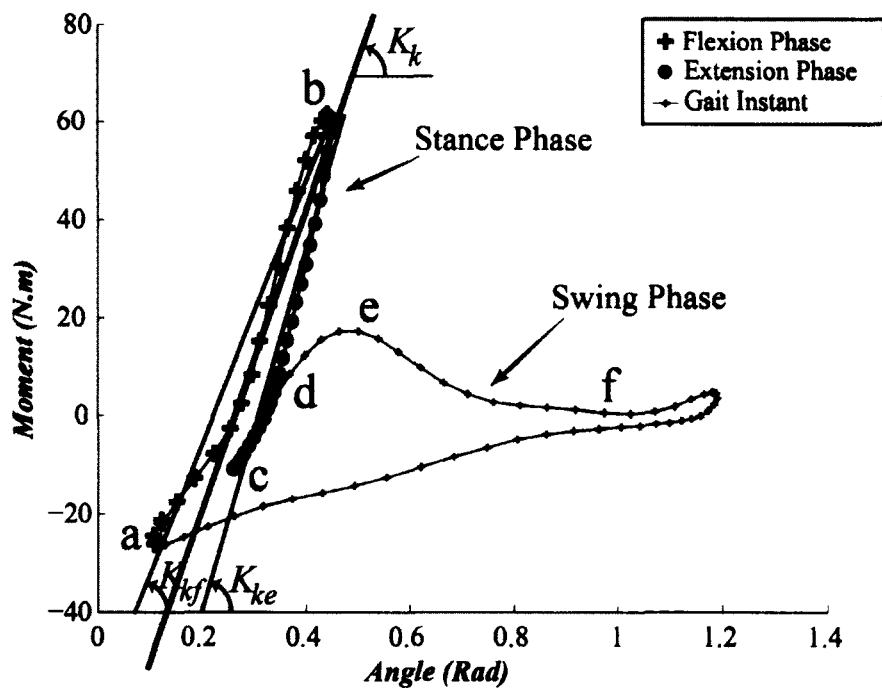
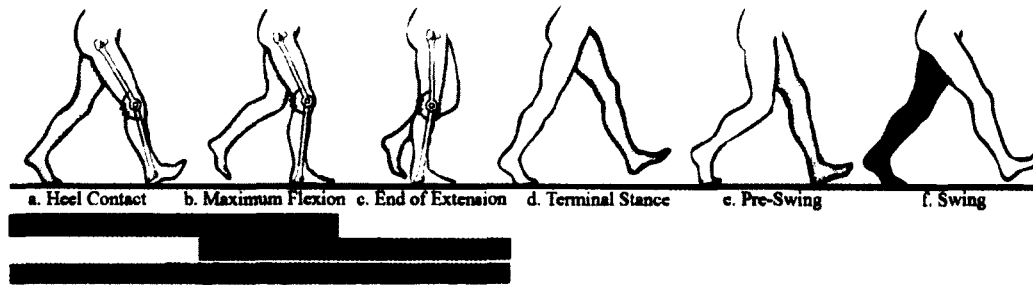


Figure 3-1. Knee moment vs. angle curve for a representative subject walking at 1.25 m/s . Letters a-f on the graph correspond to the poses shown during a typical walking cycle (top, schematic timing is adapted from [18]). Quasi-stiffness is calculated based on the slope of the best line fit to the moment-angle curve of a-b for the flexion stage (K_{kf}), and b-d for the extension stage (K_{ke}) of the weight acceptance phase (a-d). The average of these two quasi-stiffness values is defined as the quasi-stiffness of the weight acceptance phase (K_t).

We obtain the magnitude of excursion of the knee in the flexion stage (θ_{kf}) and extension stage (θ_{ke}) by subtracting the initial angle from the final angle in that particular stage. Using an averaging similar to the definition of K_k , we define the knee excursion in the weight acceptance phase (θ_k) as the mean value of θ_{kf} and θ_{ke} .

3.3 Inverse Dynamics Analysis

In this section, we derive a generic equation for the moment of the knee joint. Winter presents a detailed explanation of *step-wise* inverse dynamics analysis for gait laboratory analysis [61]. Our analyses develop the Newtonian equations of motion of foot with respect to (w.r.t.) the global coordinate system as shown by $X - Y - Z$ in Fig. 3-2. Next, we derive an expression for the moment of the ankle joint w.r.t. the anatomical coordinate frame of the foot shown by $x_f - y_f - z_f$ in Fig. 3-2. The anatomical coordinate frame of the foot is established by placing y_f on the axis connecting the toe to the ankle center, z_f along with Z and x_f along with the cross-product of y_f and z_f . The Newtonian equations of motion of the shank give us the reaction force of the knee in the global axes, using the reaction force of the ankle. Then, we apply the reaction forces of the ankle and knee in the Euler equations of motion and derive an expression for the moment of the knee w.r.t. the anatomical coordinate frame of the shank shown by $x_s - y_s - z_s$. The anatomical coordinate frame of the shank is established by placing y_s on the axis connecting the ankle center to the knee center, z_s along Z and x_s along the cross-product of y_s and z_s . Table 3-1 lists the parameters that are used in this text and brief description of each parameter.

The pair of ground reaction force (\vec{F}_G) and ground reaction moment (\vec{M}_G) is transferred to the distal joint (i.e. toe) from the center of pressure (*COP*) to obtain the distal force (\vec{R}_D^f) and the distal moment (\vec{M}_D^f) of the foot w.r.t. $X-Y-Z$. Hence w.r.t. $X-Y-Z$ we get:

$$\vec{R}_D^f = \vec{F}_G \quad (3-1-a)$$

$$\vec{M}_D^f = \vec{M}_G - \vec{F}_G \times \vec{r} \quad (3-1-b)$$

and w.r.t. $x_f - y_f - z_f$ we get:

$$\vec{R}_d^f = [GA]_f \vec{F}_G \quad (3-2-a)$$

$$\vec{M}_d^f = [GA]_f (\vec{M}_G - \vec{F}_G \times \vec{r}) \quad (3-2-b)$$

\vec{r} is the vector connecting the distal joint to *COP* and $[GA]_f$ is a proper (i.e. reserves inner product and has a determinant of 1) rotation from $X-Y-Z$ to $x_f - y_f - z_f$. The reaction force at the ankle (\vec{R}_p^f) is derived using the Newtonian equation of motion for the foot:

$$\sum \vec{F}_f = m_f \vec{a}_f \quad \therefore \vec{R}_p^f = \vec{R}_D^f + m_f \vec{a}_f + m_f g \vec{e}_y \quad (3-3)$$

where, \vec{F}_f denotes any force that is applied on the foot segment and \vec{a}_f is the acceleration of the center of mass of the foot (COM_f). m_f is the mass of the foot segment, \vec{e}_y is a unit vector along the Y -axis, and g is the acceleration due to gravity. Equation (3-1-a) gives us the proximal force of the foot w.r.t. $X-Y-Z$ as:

$$\vec{R}_p^f = \vec{F}_G + m_f \vec{a}_f + m_f g \vec{e}_y \quad (3-4)$$

which could be transformed to $x_f - y_f - z_f$ through a rotation, as:

$$\vec{R}_p^f = [GA]_f \vec{R}_p^f \quad (3-5)$$

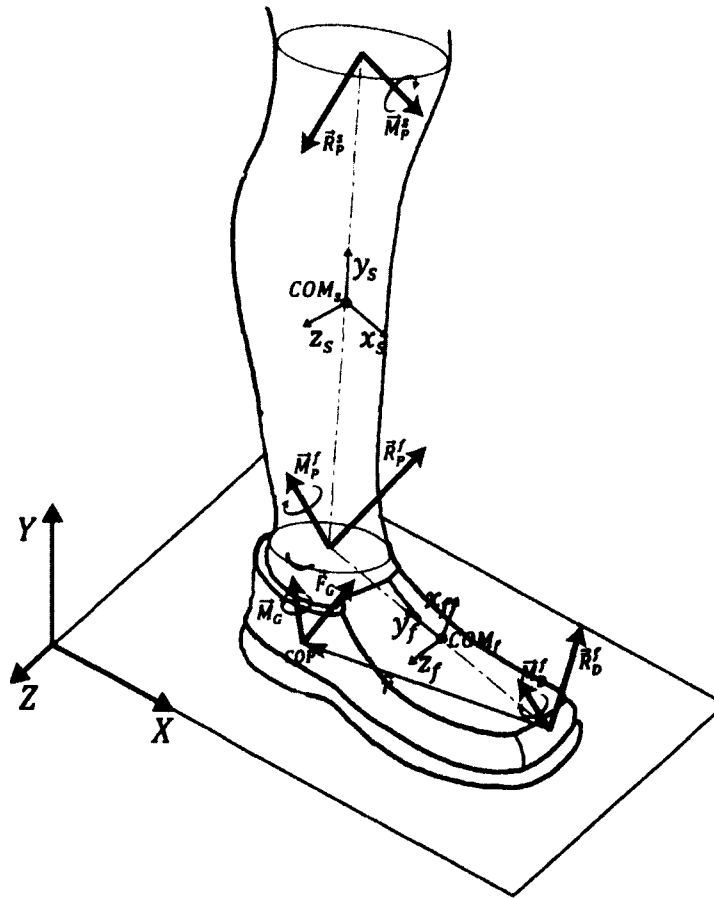


Figure 3-2. A schematic model of the support shank and foot. The figure depicts the proximal force and moments of the shank and foot segments, and the center of masses (COM_s and COM_f). The ground reaction force and moment are also shown at the center of pressure (COP).

Now, we derive the expression of the moment at its proximal joint (i.e. ankle):

$$\sum \vec{M}_f = [I_f] \vec{\dot{\omega}}_f + \vec{\omega}_f \times \vec{U}_f \quad (3-6)$$

wherein, \vec{M}_f denotes any moment that is applied on the foot segment and $[I_f]$ is the matrix of moment of inertia. $\vec{\omega}_f$ the angular velocity, $\vec{\dot{\omega}}_f$ the angular acceleration, and \vec{U}_f is the angular momentum of the foot segment. Expanding the left hand side of the above equation gives us:

$$\vec{M}_p^f = \vec{M}_d^f - \vec{R}_d^f \times \vec{d}_f + \vec{R}_p^f \times \vec{p}_f + [I_f] \vec{\dot{\omega}}_f + \vec{\omega}_f \times \vec{U}_f \quad (3-7-a)$$

Now, we develop the Euler equation of motion for the foot segment w.r.t. $x_f - y_f - z_f$ to

where, \vec{M}_p^f is the moment at the proximal joint of the foot segment expressed w.r.t. $x_f - y_f - z_f$. \vec{d}_f is the vector that connects the center of mass of the foot (COM_f) to the toe and \vec{p}_f is the vector that connects COM_f to the ankle joint both expressed w.r.t. $x_f - y_f - z_f$.

Here, the tip of the toe is chosen such that COM_f relies on the origin of $x_f - y_f - z_f$. Now, we insert the corresponding terms in equation (3-7):

$$\begin{aligned} \vec{M}_p^f = & [GA]_f (\vec{M}_G - \vec{F}_G \times \vec{r}) - [GA]_f \vec{F}_G \times \vec{d}_f \\ & + [GA]_f (\vec{F}_G + m_f \vec{a}_f + m_f g \vec{e}_y) \times \vec{p}_f + [I_f] \vec{\dot{\omega}}_f + \vec{\omega}_f \times \vec{U}_f \end{aligned} \quad (3-8)$$

Since $[GA]_f$ is a proper rotation, \vec{M}_p^f could be transformed into $X - Y - Z$ to obtain the generic equation of the ankle moment as:

$$\begin{aligned} \vec{M}_p^f = & (\vec{M}_G - \vec{F}_G \times \vec{r}) - \vec{F}_G \times [AG]_f \vec{d}_f + (\vec{F}_G + m_f \vec{a}_f + m_f g \vec{e}_y) \times [AG]_f \vec{p}_f \\ & + [AG]_f ([I_f] \vec{\dot{\omega}}_f + \vec{\omega}_f \times \vec{U}_f) \end{aligned} \quad (3-9)$$

where, $[AG]_f = [GA]_f^{-1}$. One should notice that:

$$\vec{F}_G \times L_f \vec{e}_y^f = -\vec{F}_G \times [AG]_f \vec{d}_f + \vec{F}_G \times [AG]_f \vec{p}_f \quad (3-10)$$

TABLE 3-1. Description of the Mathematical Expressions

Parameter	Description	Parameter	Description
K_{ke}	Knee quasi-stiffness in extension stage	θ_{ke}	Knee excursion in extension stage
K_{kf}	Knee quasi-stiffness in flexion stage	θ_{kf}	Knee excursion in flexion stage
K_k	Knee quasi-stiffness in weight acceptance phase	θ_k	Knee excursion in weight acceptance phase
W	Body weight	\bar{U}_f	Angular momentum of foot
V	Gait speed	\bar{U}_s	Angular momentum of shank
H	Body height	$[I_f]$	Matrix of moment of inertia of foot
\bar{M}_c	Ground reaction moment	$[I_s]$	Matrix of moment of inertia of shank
\bar{F}_c	Ground reaction force	\bar{M}_p	Shank proximal moment in global coordinate system (knee moment)
\bar{r}	Vector from toe to center of pressure	\bar{M}_d	Shank distal moment in global coordinate system
L_f	Foot length	\bar{M}'_p	Foot proximal moment in global coordinate system (ankle moment)
L_s	Shank length	\bar{M}'_d	Foot distal moment in global coordinate system
\bar{e}'_f	Unit vector along foot segment	\bar{M}''_p	Shank proximal moment in shank anatomical coordinate system
\bar{e}''_f	Unit vector along shank segment	\bar{M}''_d	Shank distal moment in shank anatomical coordinate system
m_f	Foot mass	\bar{M}'_p	Foot proximal moment in shank anatomical coordinate system
m_s	Shank mass	\bar{M}'_d	Foot distal moment in shank anatomical coordinate system
\bar{a}_f	Foot acceleration	\bar{R}_p	Shank proximal force in global coordinate system
\bar{a}_s	Shank acceleration	\bar{R}_d	Shank distal force in global coordinate system
g	Magnitude of acceleration due to gravity	\bar{R}'_p	Foot proximal force in global coordinate system
L'_p	Distance between center of mass of foot and ankle	\bar{R}'_d	Foot distal force in global coordinate system
L''_p	Distance between center of mass of shank and knee	\bar{R}''_p	Shank proximal force in shank anatomical coordinate system
$[AG]_s$	Transformation matrix from anatomical coordinate frame of shank to global coordinate frame	\bar{R}''_d	Shank distal force in shank anatomical coordinate system
$[GA]_s$	Transformation matrix from global coordinate frame to anatomical coordinate frame of shank	\bar{R}'_p	Foot proximal force in shank anatomical coordinate system
$[AG]_f$	Transformation matrix from anatomical coordinate frame of foot to global coordinate frame	\bar{R}'_d	Foot distal force in shank anatomical coordinate system
$[GA]_f$	Transformation matrix from global coordinate frame to anatomical coordinate frame of foot	$X - Y - Z$	Global coordinate system
$\bar{\omega}_s$	Angular velocity of shank	$x_s - y_s - z_s$	Anatomical coordinate system of shank
$\bar{\omega}_f$	Angular velocity of foot	$x_f - y_f - z_f$	Anatomical coordinate system of foot
$\bar{\omega}'_f$	Angular acceleration of foot	\bar{d}_f	Vector connecting center of mass of foot to toe
COM_s	Center of mass of shank	\bar{p}_f	Vector connecting center of mass of foot to ankle
COM_f	Center of mass of foot	\bar{d}_s	Vector connecting center of mass of shank to ankle
\bar{M}_s	Any moment applied on shank	\bar{p}_s	Vector connecting center of mass of shank to knee
\bar{M}_f	Any moment applied on foot	\bar{F}_s	Any force applied on shank
Fr	Froude number for walking	\bar{F}_f	Any force applied on foot
		\bar{e}_y	Unit vector vertical to the ground and along Y

where, L_f is the length of the foot segment and \bar{e}_Y^f is the unit vector along the y_f -axis of the foot segment expressed w.r.t. Y-axis. Thus, equation (3-9) can be written in the following form:

$$\bar{M}_p^f = \left(\bar{M}_G - \bar{F}_G \times \bar{r} + \bar{F}_G \times L_f \bar{e}_Y^f \right) + \left(m_f \bar{a}_f + m_f g \bar{e}_Y \right) \times L_p^f \bar{e}_Y^f + [AG]_f \left([I_f] \bar{\omega}_f + \bar{\omega}_f \times \bar{U}_f \right) \quad (3-11)$$

where, L_p^f is the distance between COM_f and the ankle.

Next, we derive the proximal moment of the shank segment (i.e. knee moment). We exploit the expressions of the proximal force and moment for the foot segment and use them as the distal force (\bar{R}_D^s) and moment (\bar{M}_D^s) of the shank. In other words w.r.t. $X - Y - Z$ we have:

$$\bar{R}_D^s = \bar{R}_p^f \quad (3-12-a)$$

$$\bar{M}_D^s = \bar{M}_p^f \quad (3-12-b)$$

which can be transformed to $x_s - y_s - z_s$ using the *proper rotation*-matrix of $[GA]_s$:

$$\bar{R}_d^s = [GA]_s \bar{R}_p^f \quad (3-13-a)$$

$$\bar{M}_d^s = [GA]_s \bar{M}_p^f \quad (3-13-b)$$

The proximal reaction force of the shank (\bar{R}_p^s) is obtained from the Newtonian equation of motion w.r.t. $X - Y - Z$, as follows:

$$\sum \bar{F}_s = m_s \bar{a}_s \quad \therefore \bar{R}_p^s = \bar{R}_D^s + m_s \bar{a}_s + m_s g \bar{e}_Y \quad (3-14)$$

where, \bar{F}_s denotes any force that is applied on the shank segment, m_s is the mass and \bar{a}_s is the acceleration of the center of mass (COM_s) for the shank segment. Applying equations (3-4-a) and (3-12-a) in (3-14), we get:

$$\bar{R}_p^s = \bar{F}_G + \left(m_f \bar{a}_f + m_s \bar{a}_s \right) + \left(m_f + m_s \right) g \bar{e}_Y \quad (3-15)$$

which could be transformed to $x_s - y_s - z_s$ as:

$$\bar{R}_p^s = [GA]_s \bar{R}_p^s \quad (3-16)$$

Now, we employ the Euler equation of motion for the shank w.r.t. $x_s - y_s - z_s$ to derive the moment at the proximal joint (i.e. knee). As such:

$$\sum \bar{M}_s = [I_s] \bar{\dot{\omega}}_s + \bar{\omega}_s \times \bar{U}_s \quad (3-17)$$

where, \bar{M}_s denotes any moment that is applied on the shank. $[I_s]$ is the matrix of moment of inertia, $\bar{\omega}_s$ the angular velocity, $\bar{\dot{\omega}}_s$ is the angular acceleration, and \bar{U}_s is the angular momentum for the shank segment. Expanding the left hand side of the above equation results in:

$$\bar{M}_p^s = \bar{M}_d^s - \bar{R}_d^s \times \bar{d}_s + \bar{R}_p^s \times \bar{p}_s + [I_s] \bar{\dot{\omega}}_s + \bar{\omega}_s \times \bar{U}_s \quad (3-18)$$

where, \bar{M}_p^s is the moment at the proximal joint of the shank (i.e. knee moment). \bar{d}_s is the vector connecting the center of mass of the shank (COM_s) to the ankle and \bar{p}_s the vector connecting COM_s to the knee both expressed in $x_s - y_s - z_s$. Inserting the corresponding expression of each term in (3-18) concludes:

$$\begin{aligned} \bar{M}_p^s = & [GA]_s \left\{ \left(\bar{M}_G - \bar{F}_G \times \bar{r} + \bar{F}_G \times L_f \bar{e}_y^f \right) + \left(m_f \bar{a}_f + m_f g \bar{e}_y \right) \times L_p^f \bar{e}_y^f \right. \\ & + [AG]_f \left\{ [I_f] \bar{\dot{\omega}}_f + \bar{\omega}_f \times \bar{U}_f \right\} \left. \right\} - [GA]_s \left(\bar{F}_G + m_f \bar{a}_f + m_f g \bar{e}_y \right) \times \bar{d}_s \\ & + [GA]_s \left(\bar{F}_G + \left(m_f \bar{a}_f + m_s \bar{a}_s \right) + \left(m_f + m_s \right) g \bar{e}_y \right) \times \bar{p}_s + [I_s] \bar{\dot{\omega}}_s + \bar{\omega}_s \times \bar{U}_s \end{aligned} \quad (3-19)$$

The proximal moment of the shank (\bar{M}_p^s) is transformed to $X - Y - Z$ to reach the following expression for the knee moment (\bar{M}_p^s):

$$\begin{aligned} \bar{M}_p^s = & \left\{ \left(\bar{M}_G - \bar{F}_G \times \bar{r} + \bar{F}_G \times L_f \bar{e}_y^f \right) + \left(m_f \bar{a}_f + m_f g \bar{e}_y \right) \times L_p^f \bar{e}_y^f + [AG]_f \left\{ [I_f] \bar{\dot{\omega}}_f + \bar{\omega}_f \times \bar{U}_f \right\} \right\} \\ & - \left(\bar{F}_G + m_f \bar{a}_f + m_f g \bar{e}_y \right) \times [AG]_s \bar{d}_s + \left(\bar{F}_G + \left(m_f \bar{a}_f + m_s \bar{a}_s \right) + \left(m_f + m_s \right) g \bar{e}_y \right) \times [AG]_s \bar{p}_s \\ & + [AG]_s \left([I_s] \bar{\dot{\omega}}_s + \bar{\omega}_s \times \bar{U}_s \right) \end{aligned} \quad (3-20)$$

where, $[AG]_s = [GA]_s^{-1}$. One should notice that:

$$\vec{F}_G \times L_s \vec{e}_Y^s = -\vec{F}_G \times [AG]_s \vec{d}_s + \vec{F}_G \times [AG]_s \vec{p}_s \quad (3-21)$$

where, L_s is the length of the shank segment and \vec{e}_Y^s is a unit vector along y_s -axis of the shank segment expressed w.r.t. $X-Y-Z$. Hence, we obtain the following generic expression for the moment of the *knee* joint:

$$\begin{aligned} \vec{M}_P^s = & \left\{ \vec{M}_G - \vec{F}_G \times (\vec{r} + L_f \vec{e}_Y^f + L_s \vec{e}_Y^s) \right\} + \\ & \left\{ (m_f \vec{a}_f + m_f g \vec{e}_Y^f) \times (L_p^f \vec{e}_Y^f + L_s \vec{e}_Y^s) + (m_s \vec{a}_s + m_s g \vec{e}_Y^s) \times L_p^s \vec{e}_Y^s \right\} + \\ & \left\{ [AG]_s \left([I_s] \vec{\omega}_s + \vec{\omega}_s \times \vec{U}_s \right) + [AG]_f \left([I_f] \vec{\omega}_f + \vec{\omega}_f \times \vec{U}_f \right) \right\} \end{aligned} \quad (3-22)$$

where, L_p^s is the distance between COM_s and the knee.

3.4 Identifying the Model Parameters and Form of Fits

We first simplify the generic equation of the knee moment (3-22) for the instant of maximum flexion in the weight acceptance phase of the gait (Fig. 3-1, point b) and extract the knee moment in the sagittal plane (X - Y). Next, we extract theoretical model-forms by investigating the terms of the equation for the knee moment on the sagittal plane and correlate them with body and gait parameters. To recall, we considered subject body weight (W) and height (H) as the body parameters, and walking speed (V), and magnitude of knee excursion (θ_k) as the gait parameters.

First, we simplify equation (3-22) for the instant of maximum flexion in the weight acceptance phase of the gait (Fig. 3-1, point b). At this instant, the ground reaction force (i.e. the force applied on the foot from the ground, GRF) shows a maximum magnitude for normal walking on level ground. Moreover, since the ground reaction moment (i.e. the moment applied on the foot from the ground) is substantially smaller than the knee moment, we neglect it (i.e. $\vec{M}_G \approx 0$). When the knee is maximally flexed in the stance phase, the support foot and shank segments are

instantaneously nearly stationary (i.e. $\vec{\omega}_s \approx 0$ and $\vec{\omega}_f \approx 0$). At this instant, the support limbs are dramatically loaded to propel the rest of the body. Thus, we assume that the effect of linear and angular acceleration of the support foot and shank is negligible compared to that of the rest of the body (i.e. $m_s \vec{a}_s \approx 0$ and $[I_s] \vec{\dot{\omega}}_s \approx 0$, and $m_f \vec{a}_f \approx 0$ and $[I_f] \vec{\dot{\omega}}_f \approx 0$). We further neglect the effect of the weight of the support limbs (i.e. $m_f \approx 0$ and $m_s \approx 0$). Applying these approximations in equation (3-22) results in the following expression for the knee moment:

$$\vec{M}_P^s = \left\{ -\vec{F}_G \times \left(\vec{r} + L_f \vec{e}_Y^f + L_s \vec{e}_Y^s \right) \right\} + \vec{C}_K \quad (3-23)$$

where, \vec{C}_K reflects the effect of the neglected terms. After our assumptions are applied, the analysis resides in a pseudo-static state which is valid for the instant of maximum moment in stance. We obtain the sagittal-plane component of the knee moment at the instant of maximum moment (point *b* in Fig. 3-1) from equation (3-23) as:

$$M_K^Z \Big|_b = -F_X \left(r_Y + L_f e_{YY}^f + L_s e_{YY}^s \right) - F_Y \left(r_X + L_f e_{YX}^f + L_s e_{YX}^s \right) + C_{KZ} \quad (3-25)$$

where, C_{KZ} is the *Z*-component of \vec{C}_K and $\vec{F}_G = [F_X \quad F_Y \quad F_Z]^T$. One should notice that $\vec{e}_Y^f = [e_{YX}^f \quad e_{YY}^f \quad e_{YZ}^f]^T$, $\vec{e}_Y^s = [e_{YX}^s \quad e_{YY}^s \quad e_{YZ}^s]^T$, and $\vec{r} = [r_X \quad r_Y \quad r_Z]^T$. \vec{e}_Y^f is assumed to be constant because the foot is instantaneously stationary when the knee is maximally flexed during the weight acceptance phase. We assume $\vec{e}_Y^s \approx [\sin \theta_k \quad \cos \theta_k \quad 0]$, provided the leg moves only on the sagittal plane with the knee slightly flexed. Considering the small amount of flexion in normal walking we assume $\vec{e}_Y^s \approx [\theta_k \quad 1 \quad 0]$. Anthropometric relationships imply that L_f and L_s are proportions of H [61]. Also, it has been shown that center of pressure (*COP*) tends to lay underneath the ankle at the instant of maximum flexion in stance [62]. Therefore, r_X and r_Y would be correlated with L_f , and hence with H . Therefore:

$$M_K^Z|_b \approx -F_x p_1 \langle H \rangle - F_y p_2 \langle H\theta, H \rangle + C_{KZ} \quad (3-26)$$

where, we note that in its general case, $p_i \langle x_1, \dots, x_n \rangle$ denotes an arbitrary first-order polynomial of x_i 's. Previous research has shown that the peaks of the normalized GRF (especially the peaks of vertical and anterior-posterior components in the stance phase) are correlated with the gait speed for normal walking on level ground [63]. In other words, at the instant of maximum moment in the weight acceptance phase we have:

$$F_x \approx W p_3 \langle V \rangle \quad (3-27-a)$$

$$F_y \approx W p_4 \langle V \rangle \quad (3-27-b)$$

Applying equations (3-27-a) and (3-27-b) in equation (3-26) results in:

$$M_K^Z|_b \approx W p_5 \langle VH, V, VH\theta, H, H\theta \rangle + C_{KZ} \quad (3-28)$$

Assuming the knee behaves nearly linearly in the weight acceptance phase of the gait [40]:

$$M_K^Z|_b \approx K_k \theta_k \approx K_{kf} \theta_{kf} \approx K_{ke} \theta_{ke} \quad (3-29)$$

Combining (3-53) and (3-54) constitutes the following analytical forms for the quasi-stiffness of the knee in the weight acceptance phase, and its flexion and extension stages:

$$K_k \approx p_6 \langle WVH / \theta_k, WV / \theta_k, WH / \theta_k, W / \theta_k, 1 / \theta_k, WH, WVH \rangle \quad (3-30-a)$$

$$K_{kf} \approx p_7 \langle WVH / \theta_{kf}, WV / \theta_{kf}, WH / \theta_{kf}, W / \theta_{kf}, 1 / \theta_{kf}, WH, WVH \rangle \quad (3-30-b)$$

$$K_{ke} \approx p_8 \langle WVH / \theta_{ke}, WV / \theta_{ke}, WH / \theta_{ke}, W / \theta_{ke}, 1 / \theta_{ke}, WH, WVH \rangle \quad (3-30-c)$$

These equations suggest that, in its most general form, K_k could be modeled by a first order polynomial of WVH / θ_k , WV / θ_k , WH / θ_k , W / θ_k , $1 / \theta_k$, WH , and WVH (and a function of only V , θ_k , H , and W); and similarly for K_{kf} and K_{ke} .

3.5 Experimental Protocols

Researchers from two different labs provided us with the knee moment and angle data, and the collection procedures for 136 trials across 14 healthy male and female adults with a reasonably wide range of mass (46-94.0 kg) and height (1.43-1.87 m). The trials included a wide range of gait speeds for the subjects (0.75-2.63 m/s). Data was compiled using:

1) Nine subjects (subjects 1 to 9 in Table 3-2) at Human PoWeR Lab, NC State University walking on a treadmill, as detailed elsewhere [21].

2) Five subjects (subjects 10 to 14 in Table 3-2) at Biomechanics Lab, East Carolina University walking on level ground. The general procedures used to obtain the ground reaction force, sagittal plane knee joint angular position and torque are described elsewhere [34]. We detail here the specific procedures relevant to the purpose of this study. All participants read and signed an informed consent form approved by the University Institutional Review Board at East Carolina University. Using a 15 m walkway, force platform (AMTI, Watertown, MA) and eight camera motion capture system (Qualisys, Gothenberg, Sweden), three dimensional ground reaction force and linear position data describing the right lower extremity and pelvis were obtained from each participant during 20 walking trials of different velocities ranging from 1.01 to 2.63 m/s. Each participant was initially tested at a self-selected, moderate walking speed the mean of which was 1.63 ± 0.03 m/s. Subsequently, the 19 remaining trials per participant were collected in an approximately random order of walking velocities. Participants were instructed to walk at various speeds with instructions such as, “walk at a moderately fast pace,” “walk at a very slow pace,” and “walk at your fastest pace.” The mean walking velocity for all trials was 1.77 ± 0.36 m/s. All participants had similar minimum and maximum walking velocities and therefore similar ranges of walking velocities. Additionally, the 20 walking velocities for each participant were moderately evenly distributed through the range of velocities from slowest to fastest velocities. Qualisys Track Manager and Visual 3D software (C-Motion, Gaithersburg, MD) were used to calculate the knee joint angular position and torque through the stance phase of walking in

each trial from the linear position and ground reaction force data. The subject consents, collection protocols and data analysis for subject groups 1 and 2 are detailed elsewhere [21,34].

3.6 Data Extraction and Statistical Analysis

For each subject, we plotted the knee moment and angle data against each other, (see Fig. 3-1-bottom for an example gait cycle). The onset of the flexion stage was identified as the point of minimum moment after the heel contacts the ground (point a), the end of flexion stage as the point of maximum moment (point b), and the end of extension stage as the point of minimum moment before the toe leaves the ground (point c). In other words, the flexion stage is composed of the data points between a and b ; and the extension stage between b and c . Then we applied linear fits between the angle and moment data points in flexion and extension stages (as described in the previous section). The slopes of the fits were correspondingly reported as K_{kf} and K_{ke} , and the average was calculated as K_k . The knee angle at point a was subtracted from the angle at point b to obtain θ_{kf} ; similarly for θ_{ke} using points b and c . We averaged θ_{kf} and θ_{ke} to obtain θ_k .

The inverse dynamics analysis of the previous section proposed three sets of collinear predictors for the models of K_{kf} , K_{ke} , and K_k . Since, the purpose of this study was to constitute predictive models for K_{kf} , K_{ke} , and K_k that are composed of these collinear predictors, we cross-validated the models structures. We removed the gait cycles of one subject at a time (stratified cross-validation) from the data pool and conducted Partial Least Square (PLS) analysis to evaluate the predictability of the predictors (i.e. parameters suggested in the previous section). For the sake of completeness, we have reported the optimal number of components that could best describe the response variables (i.e. quasi-stiffnesses) and result in minimal PRESS statistics,

TABLE 3-2. Details on Subjects and Experimental Trials used for Regression Fits

Subject	Gender	#Trial	<i>W</i>	<i>H</i>	[<i>V_{min}</i> , <i>V_{max}</i>]
1‡	M	4	92.3	1.86	[0.75,2.00]
2‡	M	4	68.4	1.70	[0.75,2.00]
3‡	M	4	65.6	1.65	[0.75,2.00]
4‡	M	4	94.0	1.86	[0.75,2.00]
5‡	M	4	68.1	1.72	[0.75,2.00]
6‡	F	4	57.7	1.43	[0.75,2.00]
7‡	F	4	63.1	1.45	[0.75,2.00]
8‡	F	4	65.7	1.75	[0.75,2.00]
9‡	F	4	75.9	1.80	[0.75,2.00]
10†	M	20	85.7	1.74	[1.26,2.43]
11†	M	20	79.2	1.82	[1.38,2.25]
12†	M	20	62.1	1.64	[1.04,2.29]
13†	M	20	62.0	1.62	[1.01,2.44]
14†	M	20	75.1	1.77	[1.30,2.63]
		Mean	72.5	1.70	1.68
		SD	11.1	0.42	0.42

W: Body weight (kg), and *H*: Body height (m).

V_{min} and *V_{max}*: Minimum and maximum gait speed (m/s)

‡: Data collected at Human PoWeR Lab, NC State University [21]

†: Data collected at Biomechanics Lab, East Carolina University [34,35]

in Table 3-4-A [64-66]. Next, based on the identified factors of equations (3-30-a to c), we evaluated these combinations for the 136 gait trials and respectively applied linear regression between them and the values of K_{kf} , K_{ke} , and K_k . We used least square regression because W and H would be known for a specific subject, and V and excursion of the knee are also assumed to be available through measurements taken from corresponding sensors on-board the user or a wearable device. In each case, stepwise, non-significant terms ($p > 0.05$) of the regressed polynomial were iteratively removed until we reached *general-form statistical models* that best explain the knee quasi-stiffnesses and that only include significant parameters.

3.7 General-Form Statistical Models

The knee demonstrated approximately linear behavior in both flexion and extension stages of stance for nearly all subjects across all gait speeds. Linear fits (similar to that shown in Fig. 3-1-bottom) demonstrated an average R^2 of 93% in the flexion stage, and 94% in the extension (Table 3-3). For each subject, the minimum and maximum values of the knee joint quasi-stiffness (K_k) and the knee joint excursion during stance (θ_k) as well as the average values of R^2 are reported in Table 3-3. Knee quasi-stiffnesses ranged from a minimum value of 81 Nm / rad for subject 7 in the extension phase of walking at 1.25 m / s to a maximum value of 745 Nm / rad for subject 14 in the flexion stage of walking at 2.43 m / s for the gait trials examined here. The average values of θ_{kf} , θ_{ke} , and θ_k were respectively calculated as 16.7° , 16.3° , and 16.5° .

As Table 3-4-A outlines, the cross-validation analyses suggest 7, 3, and 2 components that can optimally describe K_{kf} , K_{ke} , and K_k (resulting in minimal PRESS statistics). Table 3-4-A also

TABLE 3-3. Knee Quasi-Stiffnesses in the Weight Acceptance Phase

Subject	$[K_{kf}^{min}, K_{kf}^{max}]$	$[K_{ke}^{min}, K_{ke}^{max}]$	$[K_{min}, K_{max}]$	$[\theta_{min}, \theta_{max}]$	\bar{R}_{kf}^2	\bar{R}_{ke}^2	Fr when K_{kf} K_{ke}
1	[284,376]	[283,297]	[330,390]	[6,22]	90	96	0.174
2	[141,225]	[223,255]	[186,233]	[12,25]	89	95	0.191
3	[155,266]	[221,261]	[198,244]	[11,28]	90	94	0.197
4	[326,478]	[361,556]	[344,517]	[6,17]	92	95	0.174
5	[182,255]	[291,582]	[273,382]	[7,22]	91	84	0.189
6	[145,255]	[197,291]	[187,255]	[11,19]	91	97	0.227
7	[114,185]	[81,308]	[98,231]	[9,24]	87	95	0.224
8	[161,456]	[237,739]	[278,450]	[6,17]	93	94	0.185
9	[237,393]	[292,378]	[291,343]	[10,22]	93	94	0.180
10	[236,569]	[244,342]	[279,422]	[13,20]	99	96	0.254
11	[227,414]	[258,331]	[256,343]	[16,23]	98	98	0.246
12	[119,379]	[144,278]	[155,269]	[6,17]	98	96	0.234
13	[163,351]	[143,188]	[158,263]	[11,24]	99	95	0.262
14	[248,745]	[210,384]	[260,565]	[12,23]	99	96	0.247
Mean	304	263	284	16.5	93	94	0.213
SD	114	91	78	4.4	5	4	0.032

K_{kf}^{min} and K_{kf}^{max} : Minimum and maximum knee quasi-stiffness in flexion stage (Nm/rad)

K_{ke}^{min} and K_{ke}^{max} : Minimum and maximum knee quasi-stiffness in extension stage (Nm/rad)

K_{min} and K_{max} : Minimum and maximum knee quasi-stiffness in weight-acceptance phase (Nm/rad)

θ_{min} and θ_{max} : Minimum and maximum knee excursion in weight-acceptance phase (deg)

\bar{R}_{kf}^2 : Average R^2 of the linear fit on moment-angle curve in flexion stage

\bar{R}_{ke}^2 : Average R^2 of the linear fit on moment-angle curve in extension stage

Fr : Froude number

shows the values of R^2 and predicted R^2 for the PLS analysis. The PLS analysis reconfirms that the predictors that were identified through inverse dynamics analyses can constitute predicting models for K_{kf} , K_{ke} , and K_k . Next, the general-form models were obtained through Least Square Regression as listed in Table 3-4-A. We included all the components that the inverse dynamics analysis of the previous section suggested and removed the components that were not statistically significant. Table 3-4-A lists the general-form models of K_{kf} , K_{ke} , and K_k . The general-form models are listed in Table 3-4-A. Only 1, 5, and 4 data points from 136 trials exhibited outlier behavior in the regression analysis for K_{kf} , K_{ke} , and K_k , respectively. The values of R^2 and p were ($R^2 = 88.2\%$, $p < 0.001$) for K_{kf} , ($R^2 = 86.8\%$, $p < 0.001$) for K_{ke} , and ($R^2 = 80.1\%$, $p < 0.001$) for K_k , as reported in Table 3-4-A. The regression analyses showed p -values of < 0.002 for all of the coefficients of the polynomials, with the exception of 0.119 for the intercept of the model polynomial for K_k (3-30-a) and 0.026 for the coefficient of WH in the model polynomial for K_{kf} (3-30-b), implying that the intercept in (3-30-a) is not significantly greater than zero. The residuals of all three fits were normally distributed and no notable correlation with the order of data collection and magnitude of the quasi-stiffness was observed, except we found slightly greater values for the residuals of the data of subjects 10 to 14 collected at East Carolina University.

Fig. 3-3 shows the predictions of general-form models for one of the subjects with $W = 85.7Kg$ and $H = 1.74m$ close to the average adults. In this figure, both experimental data, and results of the general-form models are displayed. We observe that K_{kf} increases as the gait speed increases; whereas, K_{ke} displays a moderate decrease. We also observe that K_{kf} and K_{ke}

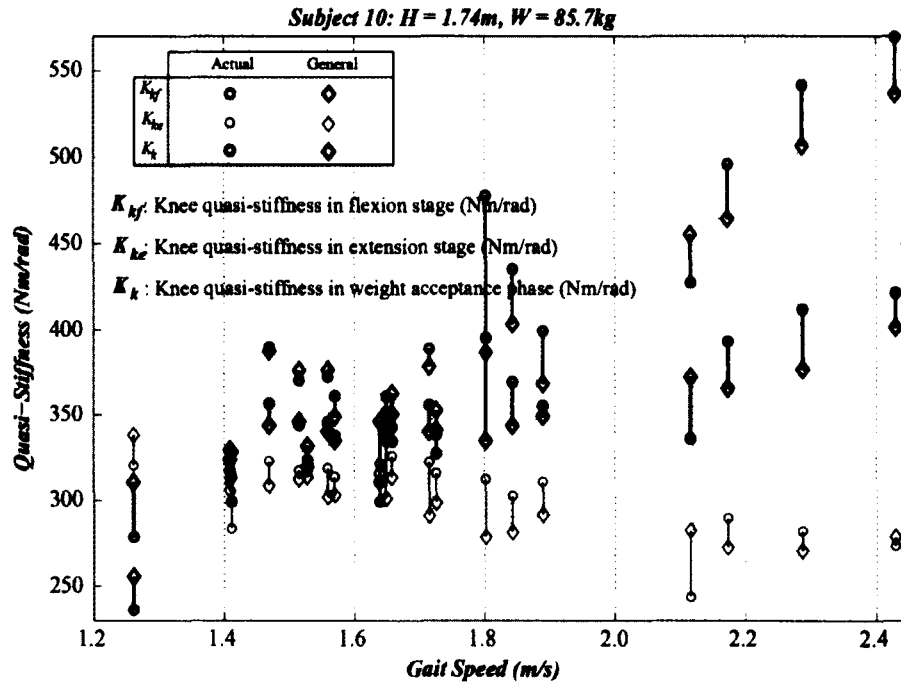


Figure 3-3. Knee quasi-stiffness for subject 10, as an example, in flexion (dark gray) and extension (light gray) stages, and weight acceptance phase (black) plotted against the gait speed. The circles indicate the experimental values and the diamonds are the predictions of the general-form models.

are nearly identical at $V = 1.46 \text{ m/s}$, which corresponds to $Fr \sim 0.254$. We observed similar phenomenon for all of the subjects. Indeed, K_{kf} and K_{ke} tend to be closest at an average gait speed of $\bar{V} = 1.31 \text{ m/s}$ with standard deviation of $\sigma_V = 0.09 \text{ m/s}$ across the subjects, which corresponds to an average Froude number of $\bar{Fr} = 0.213$ and standard deviation of $\sigma_{Fr} = 0.032$. Table 3-3 lists the values of Fr for each subject at which K_{kf} and K_{ke} are closest.

3.8 Simplification of Models for Preferred Gait Speed

To obtain more simplified models that only include the body stature (W and H), we simplified the general-form models for the preferred gait speed. Since the subjects had different body sizes, we used a non-dimensional speed (Froude number: $Fr = V^2 / gl$, where l is the leg length and g is the acceleration due to gravity) instead of the actual gait speed. $Fr = 0.25$ is an acceptable estimate of the preferred gait speed for subjects with different body size [67-70]. Assuming an anthropometric relationship of $l = 0.491 H$ [61], the optimal or “preferred” gait speed was approximated as:

$$V_{opt} = 1.097\sqrt{H} \quad (3-31)$$

To exclude the knee excursion from the general-form models, we merely substituted the mean values over the data set (i.e. $\bar{\theta}_{kf} = 16.7^\circ$, $\bar{\theta}_{ke} = 16.3^\circ$, and $\bar{\theta}_k = 16.5^\circ$) into the general-form models. The reason is twofold: a. the general-form models did not show high dependence on the knee excursion, and b. the knee excursion did not demonstrate high variability around the optimal gait speed of $Fr = 0.25$ ($\sigma_{\theta_{kf}} = 3.7^\circ$, $\sigma_{\theta_{ke}} = 4.1^\circ$, $\sigma_{\theta_k} = 3.5^\circ$). We then applied equation (3-31) and the average values in the general-form expressions to obtain a series of *stature-based models* intended to predict the quasi-stiffnesses of the knee at the preferred gait speed only as functions of H and W .

V(m/s)	1.25	1.25	1.25	1.25	1.25	1.25	1.25	1.25	1.25	1.46	1.47	1.36	1.43	1.45
θ_k (deg)	22	25	27	17	18	19	21	17	22	13	16	8	18	14
H(m)	1.86	1.70	1.65	1.86	1.72	1.43	1.45	1.75	1.80	1.74	1.82	1.64	1.62	1.77
W(kg)	92.3	68.4	65.6	94.0	68.1	57.7	63.1	65.7	75.9	85.7	79.2	62.1	62.0	75.1

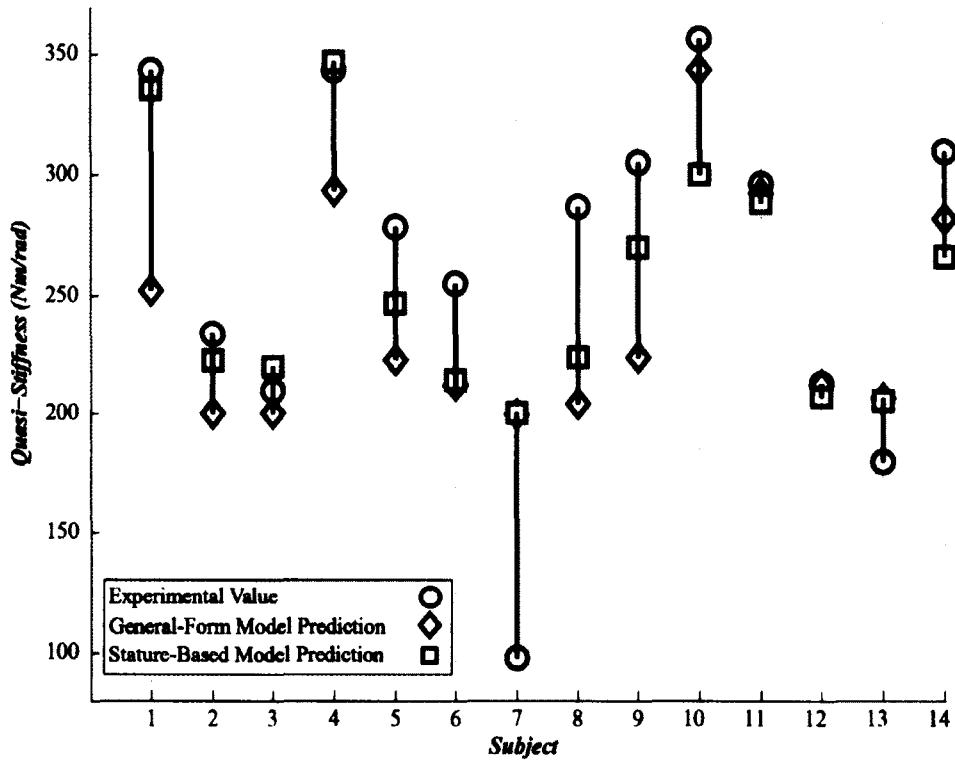


Figure 3-4. The knee quasi-stiffness in the weight acceptance phase of the gait. The experimental values are shown by circles, and the predictions of the general-form model by diamonds with average error of 45 Nm/rad (14%), and the stature-based models by squares with average error of 30 Nm/rad (9%) for the optimal gait speed.

TABLE 3-4-A. General-Form Models to Predict the Quasi-Stiffnesses of the Knee Joint in the Weight Acceptance Phase for Normal Walking

Phase	Model	Unit	Error	PLS-CV #Comp.	PLS-CV R ²	PLS-CV Predicted R ²	Fit Quality
Flexion	$K_{kf} = 437 - 2.78WH + \{95.9VHW - 120.8VW - 85.1WH + 228.0W - 7842\} / \theta_{kf}$	$\frac{Nm}{rad}$	10%	7	88.3%	75.1%	$R^2=88.2\%$ $p<0.001$
Extension	$K_{ke} = 56 + 1.05WH + \{87.8VHW - 150.0VW - 63.5WH + 119.8W\} / \theta_{ke}$	$\frac{Nm}{rad}$	10%	3	83.2%	73.6%	$R^2=86.8\%$ $p<0.001$
Stance	$K_k = 264 - \{1.37 - 0.52V\}WH + \{69.8VHW - 112.8VW - 73.6WH + 192.0W - 4458\} / \theta_k$	$\frac{Nm}{rad}$	11%	2	75.0%	59.8%	$R^2=80.1\%$ $p<0.001$

TABLE 3-4-B. Stature-Based Models to Predict the Quasi-Stiffness of the Knee Joint in Stance for Normal Walking at Optimal Gait Speed

Phase	Model	Unit	Error	Conditions
Flexion	$K_{kf} = 6.30W\sqrt{H^3} - 7.93W\sqrt{H} - 7.88WH + 13.65W - 33$	$\frac{Nm}{rad}$	11%	$\theta_{kf} = 16.7^\circ$ and $V = 1.097\sqrt{H}$
Extension	$K_{ke} = 5.91W\sqrt{H^3} - 10.09W\sqrt{H} - 2.85WH + 7.35W + 56$	$\frac{Nm}{rad}$	14%	$\theta_{ke} = 16.3^\circ$ and $V = 1.097\sqrt{H}$
Stance	$K_k = 5.21W\sqrt{H^3} - 7.50W\sqrt{H} - 5.83WH + 11.64W - 6$	$\frac{Nm}{rad}$	9%	$\theta_k = 16.5^\circ$ and $V = 1.097\sqrt{H}$

TABLE 3-4-C. Average Error Values for Different Knee Models

Parameter	General-Form	Stature-Based	Average Values
K_{kf}	10%	11%	32%
K_{ke}	10%	14%	27%
K_k	11%	9%	24%

- W : Weight (kg), H : Height (m), V : Gait Speed (m/s), and θ 's: Joint excursions (deg)

The stature-based models are reported in Table 3-4-B. Since we do not know the “true” optimal gait speed for each subject, we cannot report R^2 for the models predictions. Instead, we calculated Fr for each gait trial and chose the trial with the speed that is closest to 0.25 for each subject. These trials are shown in Fig. 3-4. Subject 7 exhibited outlier behavior of some sort. Our analysis demonstrates that the simplest (stature-based) models predict K_{kf} , K_{ke} , and K_k with an average errors of 11%, 14%, and 9% excluding the outlier number 7 (as reported in Table 3-4-B), and an average error of 15%, 19%, and 16% including it.

3.9 Conclusions and Future Work

In this chapter we established statistical models that can estimate the quasi-stiffnesses of the knee during the weight acceptance phase of human walking. To obtain the models, we extracted the generic equation of the knee moment through an inverse dynamics analysis and simplified it for the weight acceptance. The simplified equation emphasizes that the quasi-stiffnesses of the knee joint is linearly correlated with combinations of both gait and body parameters in the most general form. Using a relatively wide experimental data set and least square linear regression, we constituted expressions that statistically best describe the quasi-stiffnesses of the knee joint in the weight acceptance phase. In addition, we developed more simplified and subject-specific (i.e. stature-based) models that are independent of the knee joint excursion and gait speed. Both of these model frameworks might be used to dynamically adjust (general-form) or optimally size (stature-based) the mechanical components of wearable assistive devices.

We found high values of R^2 for linear curve fits to the moment-angle relationship at the knee in both the flexion and extension stages (as shown in Table 3-3) that are in good agreement with previous results [39,40]. We observed that the knee exhibits identical quasi-stiffness in the flexion and extension stages (*spring-type behavior*) at the non-dimensional gait speed of $Fr = 0.213$. At other gait speeds, the knee still exhibits linear behavior (more compliant at slow

speeds than at fast speeds) in both flexion and extension stages but with different equilibrium angles, which implies non-zero mechanical energy expenditure (the trend of mechanical work change vs. gait speed is shown elsewhere [40]). This finding is in accordance with the results of other researchers who showed that the rate of energy recovery is highest when the subject is walking with the preferred gait speed [67,71].

From a design point of view, our results suggest that a device (including orthoses, exoskeletons, prostheses, and biped robots) can approximate the behavior of the human knee by utilizing a spring with stiffness equal to the quasi-stiffness of the knee at the preferred gait speed. For other gait speeds, the stiffness of the device might ideally be tuned based on the equations presented in Table 3-4-A. For this purpose, the device would in a real-time mode measure the gait speed (e.g. using a GPS), knee excursion (e.g. using a goniometer), and weight. However, since realization of a variable stiffness mechanism is difficult to achieve, the net quasi-stiffness of the weight acceptance phase (K_k) might be a viable alternative for the spring constant of the envisioned device. As such, the knee might be approximately modeled by a single torsional spring with stiffness equal to the mean of the stiffness of the flexion and extension stages at the preferred gait speed of $Fr = 0.25$. This is a reasonable choice for two reasons: 1) humans prefer to walk with a speed that is dictated by their body size [67-70], and 2) K_{kf} and K_{ke} tend to be identical at the preferred gait speed and deviate at lower and higher speeds. This reemphasizes the results of our previous work [40] where we showed that the stiffness, angle of engagement, and amount of rotation of the device joint should be deliberately chosen based on the gait parameters.

Recently, researchers in the field of prosthetics have moved toward quasi-passive systems and implemented impedance control methods in their designs [11,72-74]. In most design application, the kinetic and kinematic data for the target users are not available. However, sizing orthoses and prostheses requires *a priori* knowledge of the knee quasi-stiffness variability for the users. To size the stiffness of the prosthetic and orthotic devices, the designers utilize the average quasi-

stiffness extracted from the kinetic and kinematic data of sample healthy subjects [11,13,25,73,75]. The stiffness that designers use range from $\sim 50 \text{ Nm/rad}$ to $\sim 430 \text{ Nm/rad}$, depending on the sample population that the designers have chosen and the tuning process [11,13,73]. The sample population is usually composed of individuals with weight, height, and preferred gait speed that are not necessarily representatives of the target user.

To examine the differences between a model that is based on the average data and the models developed here, we found the average values of K_{kf} , K_{ke} , and K_k for the gait data utilized in our study and examined the error between the average quasi-stiffnesses and the true subject-specific quasi-stiffnesses. Table 3-4-C compares the average error associated with the general-form models, stature-based models, and a model that merely uses the average values of K_{kf} , K_{ke} , and K_k (as reported in Table 3-3). The results show much larger errors when the average values are utilized than with our models. Therefore, we hypothesize that selection of the device stiffness based on the models presented here would result in a more natural and user/gait-adaptable performance for the knee orthoses and prostheses. All together, the models developed in this study may help researchers and clinicians tune the stiffness of knee orthoses and prostheses according to the body size and gait speed of the user, and do so without requiring to perform additional subject-specific gait analyses.

Applications of the models presented in this study are not restricted to the field of medical orthoses and prostheses. These models could also be used for the design of knee exoskeletons that are meant to augment the performance of a healthy knee. Researchers have proposed a range of sophistication in the design of exoskeletons from quasi-passive to fully active systems [3,4,6]. Our findings suggest that passive components (i.e. springs) could be further exploited in the design of these devices; provided that the passive components are properly tuned for the gait and user. In fact, the design models of Table 3-4-B suggest that the stiffness of an assistive device should ideally be adapted based on the weight and height of the subject.

Limitations: Our study had a number of methodological limitations worth addressing. Our goal was to compile a ‘large comprehensive data set’ to capture the variation in mechanical behavior of the knee joint during walking across subject size and gait speed. Despite this goal, we were only able to include a relatively modest number of gait trials (i.e. 136 gait trials across 14 adults). Therefore, our results represent a ‘first effort’ that should be added to using more and more data over time in order to gain more and more confidence in our model estimates. We caution that our results should only be generalized to the range of weight, height, and gait speed that the examined subjects represent and only to the level that the statistical significance supports.

A second potential limitation to our approach was that our experimental analyses extracted gait parameters independent of gender and whether the inverse dynamics data was acquired on a treadmill or during over ground walking. In addition, we included data from three different gait laboratories in an attempt to include the widest range of subject sizes and gait speeds possible. Although, in theory, a more comprehensive data set should be better able to capture the behavior over a wider range of humans, differences in gender and/or equipment and measurement protocols between labs could introduce variability not by factors we included in our models. To address this possibility, we examined the correlation between the residuals from the model fits and (1) the gender of the subjects, (2) the location of the laboratory data collection, and (3) whether data was acquired on a treadmill or overground. We found that although the data from East Carolina University demonstrated slightly higher residuals in the model fits than the other locations; the data from males versus females and treadmill versus overground walking showed no differences in the residuals of their model fits. Thus we felt confident that, as desired, the factors included in our model sufficiently capture variability due to subjects’ height, weight and walking speed rather than other potential factors. As mentioned earlier, ideally future studies should aim to generate highly controlled data sets from a single laboratory on many more individuals spanning larger ranges of body size and including equal numbers of males and females to gain additional confidence in the statistical estimates presented in this study.

A third limitation was that we had to apply several simplification steps in order to reduce detailed inverse dynamics equations for the knee joint moment to obtain the minimal forms for the relationships describing the knee quasi-stiffnesses in the sagittal plane as a function of stature and speed. These simplifications likely introduced small errors worth noting. For example, the eliminated terms of the generic equations for the knee moment could have introduced additional linear and non-linear predictors other than what equations (3-30-a to c) suggest. To check whether this was the case, we investigated additional potential linear forms and predictors capable of capturing the effect of the eliminated terms of the generic equation of the knee moment, and found that these additions were insignificant and resulted in no notable improvement in the models in terms of R^2 values and magnitude of residuals.

Finally, we only investigated the behavior of the knee joint during the weight acceptance phase of normal walking on level ground. We chose this period because it is when the sagittal plane moment reaches its highest peak value and exhibits nearly linear loading/unloading behavior (i.e. 'spring-like' mechanics). This phase is also the time during the stride when passive spring-loaded assistive devices would likely be most effective. Future work could extend this approach to characterize joint quasi-stiffnesses during additional locomotion behaviors including running and walking on rough terrain, sloped ground, with load carriage. It should also be possible to reformulate the generic inverse dynamics equation for different gait phases and to estimate additional gait parameters (e.g. the knee joint net work). Using similar statistical approaches to those presented here, it would also be interesting to characterize other lower extremity joints mechanics and in other clinical populations (e.g. pediatric cerebral palsy, spinal cord injury, stroke, and aging) [41,42,53,76].

Design Implications: The findings of this research suggest that designers could employ more passive components (i.e. springs) in the design of lower extremity and particularly knee exoskeletons intended to reduce biological muscle forces during walking. In both passive and active implementations of an exoskeleton, the stiffness of the spring or impedance of the motor

acting in parallel with the user's muscles will likely significantly impact the performance of the device. We expect that exoskeletons with joint stiffness selected according to the user's height and weight could help improve the performance of these devices for subjects walking on level ground. Along these lines, we have taken effort to formulate statistical models to characterizing joints quasi-stiffnesses during walking as a function of a person's height and weight across walking speed. Our models have different levels of sophistication: the general-form models can estimate the quasi-stiffnesses over a wide range of gait speeds, and the simpler stature-based models can provide estimates near the preferred gait speed only. We expect that the models developed in this study will provide a reference for designers and clinicians to size the springs of knee exoskeletons without requiring additional subject-specific gait analyses. Future studies should address the practical challenges of applying these models in the design and development of knee exoskeletons for use in both healthy and clinical populations as well as during locomotion tasks other than walking on level ground (e.g. up and downhill, with load carriage). Apart from the field of lower-limb exoskeletons, these models could also be used to improve spring-based modeling and simulations of walking, and the design of bipedal robots.

REFERENCES

1. McGeer T (1990) Passive walking with knees. Proceedings of the IEEE International Conference on Robotics and Automation. Cincinnati, USA. pp. 1640-1645.
2. Collins S, Ruina A, Tedrake R, Wisse M (2005) Efficient bipedal robots based on passive-dynamic walkers. *Science* 307: 1082-1085.
3. Zoss A, Kazerooni H, Chu A (2006) Biomechanical design of the Berkeley lower extremity exoskeleton (BLEEX). *IEEE/ASME Transactions on Mechatronics* 11: 128-138.
4. Walsh C, Paluska D, Pasch K, Grand W, Valiente A, et al. (2006) Development of a lightweight, underactuated exoskeleton for load-carrying augmentation. Proceedings of IEEE International Conference on Robotics and Automation (ICRA). Orlando, USA. pp. 3485-3491.

5. Ferris D, Lewis C (2009) Robotic lower limb exoskeletons using proportional myoelectric control. Proceedings of Annual International Conference of the IEEE Engineering in Medicine and Biology Society (EMBC). Minneapolis, USA. pp. 2119-2124.
6. Dollar A, Herr H (2008) Lower extremity exoskeletons and active orthoses: challenges and state-of-the-art. IEEE Transactions on Robotics 24: 144-158.
7. Sawicki G, Lewis C, Ferris D (2009) It pays to have a spring in your step. Exercise and Sport Sciences Reviews 37: 130-138.
8. Gordon K, Ferris D (2007) Learning to walk with a robotic ankle exoskeleton. Journal of Biomechanics 40: 2636-2644.
9. Sawicki G, Domingo A, Ferris D (2006) The effects of powered ankle-foot orthoses on joint kinematics and muscle activation during walking in individuals with incomplete spinal cord injury. Journal of Neuroengineering and Rehabilitation 3.
10. Wiggin M, Sawicki G, Collins S (2011) An exoskeleton using controlled energy storage and release to aid ankle propulsion. Proceedings of IEEE International Conference on Rehabilitation Robotics (ICORR). Zurich, Switzerland.
11. Markowitz J, Krishnaswamy P, Eilenberg M, Endo K, Barnhart C, et al. (2011) Speed adaptation in a powered transtibial prosthesis controlled with a neuromuscular model. Philosophical Transactions of the Royal Society B-Biological Sciences 366: 1621-1631.
12. Eilenberg M, Geyer H, Herr H (2010) Control of a powered ankle-foot prosthesis based on a neuromuscular model. IEEE Transactions on Neural Systems and Rehabilitation Engineering 18: 164-173.
13. Sup F, Bohara A, Goldfarb M (2008) Design and control of a powered transfemoral prosthesis. International Journal of Robotics Research 27: 263-273.
14. Hitt J, Sugar T, Holgate M, Bellman R, Hollander K (2009) Robotic transtibial prosthesis with biomechanical energy regeneration. Industrial Robot-an International Journal 36: 441-447.
15. Geyer H, Herr H (2010) A muscle-reflex model that encodes principles of legged mechanics produces human walking dynamics and muscle activities. IEEE Transactions on Neural Systems and Rehabilitation Engineering 18: 263-273.

16. Endo K, Herr H (2009) A model of muscle-tendon function in human walking. Proceedings of 2009 IEEE International Conference on Robotics and Automation (ICRA). Kobe, Japan. pp. 2790-2796.
17. Geyer H, Seyfarth A, Blickhan R (2006) Compliant leg behaviour explains basic dynamics of walking and running. Proceedings of the Royal Society B-Biological Sciences 273: 2861-2867.
18. Rose J, Gamble J (2006) Human Walking. Philadelphia, PA: Williams & Wilkins.
19. Winter D (1991) The Biomechanics and Motor Control of Human Gait : Normal, Elderly and Pathological. Waterloo, Ont.: University of Waterloo Press. 143 p.
20. DeVita P (1994) The selection of a standard convention for analyzing gait data-based on the analysis of relevant biomechanical factors. Journal of Biomechanics 27: 501-508.
21. Farris D, Sawicki G (2011) The mechanics and energetics of human walking and running: A joint level perspective. Journal of The Royal Society Interface 9: 110-118.
22. Kuo A (2002) Energetics of actively powered locomotion using the simplest walking model. Transactions of the ASME Journal of Biomechanical Engineering 124: 113-120.
23. Dean J, Kuo A (2009) Elastic coupling of limb joints enables faster bipedal walking. Journal of the Royal Society Interface 6: 561-573.
24. Srinivasan M, Ruina A (2006) Computer optimization of a minimal biped model discovers walking and running. Nature 439: 72-75.
25. Endo K, Paluska D, Herr H (2006) A quasi-passive model of human leg function in level-ground walking. Proceedings of IEEE/RSJ International Conference on Intelligent Robots and Systems (IROS). Beijing, China. pp. 4935-4939.
26. Farley C, Gonzalez O (1996) Leg stiffness and stride frequency in human running. Journal of Biomechanics 29: 181-186.
27. Alexander R (1992) A model of bipedal locomotion on compliant legs. Philosophical Transactions of the Royal Society of London Series B-Biological Sciences 338: 189-198.
28. Taga G (1995) A model of the neuro-musculo-skeletal system for human locomotion.1. emergence of basic gait. Biological Cybernetics 73: 97-111.

29. Mochon S, McMahon T (1980) Ballistic walking - an improved model. *Mathematical Biosciences* 52: 241-260.
30. Duan X, Allen R, Sun J (1997) A stiffness-varying model of human gait. *Medical Engineering & Physics* 19: 518-524.
31. Weiss P, Kearney R, Hunter I (1986) Position dependence of ankle joint dynamics: 1. passive mechanics. *Journal of Biomechanics* 19: 727-735.
32. Weiss P, Kearney R, Hunter I (1986) Position dependence of ankle joint dynamics: 2. active mechanics. *Journal of Biomechanics* 19: 737-751.
33. Silder A, Heiderscheit B, Thelen D (2008) Active and passive contributions to joint kinetics during walking in older adults. *Journal of Biomechanics* 41: 1520-1527.
34. Hortobágyi T, Herring C, Pories W, Rider P, DeVita P (2011) Massive weight loss-induced mechanical plasticity in obese gait. *Journal of Applied Physiology* 111: 1391-1399.
35. Shamaei K, Cenciari M, Dollar A (2011) On the mechanics of the ankle in the stance phase of the gait. *Proceedings of the IEEE Annual International Conference of Engineering in Medicine and Biology Society (EMBC)*. Boston, USA. pp. 8135-8140.
36. Farley C, Houdijk H, Van Strien C, Louie M (1998) Mechanism of leg stiffness adjustment for hopping on surfaces of different stiffnesses. *Journal of Applied Physiology* 85: 1044-1055.
37. Smidt G (1973) Biomechanical analysis of knee flexion and extension. *Journal of Biomechanics* 6: 79-92.
38. Edwards W (2007) Effect of joint stiffness on standing stability. *Gait & Posture* 25: 432-439.
39. Frigo C, Crenna P, Jensen L (1996) Moment-angle relationship at lower limb joints during human walking at different velocities. *Journal of Electromyography and Kinesiology* 6: 177-190.
40. Shamaei K, Dollar A. On the mechanics of the knee during the stance phase of the gait; 2011; Zurich, Switzerland.
41. Shamaei K, Sawicki G, Dollar A (2013) Estimation of quasi-stiffness and propulsive work of the human ankle in the stance phase of walking. *PLoS ONE* 8: e59935.

42. Shamaei K, Sawicki G, Dollar A (2013) Estimation of quasi-stiffness of the human knee in the stance phase of walking. *PLoS ONE* 8: e59993.
43. Shamaei K, Napolitano P, Dollar A (2013) A quasi-passive compliant stance control knee-ankle-foot orthosis. *Proceedings of the IEEE International Conference on Rehabilitation Robotics (ICORR)*. Seattle, USA.
44. Walsh C, Endo K, Herr H (2007) A quasi-passive leg exoskeleton for load-carrying augmentation. *International Journal of Humanoid Robotics* 4: 487-506.
45. Farris D, Sawicki G (2012) Linking the mechanics and energetics of hopping with elastic ankle exoskeletons. *J Appl Physiol* 113: 1862-1872.
46. Davis R, DeLuca P (1996) Gait characterization via dynamic joint stiffness. *Gait & Posture* 4: 224-231.
47. Crenna P, Frigo C (2011) Dynamics of the ankle joint analyzed through moment-angle loops during human walking: gender and age effects. *Human Movement Science* 30: 1185-1198.
48. Lark S, Buckley J, Bennett S, Jones D, Sargeant A (2003) Joint torques and dynamic joint stiffness in elderly and young men during stepping down. *Clinical Biomechanics* 18: 848-855.
49. Salsich G, Mueller M (2000) Effect of plantar flexor muscle stiffness on selected gait characteristics. *Gait & Posture* 11: 207-216.
50. Hansen A, Childress D, Miff S, Gard S, Mesplay K (2004) The human ankle during walking: implications for design of biomimetic ankle prostheses. *Journal of Biomechanics* 37: 1467-1474.
51. Kuitunen S, Komi P, Kyrolainen H (2002) Knee and ankle joint stiffness in sprint running. *Medicine and Science in Sports and Exercise* 34: 166-173.
52. Rouse E, Gregg R, Hargrove L, Sensinger J (2013) The difference between stiffness and quasi-stiffness in the context of biomechanical modeling. *IEEE Transactions on Biomedical Engineering* 60: 562-568.
53. Shamaei K, Sawicki GS, Dollar AM (2013) Estimation of quasi-stiffness of the human hip in the stance phase of walking. *PLoS ONE* 8: e81841.

54. Saunders J, Inman V, Eberhart H (1953) The major determinants in normal and pathological gait. *Journal of Bone and Joint Surgery-American* Volume 35: 543-558.
55. Ratcliffe R, Holt K (1997) Low frequency shock absorption in human walking. *Gait & Posture* 5: 93-100.
56. Gard S, Childress D (1999) The influence of stance-phase knee flexion on the vertical displacement of the trunk during normal walking. *Archives of Physical Medicine and Rehabilitation* 80: 26-32.
57. Gard S, Childress D (2001) What determines the vertical displacement of the body during normal walking? *Journal of Prosthetics and Orthotics* 13: 64-67.
58. Walsh C, Pasch K, Herr H. An autonomous, underactuated exoskeleton for load-carrying augmentation; 2006 Oct. 2006; Beijing, China. pp. 1410-1415.
59. Perry J (1992) *Gait Analysis : Normal and Pathological Function*. Thorofare, NJ: SLACK. 524 p. p.
60. Winter D, Robertson D (1978) Joint torque and energy patterns in normal gait. *Biological Cybernetics* 29: 137-142.
61. Winter D (2005) *Biomechanics and Motor Control of Human Movement*. Hoboken, New Jersey: John Wiley & Sons. 325 p.
62. Skinner S, Antonelli D, Perry J, Lester D (1985) Functional demands on the stance limb in walking. *Orthopedics* 8: 355-361.
63. Andriacchi T, Ogle J, Galante J (1977) Walking speed as a basis for normal and abnormal gait measurements. *Journal of Biomechanics*: 261-268.
64. Picard R, Cook R (1984) Cross-validation of regression models. *Journal of the American Statistical Association* 79: 575-583.
65. Geladi P, Kowalski B (1986) Partial least-squares regression: A tutorial. *Analytica Chimica Acta* 185.
66. Hoskuldsson A (1988) PLS regression methods. *Journal of Chemometrics* 2: 211-229.

67. Leurs F, Ivanenko Y, Bengoetxea A, Cebolla A, Dan B, et al. (2011) Optimal walking speed following changes in limb geometry. *Journal of Experimental Biology* 214: 2276-2282.
68. Minetti A, Ardigo L, Saibene F, Ferrero S, Sartorio A (2000) Mechanical and metabolic profile of locomotion in adults with childhood-onset GH deficiency. *European Journal of Endocrinology* 142: 35-41.
69. Minetti A, Saibene F, Ardigo L, Atchou G, Schena F, et al. (1994) Pygmy locomotion. *European Journal of Applied Physiology and Occupational Physiology* 68: 285-290.
70. Cavagna G, Franzetti P, Fuchimoto T (1983) The mechanics of walking in children. *Journal of Physiology* 343: 323-339.
71. Cavagna G, Thys H, Zamboni A (1976) Sources of external work in level walking and running. *The Journal of Physiology* 262: 639-657.
72. Herr H, Wilkenfeld A (2003) User-adaptive control of a magnetorheological prosthetic knee. *Industrial Robot: an International Journal* 30: 42-55.
73. Martinez-Vilialpando E, Herr H (2009) Agonist-antagonist active knee prosthesis: A preliminary Study in level-ground walking. *Journal of Rehabilitation Research and Development* 46: 361-373.
74. Johansson J, Sherrill D, Riley P, Bonato P, Herr H (2005) A clinical comparison of variable-damping and mechanically passive prosthetic knee devices. *American Journal of Physical Medicine & Rehabilitation* 84: 563-575.
75. Cherry M, Choi D, Deng K, Kota S, Ferris D (2006) Design and fabrication of an elastic knee orthosis: preliminary results. *Proceedings of IDETC/CIE ASME 2006 International Design Engineering Technical Conferences & Computers and Information in Engineering Conference*. Philadelphia, USA.
76. Shamaei K (2009) *On Biomechanics of Locomotion*. New Haven, USA: Yale University.

Chapter 4

Mechanics and Energetics of Human Body in Interaction with Exoskeletal Impedances in Parallel with the Knee Joint during Walking

4.1 Introduction

Lower-extremity exoskeletons have been actively investigated in the past few decades, with a number of impressive and substantial undertakings (e.g. see [1] for a thorough review). These devices generally intend to augment the locomotion performance of able-bodied users in terms of metabolic cost, load carrying capacity, fatigue, and muscle force generation (in contrast to oftentimes similar lower-limb orthoses intended for impaired subjects [2,3].) While development efforts have been extensive, lower-limb exoskeleton devices have demonstrated limited success in achieving their augmentation goals [1,4-6], highlighting the challenges in developing artificial systems that can augment the performance of the human body, which is generally substantially more efficient than engineered systems.

In terms of technical approaches to developing augmenting exoskeletons, engineers have implemented a spectrum of assistance strategies. This includes “sensitivity amplification” [7], “get out of the way” [1], “moment of inertia compensation” [8], pneumatic actuation [9,10] in fully articulated exoskeletons at one end of the spectrum, and “gravity compensation” in a passive system at the other end [11]. More closely related to the work described in this chapter, recent design efforts have focused on replication of the function of lower extremity joints by quasi-passive systems that mostly rely on energy storage/recoil using spring-clutch systems [2,3,6,12-14]. This approach was inspired by spring-type behavior observed in lower extremity joints during walking and running and proved to lead to lower weight and more functional exoskeletons [15].

The lack of successful device development has prompted a number of research efforts intended to investigate basic science questions related to the interaction between lower extremities and wearable robotic devices (e.g. [5,12,15-18]). Understanding locomotor adaptation of lower extremity joints in interaction with external engineered systems and changes in environment is also of importance to several other fields including orthotics and prosthetics [1,10,16,17,19,20], rehabilitation and physical therapy [21-23], and fundamental physiology and biomechanics [24-26]. Locomotor adaptation in the lower extremity joints is studied by exposing the human (or relevant species) lower limbs to externally-applied mechanical impedances and perturbations [27], externally added mass [28,29], and to uneven terrains in locomotion tasks [30,31]. A common message from all these research undertakings is that the human body can adapt to external loads and perturbations to exhibit stable gait.

Researchers have explored adaptation in lower extremities function to series impedances and found that upon a change in the surface stiffness, lower extremities adapt such that the overall stiffness at the human body center of mass (COM) remains invariant [32,33]. Recently, there has been growing interest in studying the behavior of lower extremity joints in interaction with parallel impedances [3,6,12,15,34-38]. These studies could prove beneficial for development of exoskeletons meant for gait assistance with able-bodied users [4,10,12-15,39], rehabilitation orthoses meant for physical therapy [40,41], and assistive orthoses meant for gait assistance to impaired users [3,42,43]. To this end, researchers have exploited robotic exoskeletons to study human motor adaptation impedances in parallel with the ankle [10,12,17,44], knee [13,14] and hip joint [6,39,41].

To date, these studies have mostly focused on the lower extremity joints performance augmentation using exoskeletal assistance and how the joints adapt to the external perturbations. In addition to the kinematic and kinetic behavior of the joints, the motion of the COM is a fundamental parameter in biomechanical analysis and characterization of gait [45,46]. It relates to

the overall motion of the human body, estimates energy changes, mechanical work, and gait efficiency, and describes gait symmetry, balance and stability [46-49].

Characterization of the effects of exoskeletal assistance, locally provided to a lower extremity joint, on the motion patterns of the COM is informative to: a. evaluate the overall energetic performance of human body in interaction with exoskeletons, b. understand the biomechanical contribution of lower extremity joints to the overall motion and energy of the COM, c. identify if the exoskeleton perturbs gait stability and symmetry, and d. evaluate the overall performance of the exoskeletons. However, only few researchers have explored the effects of exoskeletal assistance/perturbation on the movement of the COM [15].

In this chapter, we explored the interaction of the lower extremities (specifically knee joint) with externally-applied stiffnesses in parallel with the knee joint using a pair of quasi-passive robotic knee exoskeletons, as shown in Fig. 4-1. Each of the exoskeletons implemented a spring in parallel with the left and right knee joints in the stance phase and allowed free motion throughout the rest, as schematically shown in Fig. 4-2. While this pair of exoskeletons allowed for the investigation of how variation in passive external impedances affects the gait behavior of the wearer, we believe the approach of carefully-tuned external stiffness may eventually prove functional as a performance-augmenting strategy; noting that similar approaches have been proposed and implemented by others [6,14,50].

We chose to study the knee joint firstly as the knee joint demonstrates a simple spring-like behavior in the stance phase of the gait, which enables us to simply implement a spring in parallel with the knee joint to investigate the interaction with external stiffnesses [34,51]. Secondly, among the lower extremity joints, the knee joint demonstrates several major functions in walking. It primarily supports the weight of the body, absorbs the shock resulting from heel strike, and flexes in the swing phase to provide foot clearance and obstacle avoidance, allowing the leg to move forward and initiate the next gait cycle [52].

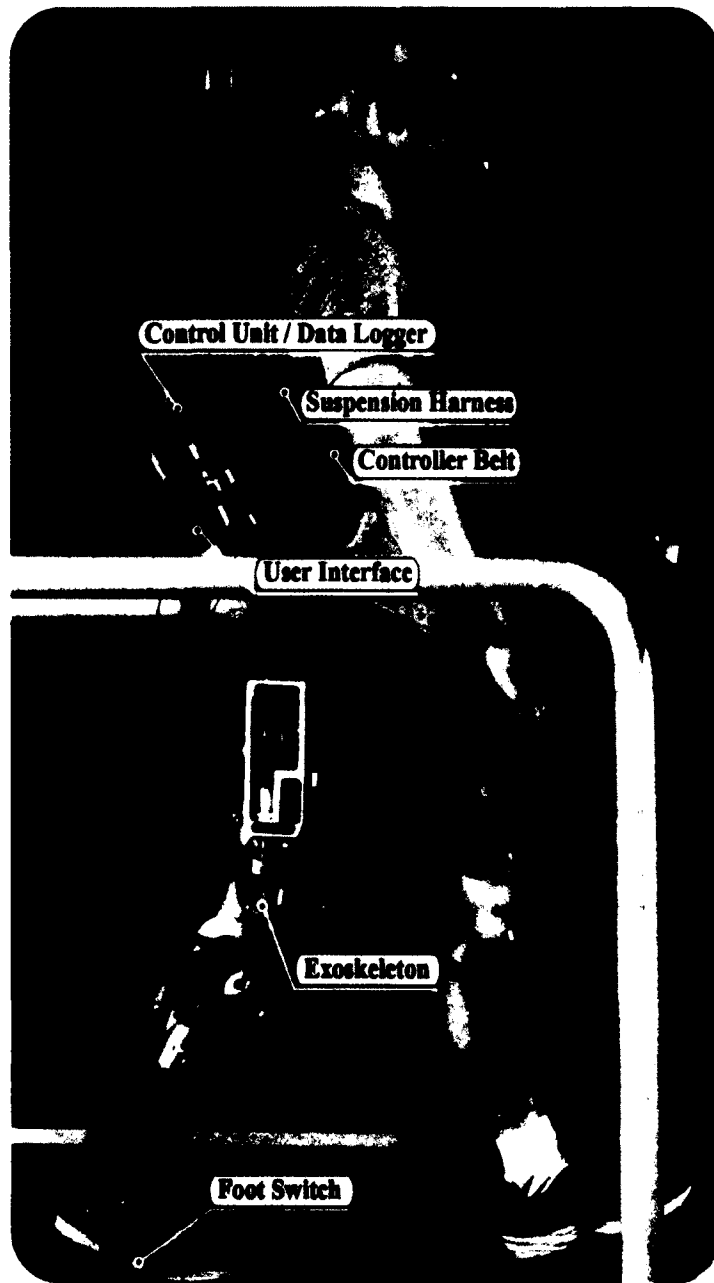


Figure 4-1. A volunteer walking with the quasi-passive knee exoskeletons. The control unit is mounted on a belt and wirelessly transfers the data to a host computer. The exoskeletons and controller are suspended with a harness from the shoulder. The exoskeleton is composed of a variable-stiffness module mounted on an adjustable knee brace equipped with a potentiometer-pulley assembly.

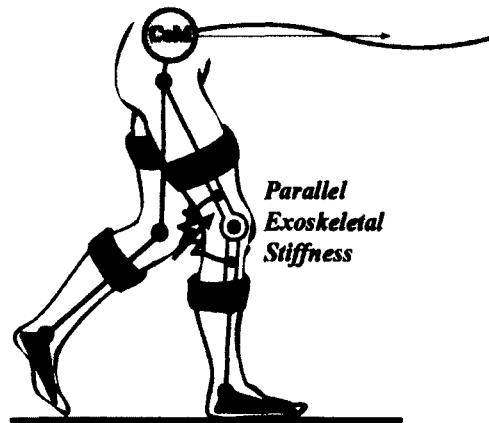


Figure 4-2. Knee complex is defined as the combination of the knee joint and exoskeleton. This work investigates the interaction between human lower extremities and parallel stiffnesses externally applied by a pair of knee exoskeletons.

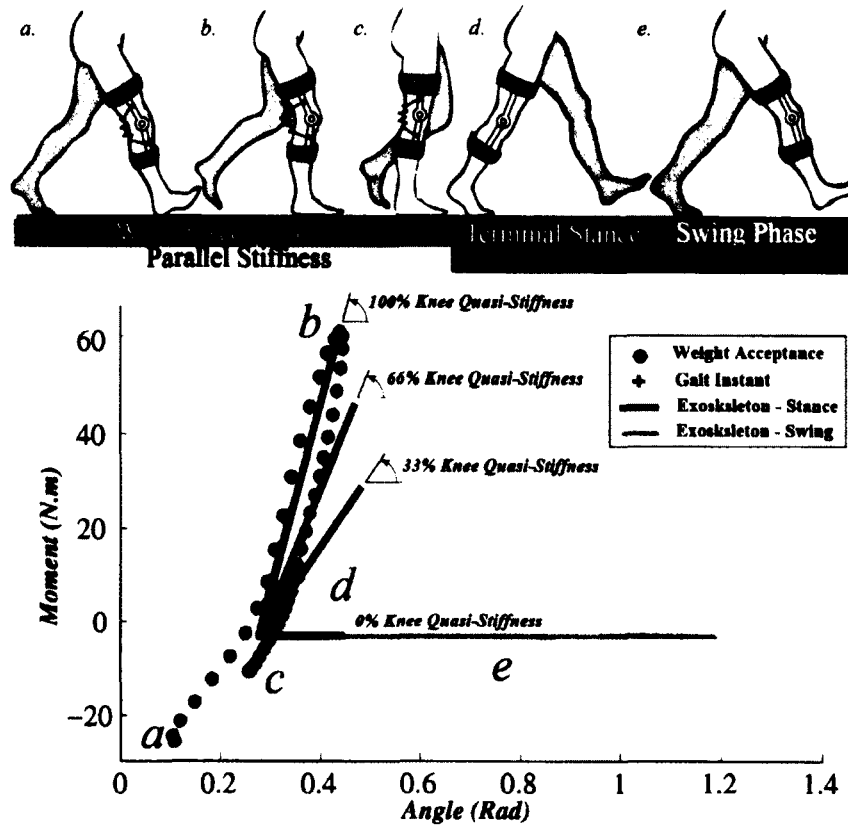


Figure 4-3. Top: The exoskeleton implements a high-stiffness spring in the weight acceptance phase of the gait and a low-stiffness spring (with negligible stiffness) throughout the rest of the gait cycle. Bottom: The exoskeleton implements 4 levels of spring stiffness including 0%, 33%, 66%, and 100% of the estimated knee quasi-stiffness.

The human knee joint experiences three consecutive phases in a gait cycle, as schematically illustrated in Fig. 4-3. The knee undergoes substantial loading in the weight acceptance phase (first ~40%, as depicted in Fig. 4-3 points *a* to *c*) and moderate loading in the terminal stance (~40-63%, as shown in Fig. 4-3 points *c* to *d*) and swing phases of gait [34,51-55]. The human knee demonstrates a linear flexion stage (points *a* to *b* in Fig. 4-3) and a linear extension stage (points *b* to *c* in Fig. 4-3) in the weight acceptance phase of the gait [34,51], which can be characterized by the concept of quasi-stiffness [34,51].

The concept of quasi-stiffness, which is the coefficient of a first order polynomial regressed to the moment-angle data of a lower extremity joint in a period of gait, is used to explain the overall behavior of the lower extremity joints in the linear loading phases of gait [35,56-62]. One should differentiate the concept of joint quasi-stiffness from the joint stiffness; in that the former refers to the overall moment-angle behavior of a joint in a locomotion task and the latter refers to static/dynamic stiffness of a joint at a certain configuration [51,61-63]. Stiffness at the leg and joint level plays an essential role in achieving stable gait [51,61,62,64,65]. Dynamic and static stiffness of the lower extremity joints have been characterized by researchers using external perturbation in conjunction with statistical system-identification techniques [27,66,67], static loading tests [68], in-vitro/vivo validation of muscle models and electromyography [69-71].

Previous research shows that the knee quasi-stiffness in the flexion and extension stages of the weight acceptance phase tend to be identical at the preferred gait speed, implying that the knee behaves close to a linear torsional spring at the preferred gait speed [34,51]. Accordingly, we model the moment-angle behavior of the knee joint in the weight acceptance phase of the gait at the preferred gait speed by a linear torsional spring with a stiffness equal to the knee quasi-stiffness in the weight acceptance phase (K_K). This chapter focuses on the interaction between the spring-type behavior of the human knee joint (with quasi-stiffness of K_K) and a spring (with stiffness of K_P) implemented in parallel with the knee in the weight acceptance phase. This

chapter also extends to the effects of the exoskeletal knee impedances on the performance of all lower extremity joints and the motion of the COM.

To this end, several hypotheses were formulated and tested as follows:

1. It was hypothesized that the overall behavior of the complex of the knee joint and parallel exoskeletal spring remains linear leading to the following equation for the knee complex quasi-stiffness (K_C):

$$K_C = K_K + K_P \quad (4-1)$$

Moreover, the moment of the knee complex (M_C) would be the summation of the knee joint moment (M_K) and parallel moment (M_P) as:

$$M_C = M_K + M_P \quad (4-2)$$

2. It was hypothesized that the knee joint quasi-stiffness and moment in the weight acceptance phase would adapt to the parallel stiffness and exoskeletal moment such that the overall quasi-stiffness and moment of the knee complex would remain invariant. In other words, an increase in K_P in equation (4-1) is negated by a decrease in K_K such that the overall knee complex quasi-stiffness remains constant:

$$\Delta K_C = 0 \implies \Delta K_K = -\Delta K_P \quad (4-3)$$

and similarly:

$$\Delta M_C = 0 \implies \Delta M_K = -\Delta M_P \quad (4-4)$$

3. It was hypothesized that the mass and articulation of an exoskeleton could affect the kinematic and kinetic patterns of the knee joint.

4. It was hypothesized that the metabolic power of walking is correlated with the rate of moment generation and mechanical work (as proposed by others [12,72-76]) suggesting that a spring in parallel with the knee joint in the weight acceptance phase can fully/partially unload the knee joint and result in a reduction in the metabolic power of walking and therefore positively influence the energetics of gait. Previous research suggests that there might be an optimal level of assistance provided by an exoskeleton [4,15], therefore this investigation included four levels of

exoskeletal assistance/stiffness as: 0%, 33%, 66%, and 100% of the estimated anatomical knee quasi-stiffness.

5. We hypothesized that an exoskeletal spring in parallel with the knee joint in the stance phase would not perturb the motion of the COM; whereas, the mass and articulations of the exoskeleton would perturb the motion of the COM.

To test these hypotheses, a series of experiments were conducted on nine healthy participants and using the exoskeletons. Furthermore, the effects of the inertia and articulation of the exoskeleton on the mechanical performance of the lower extremity joints (especially the knee joint) were studied using a pair of joint-less replicas of the exoskeletons with mass distribution that was similar to that of the exoskeletons, as shown in Fig. 4-4.

We begin this chapter by describing the mechanical design and control scheme of the exoskeletons. We continue with the moment-angle characterization of the exoskeletons and a theoretical model of the exoskeleton springs in interaction with the human limbs. We then describe experiments on nine healthy adults and present inter-subject kinematic and kinetic profiles of the lower extremity joints in the sagittal plane, moment-angle analysis of the knee joint and gait energetics. Table 4-1 lists the definition of the parameters used throughout this text.

4.2 Design and Evaluation of the Exoskeletons

4.2.1 Design Overview

The quasi-passive knee exoskeletons can demonstrate two levels of stiffness in parallel with the knee joint using a friction-based latching mechanism shown in Fig. 4-1 and in detail in Fig. 4-5. Each of the exoskeletons primarily comprises of a thigh segment including a stiffness control module (SCM) and a thigh cuff, and a shank segment including a pulley, a rotary potentiometer, and a shank cuff, as shown in Fig. 4-5. The SCM includes a shaft that is attached to the pulley by a steel tendon and can slide upward and downward as a result of knee movement.



Figure 4-4. A pair of joint-less replica devices that have mass distribution similar to that of the exoskeletons.

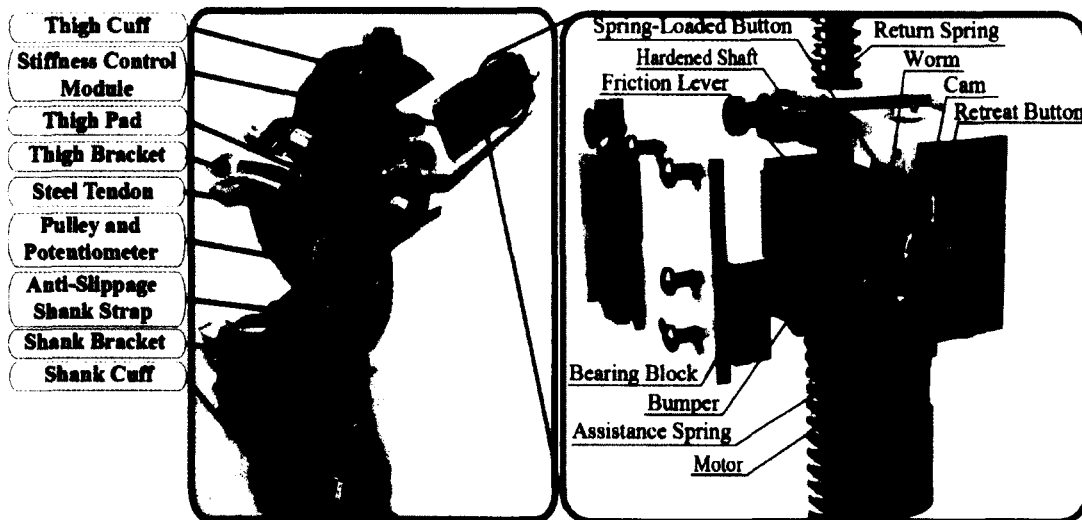


Figure 4-5. Left: Quasi-passive knee exoskeleton is composed of a stiffness control module that is assembled on the thigh segment of the exoskeleton, and a pulley on the shank segment. The shank segment is coupled to the stiffness control module through a steel tendon. Right: The stiffness control module employs a friction-based latching mechanism to engage/disengage an assistance spring. The directions of movement of the motor and worm-gear set for engagement and disengagement are illustrated. Particularly, the motor spins counterclockwise, and the cam and friction lever downward to engage and vice versa to disengage.

TABLE 4-1. Definition of Mathematical Parameters

Parameter	Unit	Definition
K_K	$\frac{N.m}{kg.rad}$	Knee joint quasi-stiffness
κ_K	-	Normalized knee joint quasi-stiffness
K_C	$\frac{N.m}{kg.rad}$	Knee complex quasi-stiffness
κ_C	-	Normalized knee complex quasi-stiffness
K_E	$\frac{N.m}{kg.rad}$	Exoskeleton stiffness
κ_E	-	Normalized exoskeleton stiffness
K_P	$\frac{N.m}{kg.rad}$	Parallel stiffness (K_E and K_S in series)
κ_P	-	Normalized parallel stiffness (κ_E and κ_S in series)
M_K	$\frac{N.m}{kg}$	Knee joint loading effort
\mathcal{M}_K	-	Normalized knee joint loading effort
M_C	$\frac{N.m}{kg}$	Knee complex loading effort
\mathcal{M}_C	-	Normalized knee complex loading effort
M_E	$\frac{N.m}{kg}$	Exoskeleton parallel assistive
\mathcal{M}_E	-	Normalized exoskeleton parallel assistive
M_P	$\frac{N.m}{kg}$	Parallel assistive (equal to M_E)
\mathcal{M}_P	-	Normalized parallel assistive (equal to \mathcal{M}_E)
K_S	$\frac{N.m}{kg.rad}$	Interface series stiffness
θ_K	deg	Knee joint excursion
θ_C	deg	Knee complex excursion
θ_E	deg	Exoskeleton excursion
θ_S	deg	Interface series excursion
i	-	A lower extremity joint, $i = \{H: \text{hip}, K: \text{knee}, A: \text{ankle}, \text{and } E: \text{exoskeleton}\}$
\bar{P}_i^+	$\frac{W}{kg}$	Average positive power of joint i
P_i	$\frac{W}{kg}$	Power of joint i at a given time
P_i^+	$\frac{W}{kg}$	Positive power of joint i at a give time
\bar{P}_T^+	$\frac{W}{kg}$	Total average positive power
P_{mat}	$\frac{W}{kg}$	Metabolic power
W_i^+	$\frac{J}{kg}$	Average positive work of joint i during a gait cycle
E	-	Efficiency of positive work
COT	$\frac{J}{kg.m}$	Metabolic cost of transport
$\dot{V}O_2$	$\frac{mL}{sec}$	Rate of oxygen uptake
W	kg	Weight of the subject
V	$\frac{m}{sec}$	Gait speed
T	sec	Duration of the gait cycle
W	kg	Body weight
H	m	Body height
\bar{M}_i^+	$\frac{Nm}{kg}$	Average positive rate of moment generation of a lower extremity joint and exoskeleton
\dot{M}_i^+	$\frac{Nm}{kg.sec}$	Positive rate of moment generation of a lower extremity joint and exoskeleton
M_i	$\frac{Nm}{kg}$	Moment of a lower extremity joint/exoskeleton in the sagittal plane
T_{exo}	sec	Exoskeleton engagement mechanism latency

The SCM includes a return spring that remains engaged at all times and pushes the SCM shaft upward throughout the gait cycle. The return spring has a relatively low stiffness and it primarily returns the shaft to its original position (most proximal) during the knee extension. The left and right exoskeletons were similarly designed and made.

The SCM employs a friction-based latching mechanism to engage and disengage the assistance spring and act on the shaft. A shaft movement due to knee flexion always compresses the return spring; whereas, a shaft movement due to flexion only compresses the assistance spring when the latching mechanism has engaged it. As such, the linear stiffness of the SCM acting on the shaft would be the summation of the stiffnesses of the assistance and return springs when the assistance spring is latched, and only the stiffness of the return spring when the assistance spring is unlatched (see Fig. 4-6 for a schematic representation of this behavior).

The tendon connected to the SCM shaft wraps around a pulley that rotates together with the knee joint and pulls the shaft of the SCM that, in turn, transforms the linear stiffness of the SCM springs to a torsional stiffness around the knee joint. Fig. 4-5-right illustrates the design of the exoskeletons latching mechanism that is composed of a friction lever, shaft, bearing block, DC Motor, worm-gear, cam, spring-loaded push-button, and retreat push-button, and additional structural components. We have reported additional details on the latching mechanism in our previous paper on the design of a compliant stance control orthosis that employs a similar mechanism [3].

The exoskeletons have been implemented on two adjustable knee braces (SPL2 from Fillauer LLC) that can fit on a wide range of subjects with heights of *1.50 m* to *1.85 m* (as suggested by the manufacturer). To minimize the effect of soft tissues and to help the exoskeletons withstand the anticipated loads, we reinforced the braces using: a. a bracket that pressed against the quadriceps femoris tendon and was located ~ 5 cm superior to the center of the patella, b. a bracket that pressed against the tibial tuberosity and was located ~ 6 cm inferior to the center of the patella, c. a solid pad that was placed posterior to the thigh and under the strap of the knee

brace thigh cuff, and d. a suspension harness strap that vertically supported the exoskeletons from the shoulder and avoided downward migration of the brace.

4.2.2 Friction-Based Latching Mechanism

The latching mechanism employs a motor to manipulate a friction lever to initiate or release a friction-based latch. The latching mechanism includes a worm-gear set that transforms motor rotation to a linear motion at the friction lever. To engage the assistance spring, the motor spins the worm gear counterclockwise to retreat the cam from the friction lever and make $\sim 2\text{ mm}$ clearance under it, as shown in Fig. 4-5-right. This movement continues until the cam presses the retreat button that sends a feedback signal to the controller. Upon the retreat of the gear, the spring loaded push-button presses the friction lever down and against the shaft to initiate a friction-based latch. The latching grip of the friction lever occurs when the shaft moves downward (as a result of a knee flexion) and the interaction force between the bearing block and the friction lever induces higher normal forces between the friction lever and the shaft. As such, the bearing block moves along with the shaft and compresses the assistance spring. An upward movement of the shaft (mainly caused by the return spring during the knee extension) relaxes the friction forces on the friction lever at the contact points and releases the latching grip when the assistance spring is fully unloaded. Therefore, the latch only initiates in the flexion direction and it is maintained during extension only if the assistance spring is engaged and loaded.

To disengage the assistance spring, the motor rotates the worm clockwise to move the cam upward and towards the friction lever. The cam lifts the friction lever and releases the latching grip. The upward movement of the lever terminates when the spring-loaded push-button is pressed and a feedback signal is sent to the controller to stop the motor. Upon disengagement of the lever, the shaft freely slides inside the bearing block and friction lever without any force being transferred to the assistance spring. Accordingly, a downward force (e.g. resulting from knee flexion in the swing phase) on the shaft only compresses the return spring. To allow free rotation in the swing phase, we chose a highly compliant return spring (5 Nm/rad), which primarily

returns the shaft to the its most proximal location after the swing phase without applying a considerable moment to the knee. A more detailed explanation of the friction-based latching mechanism can be found elsewhere [3].

4.2.3 Control Scheme

The control unit implements a finite state machine for the engagement of the assistance spring during walking. The assistance spring has to be engaged during the weight acceptance phase of gait and allow free rotation throughout the rest of gait, as schematically shown in Fig. 4-3-top. The controller identifies the states using an instrumented shoe insole that indicates the heel and toe contacts with the ground. Fig. 4-7-top shows the status of the heel and toe sensors of the insole, the sign of the knee velocity (positive for flexion) measured by a rotary potentiometer that is embedded in the exoskeleton pulleys, as well as the status of the friction lever within a gait cycle. Fig. 4-7-bottom shows the knee angle profile for a volunteer walking at $1.25 \text{ m}\cdot\text{s}^{-1}$ on level ground and the period where the assistance spring is intended to be engaged and loaded. Fig. 4-8 describes the finite state machine that consists of the following states:

a. *Weight Acceptance (WA)*: The heel sensor is on and toe sensor is off. The controller engages the assistance spring.

b. *Terminal Stance (TS)*: The toe sensor is on and heel sensor is off, or both toe sensor and heel sensor are on. The controller disengages the assistance spring after a period of time ($T_{exo} = 60 \text{ ms}$, measured on a knee simulator as explained later in this text) dictated by the latching mechanism latency plus an adjusted period of time that nearly coincides with the end of the weight acceptance phase.

c. *Swing (SW)*: The toe and heel sensors are off. The controller monitors the knee velocity direction during the swing phase to identify whether the knee is flexing or extending. The controller unlatches the friction lever during the flexion period of the swing phase and latches it

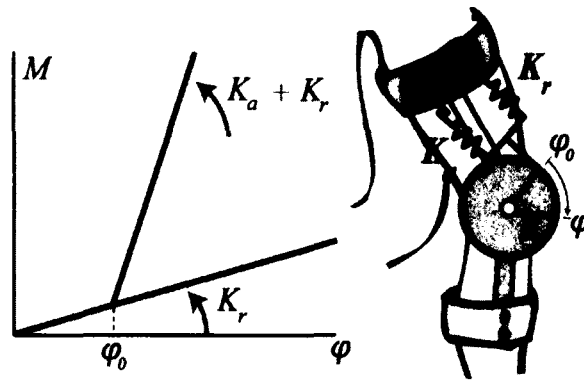


Figure 4-6. Left: The moment-angle characterization of the exoskeleton. K_a is the stiffness of the assistance spring, K_r is the stiffness of the return spring, φ is the angle of engagement, M is the exoskeleton moment, φ is the exoskeleton angle, and φ_0 is the angle at which the assistance spring is engaged. Right: Schematic model of the exoskeleton. A clutch mechanism engages/disengages the assistance spring.

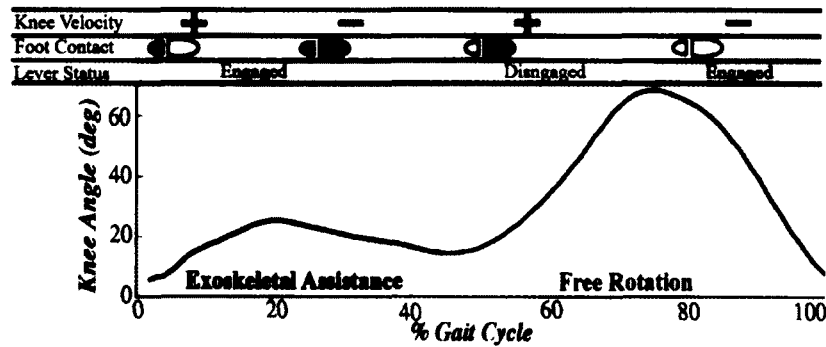


Figure 4-7. Timing of the control signals and engagement of the exoskeleton spring, Top: The statuses of the knee angular velocity (+ for flexion and – for extension), foot contact with the ground (heel and toe sensors of the instrumented shoe insole), and friction lever in a gait cycle. Bottom: Knee angle profile of a volunteer walking at 1.25 m/s. The exoskeleton assists the knee in the weight acceptance phase of the gait and allows free motion in the rest. The shades roughly show the timing of state changes.

during the extension period, as a precautionary measure against the latching mechanism latency. Because engagement of the assistance spring can only initiate in the flexion direction (positive sign of knee velocity, see also Fig. 4-7), latching of the friction lever in the extension period of the swing phase does not result in engagement and loading of the assistance spring and impeding knee joint motion.

We developed two finite state machines, one for each exoskeleton, on a Microcontroller MPC5534 from Freescale Semiconductor Co. (MPC5534EVBE). The controller measured the knee angle using a rotary potentiometer that is integrated inside the exoskeletons pulleys and the knee velocity by differentiating the potentiometer signal. The system employed an instrumented shoe insole from B & L Engineering Co., a Faulhaber 2224 DC Motor (*4.05 W*), a rotary potentiometers from Vishay Co. Model 357 for each exoskeleton, a dual H-Bridge circuit from Solarobotics Co. and a battery pack with capacity of *2500 mAh*. The controller transfers the signal from the spring-loaded push-button to identify if the friction lever is disengaged, and the signal from the retreat push-button to identify if the friction lever is engaged. A serial-to-Bluetooth adapter (Wireless RS232, Willies Computer Software Co.) was used to wirelessly transfer the data to a host LabView module implemented on a computer for data collection. The data include the left and right exoskeletons joint angles and status of engagement of the lever based on which we calculated the exoskeleton moments.

4.2.4 Moment-Angle Characterization

In the previous section, we explained that the linear stiffness of the exoskeleton (K_L) transforms to a rotational stiffness around the exoskeleton joint (K_E) through a tendon that connects the SCM shaft to the exoskeleton pulley. Fig. 4-6-right schematically shows the function of the exoskeleton. In our previous work, we showed K_L and K_E are related as [3]:

$$K_E = K_L \cdot R^2 \quad (4-5)$$

where, $R = 5 \text{ cm}$ is the radius of the exoskeleton pulleys, K_L is the stiffness of the return spring when the friction lever is disengaged, and the sum of the stiffness of the assistance spring (K_a) and return spring ($K_r \approx 0$) when the assistance spring is engaged:

$$K_L = \begin{cases} K_r + K_a & \text{engaged} \\ K_r & \text{disengaged} \end{cases} \quad (4-6)$$

Combining equation (4-5) and (4-6), the exoskeletal rotational stiffness can be expressed as:

$$K_E = \begin{cases} (K_r + K_a) \cdot R^2 & \text{engaged} \\ K_r \cdot R^2 & \text{disengaged} \end{cases} \quad (4-7)$$

Therefore, the exoskeleton assistive moment is related to the knee joint angle (φ) as follows:

$$M_E = \begin{cases} K_r \cdot R^2 \cdot \varphi + K_a \cdot R^2 \cdot (\varphi - \varphi_o) & \text{engaged} \\ K_r \cdot R^2 \cdot \varphi & \text{disengaged} \end{cases} \quad (4-8)$$

Here, φ is the knee angle and φ_o is the angle at which the assistance spring is engaged. Fig. 4-6-left schematically shows the moment-angle performance of the exoskeleton. The exoskeleton controller records φ and φ_o from the potentiometer, and status of the spring engagement for both left and right exoskeletons from the push-buttons incorporated in the SCM, and wirelessly transfers them to a host computer. We combined the controller data with the exoskeleton spring stiffnesses and obtained the exoskeleton moments.

The exoskeletons compliantly interface with the human limbs as a result of compliance in the biological soft tissues and exoskeleton cuffs and attachments. We approximate this by an additional spring between the assistance spring and the thigh. Fig. 4-9 schematically shows the configuration of the three springs of the knee complex that represent the knee joint, exoskeleton, and soft tissue behavior in the weight acceptance phase of the gait. This theoretical model suggests:

$$K_C = K_K + K_P \quad (4-9)$$

where, K_C is the quasi-stiffness of the knee complex, K_K is the quasi-stiffness of the knee joint, and K_P is the external parallel stiffness that is equal to:

$$K_P = \frac{K_E K_S}{K_S + K_E} \quad (4-10)$$

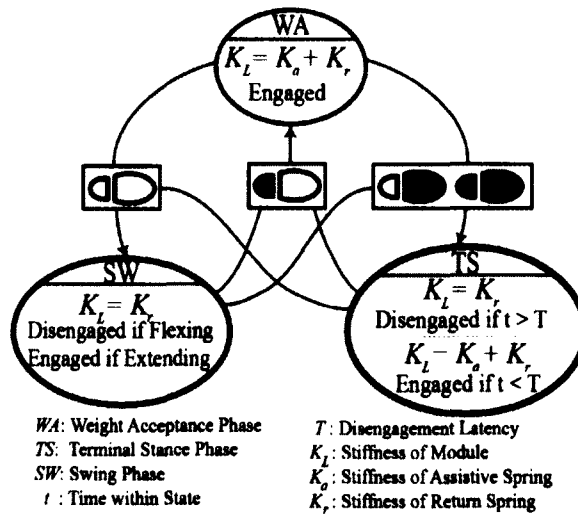


Figure 4-8. The diagram of the finite state machine that the exoskeleton controller uses to engage/disengage the assistance spring. The states include Weight Acceptance (WA), Terminal Stance (TS), and Swing (SW) and are identified using a foot sensor. The diagram also indicates the engagement status of the friction lever and stiffness of the module.

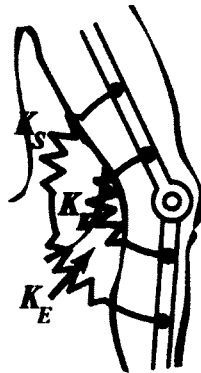


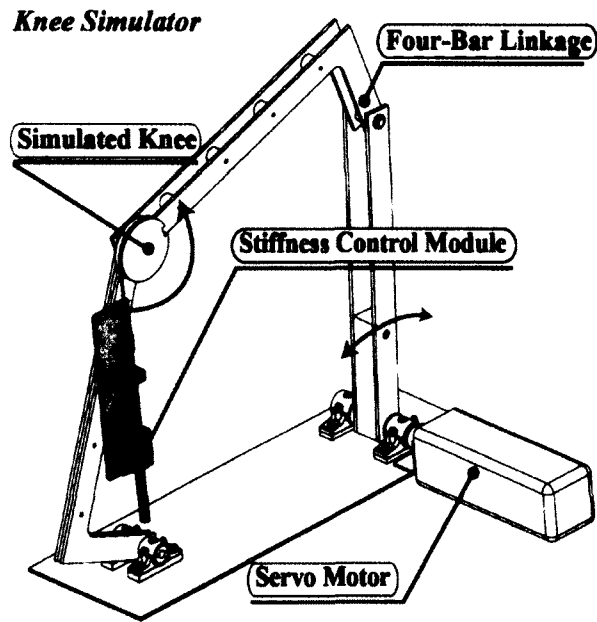
Figure 4-9. A schematic model of the knee complex comprising the knee equivalent spring, exoskeleton spring, and the compliance of the biological soft tissues of the leg and exoskeleton cuffs. The assistance condition includes modulation of K_E ; whereas, we primarily intend to investigate the effect of external parallel spring on the spring-type behavior of the knee joint.

where, K_E is the exoskeleton stiffness and K_S is the interface stiffness. In fact, K_P is the externally-applied parallel stiffness that is being perceived by the anatomical knee joint. We also define θ_C as the excursion of the knee complex, θ_K the excursion of the knee joint, θ_E the excursion of the exoskeleton, and θ_S the excursion of the interface in the weight acceptance phase. One should note that θ_E is the range of changes of φ in the weight acceptance phase.

4.2.5 Mechanical Evaluation

We tested the reliability of the exoskeleton and measured the latency of the SCM using a knee joint simulator prior to the human trials, as schematically shown in Fig. 4-10-top. In testing the reliability of the exoskeleton we conducted extensive testing to ensure that the exoskeleton can withstand the dynamic loads it would encounter in walking, and to ensure that the exoskeleton can undergo the number of gait cycles that we expect during the experiments on human volunteers.

The knee simulator primarily consists of a four-bar linkage driven by a 3-phase servomotor and servo controller (SGMAV-10A3A61 from Yaskawa and SGDVI20AE from Omron Companies) [77]. The servomotor emulates the kinematic profile of the knee joint and sends a digital signal to the SCM to engage the assistance spring during the simulated stance phase and disengage during the rest of the gait, as shown in Fig. 4-10-bottom. The simulator records the actual instances of engagement/disengagement using the feedback signals from the push-buttons embedded in the SCM. We estimate the engagement/disengagement latency by measuring the time period between the command and feedback signals. The latencies could alternatively be approximated by the properties of the DC motor and worm-gear set of the engagement mechanism; a method that was ignored because friction and other imperfection in the mechanism could not be characterized. We fabricated a prototype of the SCM and tested it on the knee joint simulator as schematically shown in Fig. 4-10-top.



Measurement of the Mechanical Latency

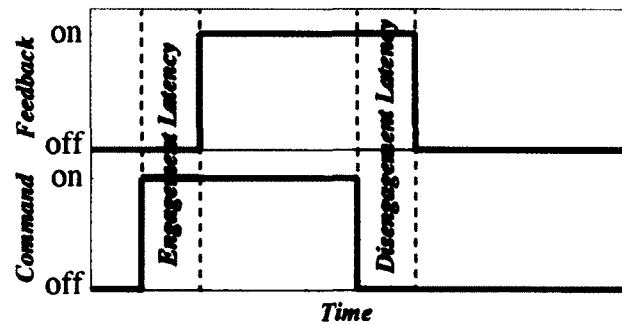


Figure 4-10. Top: The stiffness control module mechanically tested on a knee simulator. The simulator is primarily a four-bar linkage mechanism driven by a servo motor. The stiffness control module is mounted on the simulator and undergoes numerous working cycles to endure the reliability and functionality of the module and measure the mechanical latency of engagement/disengagement. Bottom: The simulator controller sends an engagement command signal to the compliance control module and receives the feedback from the pushbuttons embedded in the module. The time differences between these signals indicate the mechanism engagement/disengagement latency.

The prototype successfully underwent $\sim 30,000$ gait cycles (with maximum moment of 60 Nm/rad) on the knee simulator without any failure in the mechanical components and engagement occurrence. The average latencies for both engagement and disengagement were also measured using the test machine and were found to be $T_{exo} = \sim 60 \text{ ms}$. We explained earlier that the exoskeleton transferred the engagement signal to a host computer to calculate the exoskeleton moment profiles. The engagement signal was extended by T_{exo} to capture the effect of the disengagement mechanism latency. T_{exo} was also used in the design of the state machine of Fig. 4-8. One should note that the engagement latency was not used because the exoskeletons engage the spring in the extension period of the swing phase and prior to the heel contact with the ground. The mechanical function of the exoskeletons was also monitored using a high-speed camera to visually inspect the mechanism function in additional detail. The video inspection confirmed that the engagement mechanism functioned as desired throughout the experiments.

4.3 Experimental Conditions and Protocols

4.3.1 Subjects

Nine healthy adult volunteers were recruited from the US Army Soldiers assigned to Headquarters, Research, and Development Detachment of Natick Soldier System Center. Inclusion criteria were a body height between 1.50 and 1.85 m and a body weight less than 130 kg according to the size limitations of the exoskeleton. Table 4-2 lists the demographics of the volunteers, including the means and standard deviations (SD) of weight and height of each volunteer. Written informed consent was obtained from each volunteer enrolled in the study prior to participation in the study. The study protocol was approved by Yale University Institutional Review Board, Human Use Review Committee of United States Army Research Institute of Environmental Medicine, Army Human Research Protections Office, and Battelle Institutional Review Board in accordance with DoD 3216.02, protection of human subjects.

4.3.2 Data Collection Instrumentation

The experiments took place in the Center for Military Biomechanics Research at the Natick Soldier Research, Development and Engineering Center, Natick, MA. The experimental conditions included walking on an instrumented treadmill (AMTI, Watertown, MA). The treadmill comprises two synchronized treadmill belts positioned side-by-side, each on a separate force platform with a gap smaller than 1 cm. A motion capture system of ten cameras (Qualisys, Gothenberg, Sweden) and the Qualisys Track Manager Software were used to record three dimensional motion data of the volunteers walking on the treadmill at a frequency of 240 frames/sec.

The exoskeleton simultaneously transferred data of the right and left knee angles, heel and toe sensors status, and feedback signal from the exoskeleton as indicators of the status of the engagement of the high-stiffness spring through the serial port using a wireless serial to Bluetooth adapter (from Willies Computer Software Co.) to a host computer that records the data using a LabView module. The exoskeleton also sent a synchronization signal to the Qualisys camera system that allowed us to synchronize the data from the exoskeleton with the data from the motion capture system and the force plates. Kinematic and kinetic profiles of the joints were calculated using Visual3D software (C-Motion, Gaithersburg, MD). The rest of analyses were done in Matlab software (Mathworks, Natick, MA).

The rate of oxygen uptake ($\dot{V}O_2$, mL/min) was measured using a K4b² portable metabolic measurement system (COSMED, Rome, Italy). First, $\dot{V}O_2$ was measured for a 2-min standing trial as a baseline for each subject. For each walking trial, $\dot{V}O_2$ was measured during minutes 8-10 and were averaged over 20 secs increments for the 2-min collection period. We ensured that the rate of oxygen uptake was steady for each trial. Net rate of oxygen uptake ($\dot{V}O_2'$) for each trial was calculated as the average value of $\dot{V}O_2$ during walking subtracted by the average $\dot{V}O_2$ of the standing trial.

TABLE 4-2. Demographic data of the participants and exoskeleton stiffnesses

No.	H (m)	W (kg)	V(m/s)	Measured K_E (Nm/rad)	Estimated K_E (Nm/rad)	33% K_E (Nm/rad)	66% K_E (Nm/rad)	100% K_E (Nm/rad)
1	1.73	86.0	1.30	321	299	103	203	328
2	1.80	68.0	1.43	143	243	82	166	239
3	1.83	68.0	1.21	117	247	81	160	239
4	1.68	71.0	1.12	156	240	81	160	239
5	1.69	78.5	1.39	257	267	89	174	239
6	1.70	79.9	1.43	258	274	92	174	239
7	1.76	67.0	1.03	110	235	81	160	239
8	1.89	103.8	1.34	318	393	128	239	328
9	1.77	66.7	1.21	149	235	81	160	239
Mean	1.76	76.5	1.27	203	270	91	177	259
SD	0.1	12.3	0.14	85	51	16	27	39

TABLE 4-3. Mass properties of the exoskeleton

Side	Segment	Mass (kg)	I_{xx} (kg.m ²)	I_{yy} (kg.m ²)	I_{zz} (kg.m ²)
Right	Thigh	1.68	0.02370	0.02312	0.00211
	Shank	0.77	0.00217	0.00249	0.00122
Left	Thigh	1.81	0.02370	0.02312	0.00211
	Shank	0.82	0.00217	0.00249	0.00122

Left Exoskeleton Weight = 2.63 kg
 Right Exoskeleton Weight = 2.45 kg
 Controller Unit Weight = 2.4 kg
 Total Weight = 7.48 kg

4.3.3 Experimental Conditions

The hypotheses were tested experimentally using the following six experimental conditions of treadmill walking:

1. *Control Condition (CTRL)*: Without wearing the exoskeletons or mass replicas
2. *Exoskeleton Mass (MASS)*: Wearing the joint-less mass replicas
3. *Exoskeleton Articulation (0%)*: Wearing the exoskeleton unpowered with exoskeleton steel tendon detached
- 4-6. *Exoskeleton Stiffness (33%, 66%, and 100%)*: Wearing the exoskeleton with assistance spring stiffness equivalent to 33%, 66%, and 100% of the quasi-stiffness of the anatomical knee in normal walking at the preferred gait speed

To size the exoskeleton spring (K_E), we used a previously developed statistical model to estimate knee quasi-stiffness in the weight acceptance phase of gait based on the subject's body size as follows [51]:

$$K_E = 5.21 W \sqrt{H^3} - 7.50 W \sqrt{H} - 5.83 WH + 11.64 W - 6 \quad (4-11)$$

where, W (kg) is the body weight and H (m) is the height of the volunteer. This model shows a 9% error of estimation and was established for volunteers with a wide range of body weight (from 67.7 kg to 94.0 kg) and height (from 1.43 m to 1.86 m). Once the volunteer's knee quasi-stiffness was estimated using equation (4-11) for condition 6, it was then scaled to 33% and 66% for conditions 4 and 5, respectively. The values of gait speed, the estimated subject's quasi-stiffness, and the spring constants of the high-stiffness springs used for each volunteer are listed in Table 4-2.

4.3.4 Experimental Protocols

The study volunteers had three visits in total, including two orientation sessions and one data collection session. On all visits, the participants wore shorts, t-shirts, socks, and their own athletic shoes. The three visits took place within a single week with one to two day(s) in between to provide rest and prevent any fatigue that could affect the results. Volunteers' weight and height

were measured on the first visit to estimate each volunteer's knee quasi-stiffness (K_k) and size the assistance spring stiffness values for the assistance conditions using equation (4-11).

Orientation Sessions: Two orientation sessions were included prior to the data collection session to allow the volunteers to become familiar with walking while wearing the exoskeletons. On the first visit, participants walked on the treadmill for *3 mins* at *4.83 km/h* to become familiar with treadmill walking, after which they were given a 3-5 min rest break. Each participant was then instructed to walk on the treadmill with a speed that slowly increased from the zero-speed state up to a self-selected comfortable pace. This pace was then used as the preferred gait speed throughout the experiments. Next, the exoskeletons were fitted on the volunteers while seated and the alignment of the exoskeletons joint with the knee joints was ensured. In an effort to minimize the vertical migration of the exoskeleton, suspension harness straps were also put on the volunteer and fastened to the controller belt, which was strapped around the chest and shoulders. Lastly, the tension of the suspension straps was adjusted as the volunteers slowly stood up. The volunteers were asked to walk overground wearing the exoskeleton for each of the experimental conditions with the exception of the control condition. For each condition, the subjects walked overground for about *640 m* at their own pace, covering a distance approximately equivalent to the distance covered in *8 mins* of treadmill walking. A 5-min seated rest break was given to the volunteers before they walked on the treadmill in the same condition for *8 mins* at their preferred gait speed. The order of the conditions for the first session was ordered from condition 2 to condition 6, and not randomized across volunteers.

The second orientation session included only treadmill walking trials of 10-min duration. The order of the six conditions was randomized (using 6x6 Latin squares design) for each volunteer. The order of the conditions during each volunteer's second orientation session was the same as the order followed during the volunteer's data collection session. To summarize, volunteers walked a total *18 mins* on the treadmill and about *10 mins* overground for each experimental

condition during the first two orientation sessions to become more familiar with walking while wearing the exoskeletal device.

Data Collection Sessions: Reflective markers were placed on body landmarks according to convention described elsewhere [78], with slight differences in that four-marker clusters were placed on the shank and the thigh such that the exoskeleton cuffs could fit on the limbs without blocking their visibility from the cameras. Additionally, a four-marker cluster was placed on the chest to track the trunk and pelvis as a single segment. Within each trial, a 30-second long data recording was taken after *4 mins* from the start of the trial.

4.3.5 Kinematic and Kinetic Analysis

Visual3D software (C-Motion, Gaithersburg, MD) was used to calculate the lower extremity joints angle, moment, and power profiles for all conditions. To obtain the moment and power profiles for conditions 2-6, which included a device, we first calculated the mass, moment of inertia, and the center of mass of the thigh and shank segments of the exoskeleton and mass replicas in SolidWorks (Dassault Systèmes SolidWorks Corp., Waltham, MA), as listed in Table 4-3. Next, we updated the mass, center of mass, and moment of inertia of the shank, thigh, and trunk segments of the limb models in Visual3D as a gross average of the human limbs and exoskeleton components. Inverse dynamics analysis was then performed to obtain the moment and power profiles of the ankle and hip joints and knee complex in the sagittal plane for the left and right side. The kinetic and kinematic intra-subject profiles of the left side and right side were averaged to obtain the final mean profiles. A third-order Butterworth filter with cut-off frequency of *8 Hz* was used to filter the kinetic and kinematic profiles. The rest of analyses were carried out in Matlab (Mathworks, Natick, MA). The exoskeleton moment was calculated using equation (4-8) and the data received from the exoskeleton. To approximate the moment of the knee joint in the sagittal plane, the synchronized moment of the exoskeleton was subtracted from the moment of the complex assuming that the axis of exoskeleton joint and knee joint were perfectly aligned.

Visual3D software was also used to calculate the acceleration of the COM in the sagittal, frontal, and horizontal (i.e. transverse) planes from the corresponding ground reaction forces. To obtain the motion of the COM, a Visual3D model of the limbs was used, which included the mass of the replicas for the MASS condition and the exoskeletons for the other conditions. The velocity and travel profiles of the COM were then calculated as the first and second time-integral of the acceleration profile. The motion (travel and velocity) profiles of the COM were normalized with respect to the body height. The remaining analysis was carried out in Matlab.

The gait cycles were identified by the right heel strikes. Four consecutive gait cycles for each trial were identified from the force plate signals and complete marker data. We also verified that the calculated intra-subject averages for the joint angle and moment profiles from the four consecutive cycles were consistent among all trials. Additionally, the intra-subject mean profiles of the joint angles were normalized with respect to the standing configuration, the moment and power profiles with respect to the body weight, and motion of the COM with respect to the body height. The inter-subject mean and SD profiles were subsequently obtained from the corresponding intra-subject mean profiles (which were averaged across left and right sides for the angle, moment, and power). The inter-subject mean angle, moment, and power profiles in the sagittal plane are plotted in Fig. 4-11 to 13. The coefficient of variability (CV; described elsewhere [54]) was calculated for each profile using the mean and SD profiles. The inter-subject mean travel profiles of the COM along the vertical, mediolateral, and anteroposterior axes are plotted in Fig. 4-14. Additionally, travel and velocity trajectories of the COM were plotted for the sagittal, frontal, and horizontal planes in Fig. 4-15 and 16.

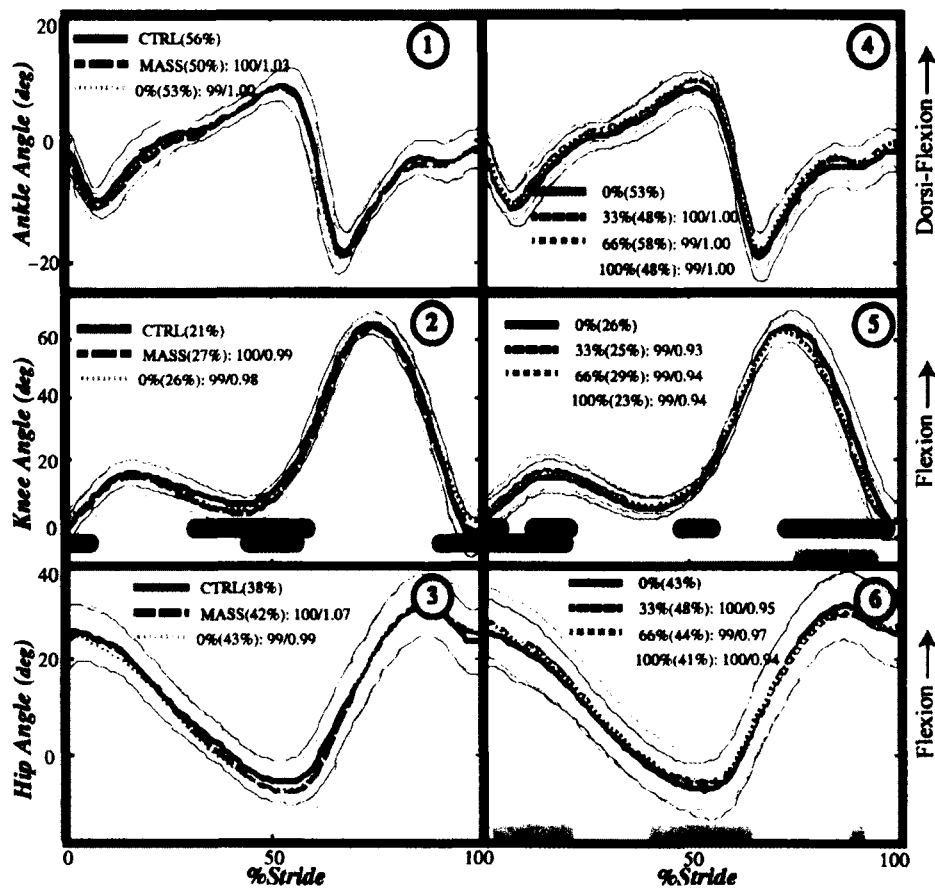


Figure 4-11. Inter-subject mean angle profiles. We have separately indicated the first three conditions (CTRL, MASS, and 0%) in the left column and the assistance conditions (0% to 100%) in the right column. The thick solid lines indicate the inter-subject mean profiles and the thin lines boundaries defined by ± 1 SD. The legends of each graph report the CV of each profile in parentheses followed by the R^2 /Scale of the regression comparison. The values of R^2 /Scale for the MASS condition are presented with respect to CTRL condition, and 0% condition with respect to the MASS condition, whereas 33%, 66%, and 100% are with respect to 0%. On the bottom of each graph, a series of stripes are plotted that indicate the periods during which two profiles are significantly different. The stripe colors correspond to the profile with similar color. The comparison is made between MASS and CTRL, 0% and MASS, 33% and 0%, 66% and 0%, and 100% and 0%.

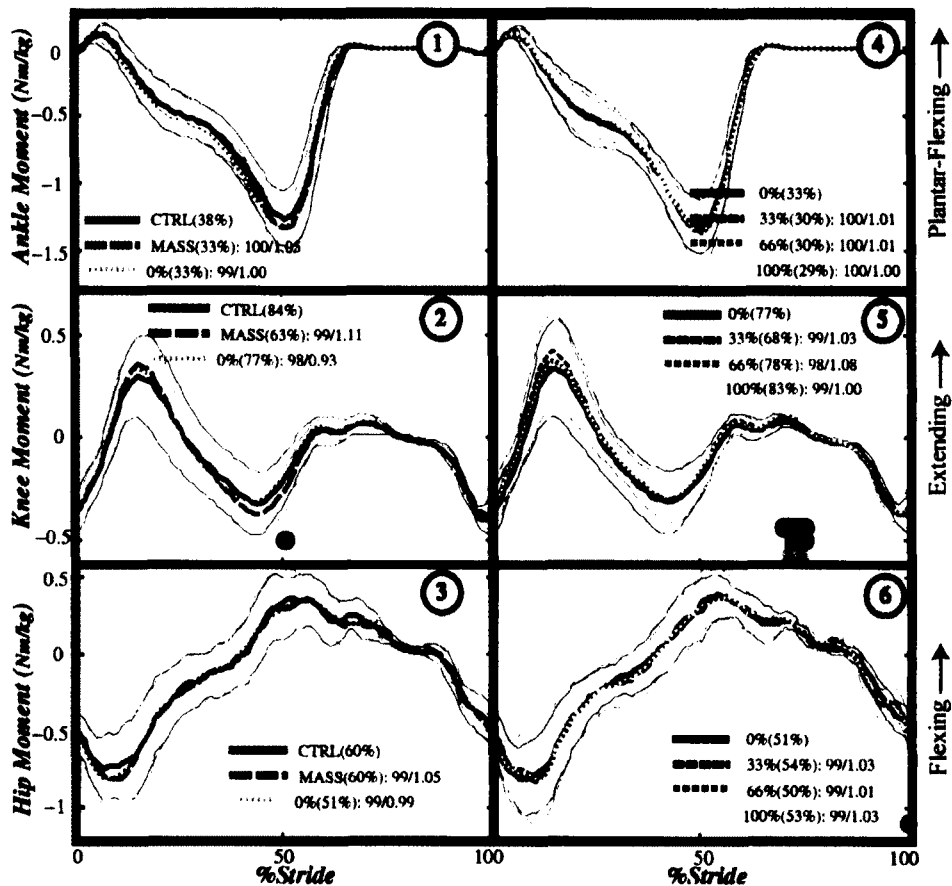


Figure 4-12. Inter-subject mean moment profiles. We have separately indicated the first three conditions (CTRL, MASS, and 0%) in the left column and the assistance conditions (0% to 100%) in the right column. The thick solid lines indicate the inter-subject mean profiles and the thin lines boundaries defined by ± 1 SD. The legends of each graph report the CV of each profile in parentheses followed by the R^2 /Scale of the regression comparison. The values of R^2 /Scale for the MASS condition are presented with respect to CTRL condition, and 0% condition with respect to the MASS condition, whereas 33%, 66%, and 100% are with respect to 0%. On the bottom of each graph, a series of stripes are plotted that indicate the periods during which two profiles are significantly different. The stripe colors correspond to the profile with similar color. The comparison is made between MASS and CTRL, 0% and MASS, 33% and 0%, 66% and 0%, and 100% and 0%.

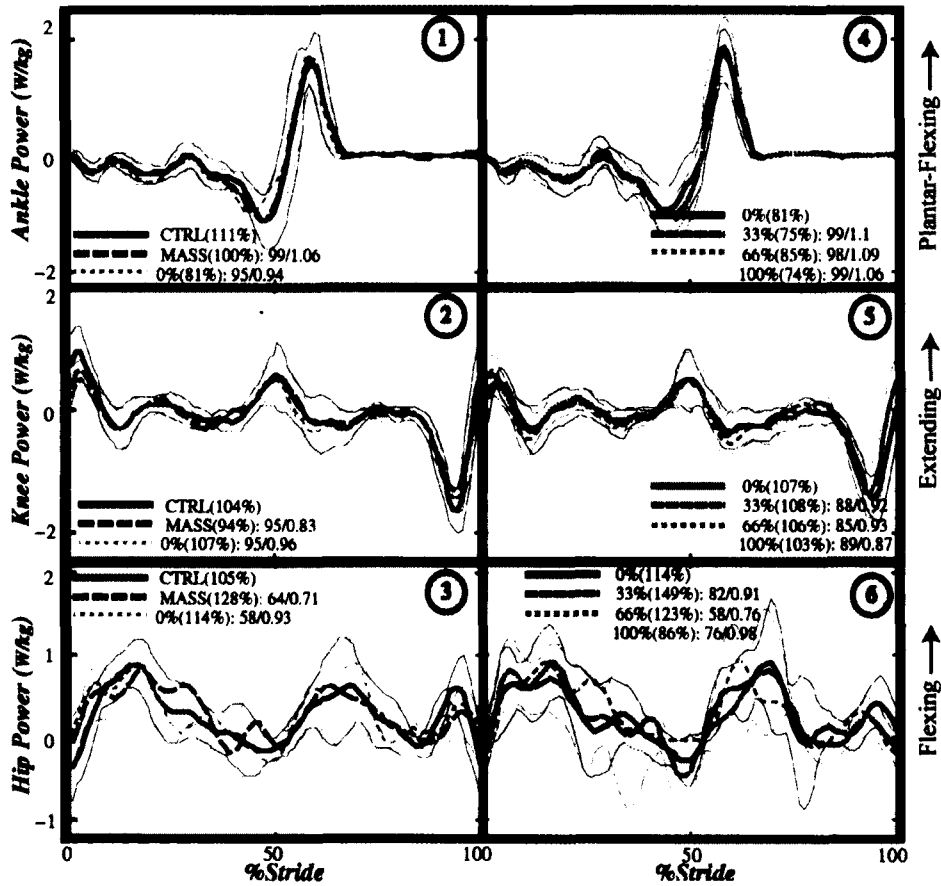


Figure 4-13. Inter-subject mean power profiles. We have separately indicated the first three conditions (CTRL, MASS, and 0%) in the left column and the assistance conditions (0% to 100%) in the right column. The thick solid lines indicate the inter-subject mean profiles and the thin lines boundaries defined by ± 1 SD. The legends of each graph report the CV of each profile in parentheses followed by the R^2 /Scale of the regression comparison. The values of R^2 /Scale for the MASS condition are presented with respect to CTRL condition, and 0% condition with respect to the MASS condition, whereas 33%, 66%, and 100% are with respect to 0%. On the bottom of each graph, a series of stripes are plotted that indicate the periods during which two profiles are significantly different. The stripe colors correspond to the profile with similar color. The comparison is made between MASS and CTRL, 0% and MASS, 33% and 0%, 66% and 0%, and 100% and 0%.

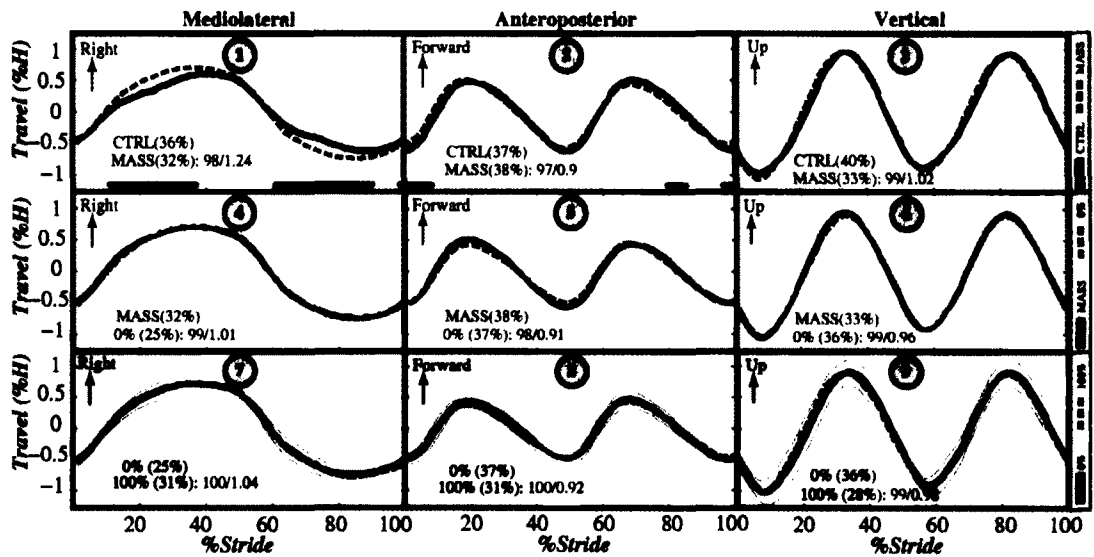


Figure 4-14. Inter-subject mean \pm SD profile of the travel of the body center of mass in mediolateral (left column), anteroposterior (middle column), and vertical (right column) direction. The first to third rows respectively include the profiles of the CTRL and MASS conditions, MASS and JOINT conditions, and JOINT and SPRING conditions. The stripe on the bottom of top left and top middle graph shows the period where the two profiles are significantly different. No other pair-wise comparison of profiles shows statistical differences. The shaded area in the third row shows the period where the exoskeleton spring was engaged.

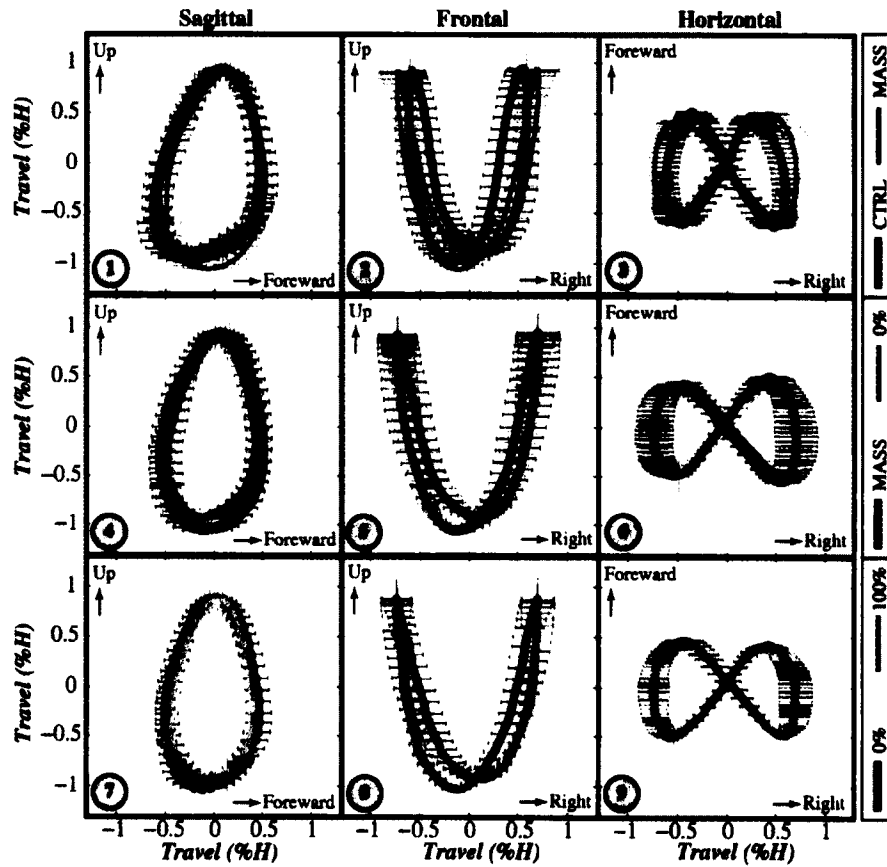


Figure 4-15. Inter-subject mean \pm SD trajectory of the body center of mass.

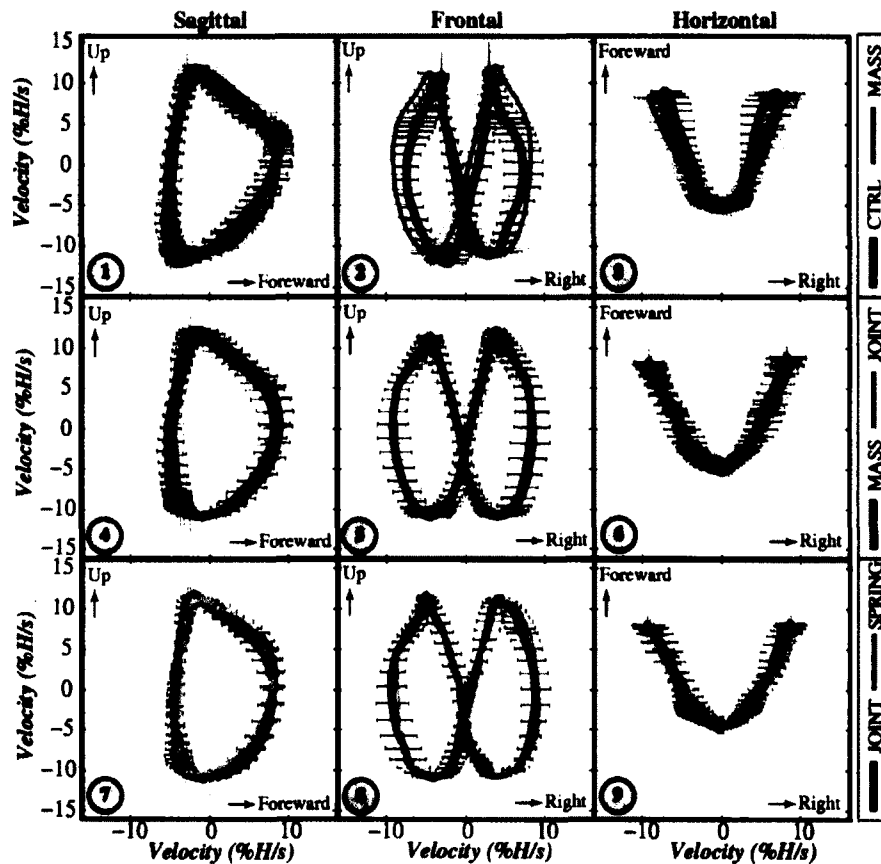


Figure 4-16. Inter-subject mean \pm SD velocity trajectory of the body center of mass.

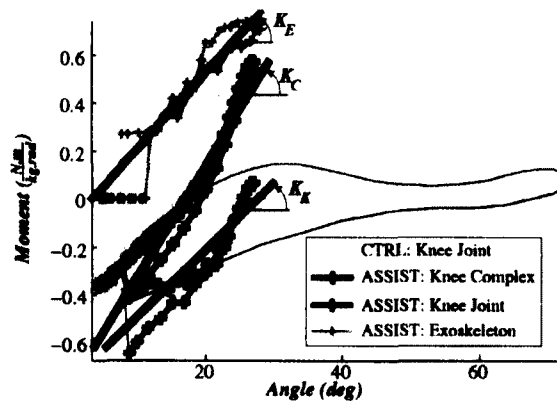


Figure 4-17. A sample moment-angle graph for one of the subjects. Two gait cycles are included: 1. Control condition (light gray circles), 2. Assistance condition (shown by crosses) that includes the graph of the knee complex, knee joint, and exoskeleton. The graph also includes the quasi-stiffness of the knee complex (K_c) and knee joint (K_k) in the weight acceptance phase as well as the stiffness of the exoskeleton (K_e).

4.3.6 Profile Comparison Measures

To compare the profiles, we performed pair-wise t-test between all 100 points of the profiles of CTRL and MASS, MASS and 0%, 0% and 33%, 0% and 66%, and 0% and 100% conditions which was also verified by false discovery rate control as explained elsewhere [79]. The angle and moment profiles of the conditions (similar pairs of conditions used for the t-test) were compared using linear regression between the inter-subject mean profiles in these two conditions, as explained elsewhere [10]. The R^2 value of the regression indicates the degree of similarity of the patterns, while the slope refers to the scaling factor. For example, a profile identical to the baseline profile would have a R^2 and a scale of 1; whereas, a down scaled profile (i.e. smaller range of values) with identical pattern would have $R^2=1$ and slope < 1 . One should note that the scale is not very meaningful when R^2 is relatively low.

4.3.7 Knee Complex Moment-Angle Analysis

In previous sections, we explained the method to calculate the knee complex and joint angles and moments for conditions 3-6 that include the exoskeleton. To obtain the quasi-stiffness of the knee complex (K_C) and knee joint (K_K), linear polynomials were respectively regressed on the moment-angle data of the knee complex and knee joint in the weight acceptance phase of the gait cycle (a sample moment-angle graph and the associated analysis are illustrated in Fig. 4-17). The slopes of the corresponding linear fits represented K_C and K_K , and the coefficient of determination (R^2) indicated the goodness of the fit representative of the linearity of the behavior of the knee complex and knee joint in the weight acceptance phase. K_K was subtracted from K_C to calculate K_P and equation (4-10) was used to calculate K_S . We also define θ_C as the excursion of the knee complex, θ_K the excursion of the knee joint, θ_E the excursion of the exoskeleton, and θ_S is the excursion of the interface. We subtracted the minimum angle from maximum angle of the knee complex in the weight acceptance phase to calculate θ_C and θ_K (Note that $\theta_C = \theta_K$). We similarly calculated θ_E by subtracting the minimum from maximum angles of the exoskeleton in the weight acceptance phase, and θ_S by subtracting θ_E from θ_C .

This study also aimed to investigate if and to what extent an external parallel spring can reduce the human knee joint moment in the weight acceptance phase of the gait. To address this question, the loading effort of the knee joint (M_K) and complex (M_C) were respectively defined as the sum of the moment profiles of the knee joint and knee complex in the weight acceptance phase. Parallel assistance (M_P) was defined as the sum of the parallel/exoskeletal moment profile in the weight acceptance phase of the gait. These parameters allowed us to investigate the overall effect of the exoskeleton assistance on the reduction of the knee moment throughout the weight acceptance phase of the gait. Finally, the mechanical work of the knee joint in the weight acceptance phase and the entire gait cycle were calculated as the area enclosed in the moment-angle graphs of the corresponding period. The aforementioned parameters are plotted in Fig. 4-18. One should note that the knee complex and knee joint were identical for CTRL and MASS conditions, due to the lack of external exoskeleton joints or stiffness in those conditions.

To study the effect of exoskeleton mass and articulation, a pair-wise comparison was performed between the values of quasi-stiffness, excursion, R^2 , work, and loading efforts of CTRL and MASS, and MASS and 0% conditions using t-test at a significance level of *0.05*. To study the effect of externally-applied stiffnesses, a one-way ANOVA was performed on the aforementioned parameters for conditions 0%, 33%, 66%, and 100% in addition to a post hoc t-test with Bonferroni correction leading to a significance level of *0.008*.

4.3.8 Locomotor Adaptation to Parallel Stiffness

We investigated locomotor adaptation of the knee joint to externally-applied parallel stiffnesses in terms of variations of: a. the quasi-stiffness of the knee joint and complex as functions of the parallel stiffness, and b. the loading efforts of the knee joint and complex as functions of the parallel assistance. These analyses included the entire gait cycles for the left and right sides for only the assistance trials (namely conditions 3-6 which correspond to 0% to 100% of the knee quasi-stiffness).

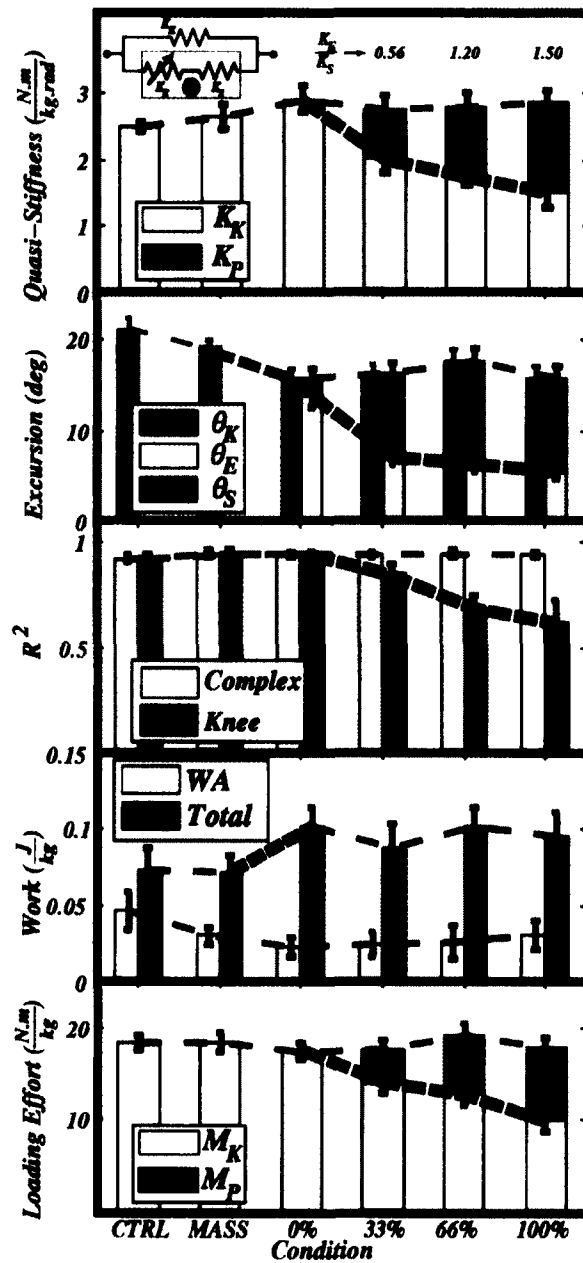


Figure 4-18. Inter-subject moment-angle analysis of the knee complex, joint, and exoskeleton in the sagittal plane. The first to fifth rows are respectively the quasi-stiffness, excursion, R^2 , work, and loading efforts in the weight acceptance phase.

The values of quasi-stiffnesses and loading efforts were normalized with respect to the intra-subject mean values for the 0% condition. To obtain the normalized quasi-stiffnesses of the knee joint (κ_K), the intra-subject mean value of K_K was first calculated for the 0% condition for each subject. Next, the values of K_K for conditions 3-6 were divided by the intra-subject mean of K_K for the corresponding subject as the baseline for that subject. Normalized quasi-stiffnesses of the knee complex (κ_C) were similarly calculated by dividing the values of K_C for conditions 3-6 by the intra-subject mean value of K_C in the 0% condition for each subject (Note that for $K_K = K_C$ condition 0%). The normalized parallel stiffness (κ_P) was also obtained by dividing K_P by the intra-subject mean value of K_K in the 0% condition for each subject. In a similar fashion, the normalized loading effort of the knee joint (\mathcal{M}_K) and complex (\mathcal{M}_C) were obtained by respectively dividing M_K and M_C by their intra-subject mean values in the 0% condition, and the normalized parallel assistance (\mathcal{M}_P) by dividing M_P for each gait cycle by the intra-subject mean values of M_K in the 0% condition for each subject.

Lastly, the normalized knee joint and complex quasi-stiffnesses (κ_K and κ_C) were plotted with respect to the normalized external parallel stiffness (κ_P), and the normalized loading efforts of the knee joint and complex (\mathcal{M}_K and \mathcal{M}_C) with respect to the normalized exoskeleton assistance (\mathcal{M}_P). The theoretical equations (4-3) and (4-4) were also plotted on the corresponding graphs to compare with the experimental values, as appears in Fig. 4-19.

4.3.9 Calculation of Mechanical and Metabolic Power

Average Metabolic Power: The rate of oxygen uptake was used to calculate the average metabolic power as [80]:

$$P_{met} = 21 \dot{V}O_2' / W \quad (4-12)$$

The metabolic cost of transport (COT) was calculated as [12,72]:

$$COT = \frac{P_{met}}{w.v} = 20.1 \frac{\dot{V}O_2}{w.v} \quad (4-13)$$

Average Positive Power: For each gait cycle, the average positive power of each lower extremity joint and exoskeleton ($i = \{H: \text{Hip}, K: \text{Knee}, \text{and } A: \text{Ankle}\}$) was calculated as [12]:

$$\bar{P}_i^+ = \frac{W_i^+}{T} \quad (4-14)$$

where, T is the duration of the gait cycle and W_i^+ is the positive mechanical work that was calculated using the following equation:

$$W_i^+ = \int P_i^+(t) dt \quad (4-15)$$

Here, P_i^+ is:

$$P_i^+(t) = \begin{cases} P_i(t) & \text{if } P_i(t) > 0 \\ 0 & \text{if } P_i(t) \leq 0 \end{cases} \quad (4-16)$$

where $P_i(t)$ is the power in the sagittal plane at instant t . The total average positive mechanical power (\bar{P}_T^+) was calculated as the summation of the positive power of the hip, knee, and ankle joints. The efficiency of positive power was calculated as:

$$\bar{E} = \frac{\bar{P}_T^+}{P_{met}} \quad (4-17)$$

Average Rate of Positive Moment Generation: Average positive rate of moment generation of a lower extremity joint and exoskeleton (\bar{M}_i^+) was calculated as:

$$\bar{M}_i^+ = \int \dot{M}_i^+(t) dt / T \quad (4-18)$$

where:

$$\dot{M}_i^+(t) = \begin{cases} \frac{dM_i}{dt} & \text{if } \frac{dM_i}{dt} > 0 \\ 0 & \text{if } \frac{dM_i}{dt} \leq 0 \end{cases} \quad (4-19)$$

where, $M_i(t)$ is the moment of the joint/exoskeleton in the sagittal plane at instant t .

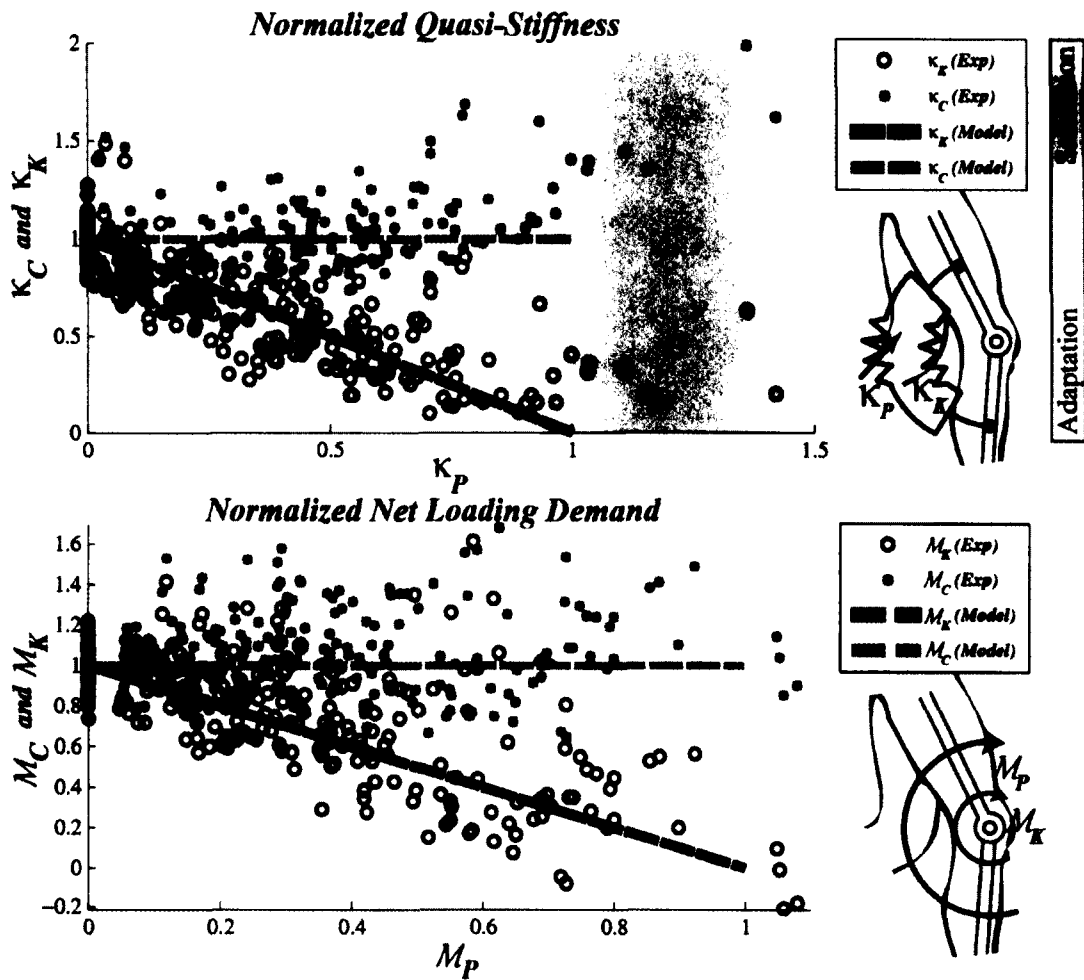


Figure 4-19. Top: Normalized quasi-stiffness of the knee complex and joint with respect to the normalized parallel stiffness. The knee joint adaptation shows saturation to parallel stiffnesses starting at ~80% of the knee quasi-stiffnesses. Bottom: Normalized loading effort of the knee complex and joint with respect to normalized parallel assistance. The knee joint shows full adaptation to the parallel assistive moments.

The means and SD of \bar{M}_i^+ , \bar{P}_i^+ , P_{met} , \bar{E} , and COT were calculated and shown across the conditions in Fig. 4-20 to 22. The effects of exoskeleton assistance on these parameters were investigated using one-way ANOVA across the conditions as well as a post hoc t-test with Bonferroni correction that resulted in a *p-value* of 0.008. To inspect potential correlation between the metabolic cost and the moment generation rate and mechanical work, we plotted P_{met} with respect to \bar{M}_K^+ and \bar{P}_K^+ , and applied linear regression for each trial, as shown in Fig. 4-23.

4.4 Kinematic and Kinetic Profiles

Fig. 4-11 to 13 respectively include the inter-subject mean angle, moment, and power profiles for the lower extremity joints in the sagittal plane. In Fig. 4-11 to 13, the left column include CTRL, MASS, and 0% conditions, and the right column include 0% to 100% conditions. The inter-subject mean travel profiles of the COM along the vertical, mediolateral, and anteroposterior axes are plotted in Fig. 4-14. Additionally, travel and velocity trajectories of the COM were plotted for the sagittal, frontal, and horizontal planes in Fig. 4-15 and 16. It was found that the motion patterns of the COM were invariant under the effect of the exoskeleton stiffness allowing us to exclude conditions 33% and 66% from Fig. 4-14 to 16, for the sake of simplicity.

4.4.1 Effects of Exoskeleton Mass

The values of $R^2 = 100\%$ and $Scale = 0.99$ to 1.07 for the angle profiles in Fig. 4-11 (graph 1-3) show that the exoskeleton mass did not notably change the overall kinematic patterns of gait in the sagittal plane. However, the exoskeleton mass resulted in a significantly more extended knee in the terminal stance phase and more flexed knee at the heel contact with the ground (notice the dark gray stripes on graph 3), which is in agreement with our previous results [34]. The values

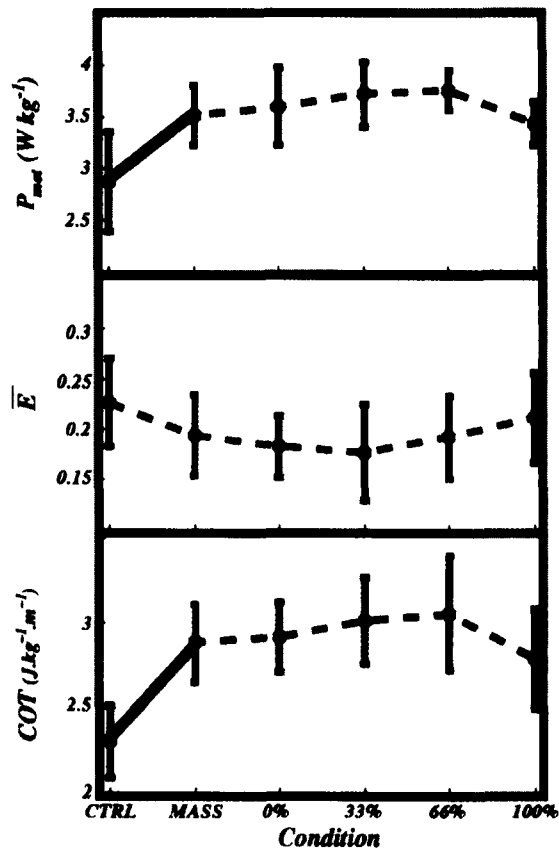


Figure 4-20. Mean \pm SD of metabolic power, efficiency of positive work, and cost of transport across the conditions. Solid lines between conditions indicate statistically significant differences.

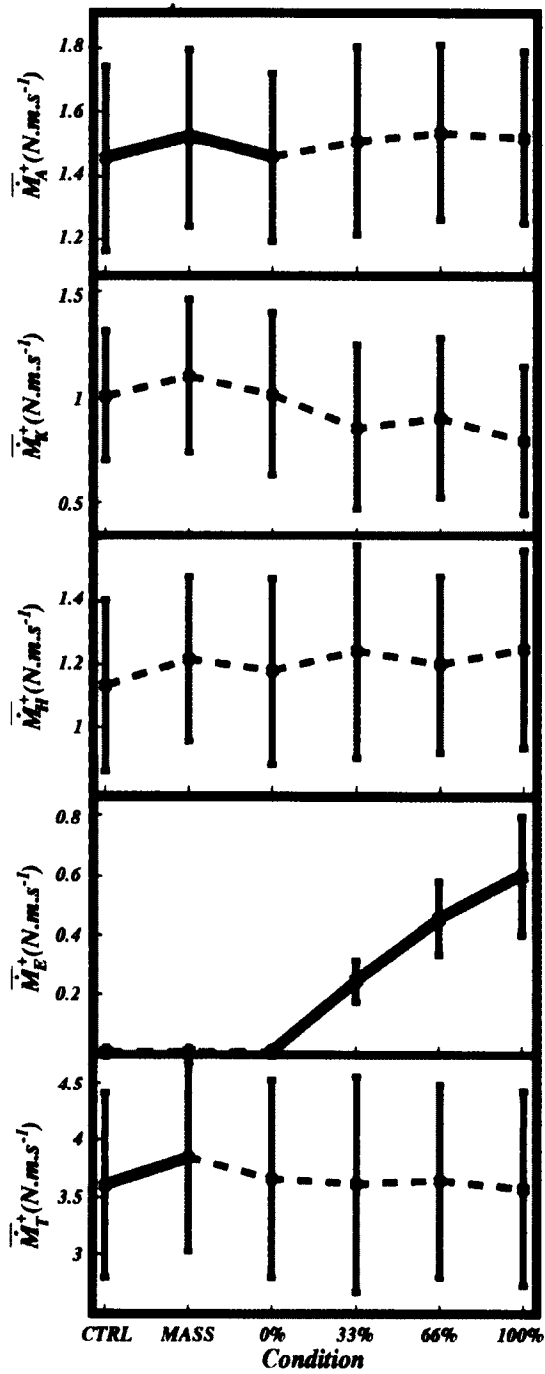


Figure 4-21. Mean \pm SD of average positive rate of moment generation for the ankle joint, knee joint, hip joint, exoskeleton, and total respectively from top to bottom across the conditions. Solid lines between conditions indicate statistically significant differences.

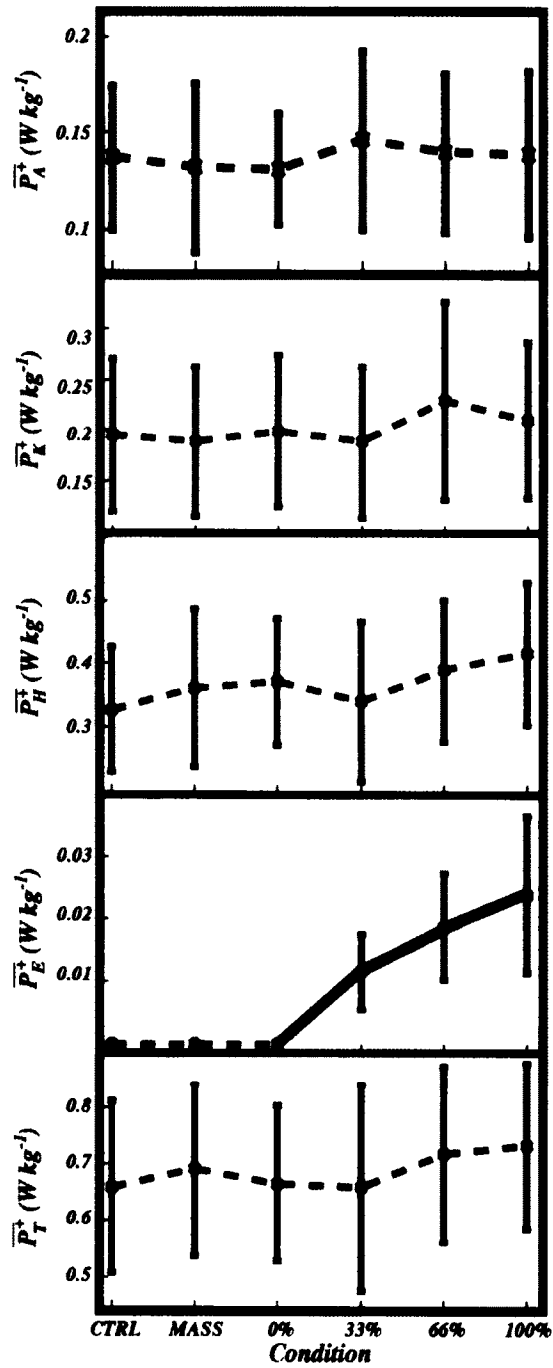


Figure 4-22. Mean \pm SD of average positive power for the ankle joint, knee joint, hip joint, exoskeleton, and total respectively from top to bottom across the conditions. Solid lines between conditions indicate statistically significant differences.

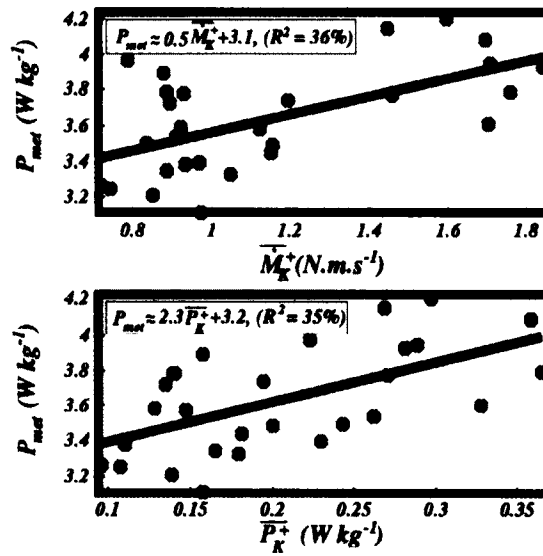


Figure 4-23. Average positive rate of moment generation (top) and average positive power (bottom) with respect to the metabolic power. The graphs also include linear fits that show significant correlation ($p < 0.01$ for the coefficients of the fit) between the parameters.

of $R^2 = 99\%$ to 100% and $Scale = 1.05$ to 1.11 for the moment profiles in Fig. 4-12 (graphs 1-3) show that the exoskeleton mass did not notably change the moment profiles patterns in the sagittal plane but led to a slight overall upscale in the moment profiles. The exoskeleton mass did not significantly change the power profiles of the joints, as shown in Fig. 4-12 (Graphs 1-3); yet, it resulted in an increase in the range of hip power values ($Scale = 1.06$), but a decrease in the range of knee ($Scale = 0.83$) and ankle ($Scale = 0.73$) values. It is observed in Fig. 4-14 (Graphs 1-3) that the exoskeleton mass was the major contributor to the changes in the motion of the COM with the most changes along the mediolateral direction. It is also observed in Fig. 4-15 and 16 (Graphs 1-3) that the motion and velocity trajectories of the COM mediolaterally extended under the effect of the exoskeleton mass. Interestingly, the motion of the COM along the vertical direction remained invariant under the effect of the exoskeleton mass.

4.4.2 Effects of Exoskeleton Articulations

The values of $R^2 = 99\%$ and $Scale = 0.98$ to 1.00 for the angle profiles in Fig. 4-11 (graphs 1 to 3) show that the kinematic constraint imposed by the exoskeleton articulation did not notably affect the knee angle patterns and profiles in the sagittal plane. However, the knee joint was significantly more extended during the heel contact and terminal stance phase (notice the light gray stripes on graph 2). The values of $R^2 = 98\%$ to 99% and $Scale = 0.93$ to 1 for the moment profiles of the hip and ankle joints in Fig. 4-12 (graphs 1 to 3) show that the exoskeleton articulation does not notably affect the moment patterns of the hip and ankle but led to an overall downscale in the knee moment profile. Particularly, the moment profile of the knee complex did not show a pattern change ($R^2 = 98\%$), but showed a notable downscale ($Scale = 0.93$) under the effect of the exoskeleton articulation. The exoskeleton joint did not significantly change the power profiles of the joints, as shown in Fig. 4-13 (Graphs 1-3). It is observed in Fig. 4-14 to 16 (Graphs 4-6) that the exoskeleton joint did not cause significant changes in the motion and trajectories of the COM.

4.4.3 Effects of Exoskeleton Stiffness

The values of $R^2=99\%$ to 100% for the ankle and hip angle and moment profiles for conditions 33%, 66%, and 100% in Fig. 4-11 and 12 (graphs 4-6) show that the external assistance did not have a considerable effect on the overall kinematic and kinetic patterns for those joints in the sagittal plane. It is worth mentioning that the hip angle profile started to deviate from the baseline upon high exoskeletal stiffness (notice the light gray stripes on graph 6, left). The angle and moment profiles of the knee complex exhibited invariant overall patterns under the exoskeleton assistance ($R^2=98\%$ to 99%), with significant local variations in the angle profiles at the initial stance and terminal swing phase (notice the stripes on graph 5, left) and significant local variation in the moment profile at the initial swing phase (notice the stripes on graph 5, right). A slight downscale in the values of the angle profiles of the knee and hip in the sagittal plane were observed and an upscale in the values of the knee and hip moments were observed in the sagittal plane. The exoskeleton stiffness did not significantly change the power profiles of the joints, as shown in Fig. 4-13 (Graphs 4-6); yet, it resulted in an increase in the range of hip power values (*Scale = 1.06 – 1.10*), but a decrease in the range of knee (*Scale = 0.87-0.92*) and ankle (*Scale = 0.76-0.98*) values. It is observed in Fig. 4-14 to 16 (Graphs 7-9) that the exoskeleton stiffness did not cause significant changes in the motion and trajectories of the COM.

4.5 Effects of Exoskeleton Impedance on Moment-Angle Behavior of the Knee Joint

4.5.1 Moment-Angle Performance of the Knee Complex

Fig. 4-18 shows the parameters that explain inter-subject moment-angle behavior of the knee in the weight acceptance phase of gait. The first to fifth rows respectively include the quasi-stiffness, excursion, and R^2 of the weight acceptance phase, the mechanical work of the weight acceptance phase and entire gait cycle, and the loading efforts of the weight acceptance phase. The dashed lines illustrate the trends and the thick trend lines indicate those values that are

statistically different from the baseline measure according to the statistical comparison explained in section 4.6.

Quasi-Stiffness: The inter-subject mean and SD of the knee joint quasi-stiffness (K_K) and parallel stiffness (K_P) in the weight acceptance phase of gait are shown in the first row of Fig. 4-18. A non-significant increase in the quasi-stiffness of the knee complex (K_C) was observed as a result of the exoskeleton mass, and a non-significant increase in K_C as a result of the kinematic constraints imposed by the exoskeleton articulations was observed. K_C remained invariant across the assistance conditions. However, a significant ($p < 0.008$) decrease in the knee joint quasi-stiffness relative to the 0% condition was observed for each level of exoskeletal assistance (33%, 66% and 100%).

Excursion: The inter-subject mean and SD of the knee joint excursion (θ_K), exoskeleton excursion (θ_E), and soft tissue excursion (θ_S) in the weight acceptance phase of gait are shown in the second row of Fig. 4-18. A non-significant decrease in θ_K was observed in MASS condition relative to CTRL condition and a significant decrease was observed for the knee excursion in 0% condition relative to MASS condition ($p < 0.05$). The knee excursion remained relatively constant across the different assistance conditions. However, θ_E significantly decreased with exoskeleton assistance (33%, 66%, and 100%) as compared to the 0% condition ($p < 0.008$).

Linearity of the Knee Behavior: The inter-subject mean and SD of the R^2 values for the linear fits to the moment-angle graphs of the knee complex and knee joint in the weight acceptance phase of gait are shown in the third row of Fig. 4-18. There was no significant change in R^2 values for the knee complex across all of the conditions, implying that the overall behavior of the knee complex remained linear. However, a significant reduction ($p < 0.008$) in R^2 values was observed for the knee joint across the assistance conditions (33%, 66% and 100%) relative to the 0% condition, implying that the moment-angle behavior of the knee joint becomes less linear with external assistance.

Mechanical Work: The inter-subject mean and SD of the knee joint mechanical work in the weight acceptance phase and throughout the entire gait cycle are shown in the fourth row of Fig. 4-18. No significant changes in the mechanical work of the knee joint in the weight acceptance phase and throughout the gait cycle were observed; except a significant increase ($p < 0.05$) in the gait phase work was observed for the 0% condition as compared to the MASS condition.

Loading Effort: The inter-subject mean and SD of the loading efforts of the knee joint and complex as well as the exoskeleton assistance are shown in the fifth row of Fig. 4-18. A significant ($p < 0.008$) decrease in the loading effort of the knee joint was observed with the exoskeletal assistance conditions as compared to the 0% condition. The values of M_C (equal to $M_K + M_P$) do not exhibit a notable change across the different conditions.

4.5.2 Adaptation of Knee Moment and Quasi-Stiffness

Fig. 4-19-top shows the graph of normalized quasi-stiffness of the knee joint and complex (κ_K and κ_C) with respect to the normalized parallel stiffness (κ_P). Fig. 4-19-bottom shows the graph of normalized loading effort of the knee joint and complex (\mathcal{M}_K and \mathcal{M}_C) with respect to the normalized parallel assistance (\mathcal{M}_P). The theoretical models explained by equations (4-3) and (4-4) are also plotted on each graph (dashed lines). According to these equations, the quasi-stiffness of the knee complex would remain invariant as the parallel stiffness increases due to an equal decrease in the quasi-stiffness of the knee joint. These equations predict a similar behavior for the knee joint and complex loading efforts. Fig. 4-19 only includes the gait cycle data for the assistance conditions 0% to 100%.

As seen in Fig. 4-19, the theoretical models are in close agreement with the trends of the experimental values of κ_K and κ_C . Starting at $\kappa_P = \sim 0.8$, however, the experimental values start to deviate from the theoretical models; in that, κ_K tends to remain relatively constant and κ_C tends to increase. In contrast, the experimental values of \mathcal{M}_K and \mathcal{M}_C appear to follow the theoretical models throughout the range of experimental values of \mathcal{M}_P .

4.6 Effects of Exoskeleton Impedance on Gait Energetics

4.6.1 Metabolic Power

The inter-subject means \pm SD of P_{met} , \bar{E} , and COT are shown in Fig. 4-20 across the experimental conditions. The solid lines show significant trends; whereas, the dashed lines only help observe the trends. It can be observed that P_{met} and COT significantly increased as a result of the exoskeleton mass. The exoskeleton mass, joint, and assistance did not result in a significant change in \bar{E} . It is observed that the exoskeleton assistance did not significantly affect P_{met} , \bar{E} , and COT . Comparing 0% and 100% conditions, the exoskeleton assistance non-significantly reduced P_{met} by 5%; however, the exoskeleton assistance did not reduce the metabolic cost of walking when comparing 100% and CTRL conditions.

4.6.2 Determinants of Metabolic Power

The inter-subject means \pm SD of \bar{M}_i^+ and \bar{P}_i^+ ($i = \{\text{ankle joint, knee joint, hip joint, exoskeleton, and total}\}$) are shown in Fig. 4-21 and 22 across the experimental conditions. The solid lines show significant trends; whereas, the dashed lines only help observe the trends. The exoskeleton mass resulted in significant increase in \bar{M}_A^+ ($p < 0.03$) and \bar{M}_T^+ ($p < 0.04$), and the exoskeleton joint resulted in significant decrease in \bar{M}_A^+ ($p < 0.04$). Other trends of \bar{M}_i^+ and \bar{P}_i^+ were non-significant. Particularly, the exoskeleton assistance caused a mild noticeable reduction in \bar{M}_K^+ , which is non-significant.

Fig. 4-23 includes the graphs of P_{met} with respect to \bar{M}_K^+ and \bar{P}_K^+ as well as first order polynomials fitted to the data. The coefficients of the polynomials are significantly different than zero ($p < 0.05$) indicating that P_{met} has significant correlations with both \bar{M}_K^+ ($R^2=36\%$) and \bar{P}_K^+ ($R^2=35\%$).

4.7 Conclusions and Future Work

In this chapter, we described a quasi-passive knee exoskeleton that implements a spring with a desired stiffness in parallel with the knee joint in the weight acceptance phase of the gait cycle where the knee behaves close to a linear torsional spring. Using a pair of the exoskeletons in a series of experiments on healthy adults, we experimentally studied motor adaptation in lower extremity joints to externally-applied stiffnesses in parallel with the knee joint during the weight acceptance phase of gait. The experiments included treadmill walking with exoskeletons with four levels of stiffness, which were roughly equal to 0%, 33%, 66% and 100% of the knee quasi-stiffness, in parallel with the knee joint during the stance phase as well as walking with the replicas of the exoskeletons. The experimental results revealed that the lower extremity joints demonstrate substantial adaptation to parallel stiffnesses leading to invariant kinematic and kinetic patterns. The exoskeleton mass did not impose notable disturbance on the moment and angle patterns but resulted in an overall higher range of moments. The exoskeleton articulation was found to impose inconsequential kinematic and kinetic constraints on the overall angle and moment patterns, implying that a simple uniaxial hinge joint can be a viable design choice for knee exoskeletons. The exoskeleton mass, articulation, and stiffness were mostly found to locally affect the knee joint moment and angle profiles around the initial and terminal stance as well as terminal swing phase.

A detailed analysis of the knee joint moment-angle during the weight acceptance phase of gait revealed that the knee joint quasi-stiffness adapts to externally applied stiffnesses such that the overall stiffness of the complex of the knee joint and exoskeleton remains invariant; a behavior that was also observed for the knee complex moments. It was also observed that the exoskeleton assistance nonlinearized the moment-angle behavior of the knee joint as R^2 values decreased as exoskeleton assistance increased; whereas, the overall moment-angle behavior of the knee complex remained linear with R^2 values abiding near 1 in all experimental conditions. This suggests that the human body prefers to experience a linear behavior at the knee joint during the

weight acceptance phase, which could be associated with higher rates of energy recovery [34,51]. The exoskeleton stiffness did not have a significant effect on the mechanical work of the knee joint in the weight acceptance phase implying that the adaptation to the exoskeletal stiffnesses does not necessitate additional mechanical work.

The analysis of the adaptation in knee joint quasi-stiffness to parallel stiffnesses showed that the knee joint exhibits smaller quasi-stiffnesses in the presence of a parallel stiffness such that the overall stiffness remains invariant. This quasi-stiffness adaptation saturates when the parallel stiffness reaches ~80% of natural knee quasi-stiffness, after which the knee joint quasi-stiffness remains relatively constant and a further increase in the parallel quasi-stiffness causes an increase in the overall quasi-stiffness. Furthermore, it was observed that the loading effort of the knee joint and knee complex show complete adaptation to parallel assistance suggesting that the knee joint can fully accommodate external assistance. Therefore, *the knee joint can well accommodate a parallel spring with a wide range of stiffnesses up to ~80%, after which the parallel spring still provides assistance but the knee complex stiffness increases above the normal rate.* This finding also strengthens the assumption that *the knee joint can be theoretically modeled by a linear torsional spring in the weight acceptance phase of the gait.* The saturation of the quasi-stiffness adaptation could be attributable to existence of bi-articular muscles leading us to speculate that the exoskeletal assistance can only unload the mono-articular muscles. Future research is needed to investigate this hypothesis through analysis of the EMG signals of mono-articular and biarticular muscles.

The findings of this research can give insight to the design of exoskeletons/orthoses for lower extremity joints (specifically the knee joint). Replication of the moment-angle behavior of the lower extremity joints by an exoskeletal device can be a viable strategy to assist and unload these joints. The compliance of the biological soft tissues of the leg as well as the interface components of the exoskeleton can neutralize the assistance of the exoskeletons. This is especially true for exoskeletons attached to the thighs, due to the large amount of soft tissue located at those

segments. Therefore, the design of exoskeletons should minimize the effect of the soft tissues with additional considerations such as larger pads and more carefully chosen strap locations. Moreover, the control algorithm of the exoskeletons should not solely rely on the angular movement of the exoskeleton, which could be disturbed by the excursion of the soft tissues.

The exoskeleton uniaxial joint did not substantially perturb the gait patterns implying that a uniaxial joint can be a suitable choice in the design of knee exoskeletons. The kinematic constraints imposed by the exoskeletons joint resulted in a slightly more flexed knee at the heel strike, which could be a result of limited range of motion of the exoskeleton joints (as fabrication imperfection), as was reported by the participants for the left exoskeleton. The exoskeleton mass caused an upscale in the range of joint moments suggesting that minimization of the exoskeleton mass should be a main goal in the design of exoskeletons. The knee joint complex behaved linearly under all six conditions implying that the human body prefers to experience a linear behavior at the knee complex. This preferred linear behavior may be related to the energetics of gait, damping function of the knee, or preferred gait speed [34,81-83]. Regardless of the reason, a knee exoskeleton should ideally demonstrate a linear behavior in the weight acceptance phase of gait.

The current study necessitated several assumptions. The reflective markers of the study were mounted on the skin of the volunteer; hence, the kinematic profiles of the knee complex and anatomical joint are assumed to be identical. Moreover, the exoskeleton moment was calculated by equation (4-8). Alternatively, load cells could have been implemented in the exoskeletons to directly measure the exoskeleton moment; a method that was avoided in the current study in order to minimize the exoskeleton mass and experimental complications. The exoskeleton was suspended from the shoulders using a pair of suspension harnesses to limit the vertical migration of the exoskeleton. These suspension straps may have caused confounding factors in the results and affected the kinetic and kinematic behavior of the joints.

To carry out the inverse dynamics analysis, several assumptions were made. The knee joint and exoskeleton were considered one single joint. Despite the independence of the inverse dynamics analysis of the morphology of the joints, this assumption can have nuisance effects on the joint center estimations and the calculations of the kinetic profiles. The exoskeleton moment of inertia and center of mass were obtained from a computer-aided design (CAD) model of the exoskeleton and exoskeleton replica, which ignores the effect of small movements of the exoskeleton with respect to limbs and slight differences between the actual device and the computer models. Furthermore, it should be noted that as the exoskeletal stiffness increased the knee joint behavior became less linear (lower R^2 values, Fig. 4-18), which could make the calculations of the knee joint quasi-stiffness less accurate and the linear models of equations (4-3) and (4-4) less accurate.

The knee joint levels of quasi-stiffness in the 33%, 66%, and 100% conditions were estimated using a previously developed statistical model, because a priori knowledge of the natural knee quasi-stiffness of each volunteer was not available [3,51]. The estimation models were developed in previous studies for the design of lower extremity orthoses and prostheses [51,61,62]. Table 4-2 lists the knee quasi-stiffness of each volunteer for the CTRL condition as calculated using the moment-angle data, which shows that the values estimated using the models are different from the experimental values. This inaccuracy was addressed by normalizing the quasi-stiffness of each assistance level (0%, 33%, 66%, and 100%) by the natural knee stiffness measured during the 0% condition for each volunteer in the analysis of motor adaptation presented in Fig. 4-19.

To study adaptation in the knee joint moment, we examined the correlation between the loading effort, which is the summation of the knee joint moments and knee complex moments during the weight acceptance phase, and parallel assistance, which is the summation of the exoskeleton moments during the weight acceptance phase. Alternatively, we could only investigate the maximum moment of the knee joint and complex in the weight acceptance phase. However, for some of the trials we observed that the exoskeletons springs disengaged before the

end of the weight acceptance phase of gait depending on the gait patterns and timing of the toe and heel contact with the ground. Therefore, using the maximum moment of the knee joint and complex would not have given a complete picture of the effect of the exoskeleton assistance on the knee joint loading effort throughout the weight acceptance phase.

This research also includes the effects of the assistance provided by the exoskeletons on the energetics of walking. It was found that the exoskeleton assistance did not significantly reduce the metabolic power of walking and the major contributor to the increase in the metabolic power of walking was the exoskeleton mass. We considered the average positive rate of moment generation (as an indicator of force generation of the muscles) and positive power as two determinants of the metabolic cost of walking, as suggested by others [12,72-76]. We found that the metabolic power is correlated with both positive rate of moment generation and average positive mechanical power. This finding is in agreement with findings of research regarding exoskeletal augmentation of the ankle during gait [12,76]. Considering that the knee joint generates negligible mechanical work during the weight acceptance phase, the findings of this research suggest that reducing the rate of moment generation can be a viable method in the design of augmenting exoskeletons to reduce the metabolic power of walking.

As future steps for this research, we intend to investigate the EMG activities of the muscles adjacent to the knee joint and analyze the performance of both mono-articular and bi-articular muscles in interaction with the exoskeletons. We also intend to analyze the behavior of the adjacent joints (i.e. ankle and hip) under the effect of assistance to the knee joint to examine the locality of the external stiffness effects. This research could also be extended to other joints, different periods of the gait cycle, and different regimes of locomotion.

REFERENCES

1. Dollar A, Herr H (2008) Lower extremity exoskeletons and active orthoses: challenges and state-of-the-art. *IEEE Transactions on Robotics* 24: 144-158.

2. Dollar A, Herr H, Chatila R, Kelly A, Merlet J (2008) Design of a quasi-passive knee exoskeleton to assist running. *Proceedings of the 2008 IEEE/RSJ International Conference on Robots and Intelligent Systems (IROS)*: 747-754.
3. Shamaei K, Napolitano P, Dollar A (2013) A quasi-passive compliant stance control knee-ankle-foot orthosis. *Proceedings of the IEEE International Conference on Rehabilitation Robotics (ICORR)*. Seattle, USA.
4. Gregorczyk K, Hasselquist L, Schiffman J, Bensek C, Obusek J, et al. (2010) Effects of a lower-body exoskeleton device on metabolic cost and gait biomechanics during load carriage. *Ergonomics* 53: 1263-1275.
5. Ronsse R, Lenzi T, Vitiello N, Koopman B, van Asseldonk E, et al. (2011) Oscillator-based assistance of cyclical movements: model-based and model-free approaches. *Medical & Biological Engineering & Computing* 49: 1173-1185.
6. Walsh C, Endo K, Herr H (2007) A quasi-passive leg exoskeleton for load-carrying augmentation. *International Journal of Humanoid Robotics* 4: 487-506.
7. Kazerooni H, Steger R, Huang L (2006) Hybrid control of the Berkeley lower extremity exoskeleton (BLEEX). *International Journal of Robotics Research* 25: 561-573.
8. Aguirre-Ollinger G, Colgate J, Peshkin M, Goswami A (2011) Design of an active one-degree-of-freedom lower-limb exoskeleton with inertia compensation. *International Journal of Robotics Research* 30: 486-499.
9. Wehner M, Quinlivan B, Aubin P, Martinez-Villalpando E, Baumann M, et al. (2013) A lightweight soft exosuit for gait assistance. *Proceedings of the IEEE International Conference on Robotics and Automation (ICRA)*. pp. 3362-3369.
10. Kao P, Lewis C, Ferris D (2010) Invariant ankle moment patterns when walking with and without a robotic ankle exoskeleton. *Journal of Biomechanics* 43: 203-209.
11. Agrawal S, Banala S, Fattah A, Sangwan V, Krishnamoorthy V, et al. (2007) Assessment of motion of a swing leg and gait rehabilitation with a gravity balancing exoskeleton. *IEEE Transactions on Neural Systems and Rehabilitation Engineering* 15: 410-420.
12. Farris D, Sawicki G (2012) Linking the mechanics and energetics of hopping with elastic ankle exoskeletons. *J Appl Physiol* 113: 1862-1872.

13. Elliott G, Sawicki G, Marecki A, Herr H (2013) The biomechanics and energetics of human running using an elastic knee exoskeleton. Proceedings of IEEE Conference on Rehabilitation Robotics (ICORR). Seattle, USA.
14. Cherry M, Choi D, Deng K, Kota S, Ferris D (2006) Design and fabrication of an elastic knee orthosis: preliminary results. Proceedings of IDETC/CIE ASME 2006 International Design Engineering Technical Conferences & Computers and Information in Engineering Conference. Philadelphia, USA.
15. Grabowski A, Herr H (2009) Leg exoskeleton reduces the metabolic cost of human hopping. *Journal of Applied Physiology* 107: 670-678.
16. Sawicki G, Domingo A, Ferris D (2006) The effects of powered ankle-foot orthoses on joint kinematics and muscle activation during walking in individuals with incomplete spinal cord injury. *Journal of Neuroengineering and Rehabilitation* 3.
17. Ferris D, Bohra Z, Lukos J, Kinnaird C (2006) Neuromechanical adaptation to hopping with an elastic ankle-foot orthosis. *Journal of Applied Physiology* 100: 163-170.
18. Roy A, Krebs H, Williams D, Bever C, Forrester L, et al. (2009) Robot-aided neurorehabilitation: A novel robot for ankle rehabilitation. *IEEE Transactions on Robotics* 25: 569-582.
19. Kao P, Lewis C, Ferris D (2010) Short-term locomotor adaptation to a robotic ankle exoskeleton does not alter soleus Hoffmann reflex amplitude. *Journal of Neuroengineering and Rehabilitation* 7: 33.
20. Eilenberg M, Geyer H, Herr H (2010) Control of a powered ankle-foot prosthesis based on a neuromuscular model. *IEEE Transactions on Neural Systems and Rehabilitation Engineering* 18: 164-173.
21. Jezernik S, Colombo G, Morari M (2004) Automatic gait-pattern adaptation algorithms for rehabilitation with a 4-DOF robotic orthosis. *IEEE Transactions on Robotics and Automation* 20: 574-582.
22. Marchal-Crespo L, Reinkensmeyer D (2009) Review of control strategies for robotic movement training after neurologic injury. *Journal of Neuroengineering and Rehabilitation* 6.
23. Ferris D, Sawicki G, Domingo A (2005) Powered lower limb orthoses for gait rehabilitation. *Topics in spinal cord injury rehabilitation* 11: 34.

24. Ferris D, Farley C (1997) Interaction of leg stiffness and surface stiffness during human hopping. *Journal of Applied Physiology* 82: 15-22.
25. Ortega J, Farley C (2005) Minimizing center of mass vertical movement increases metabolic cost in walking. *Journal of Applied Physiology* 99: 2099-2107.
26. Choi J, Bastian A (2007) Adaptation reveals independent control networks for human walking. *Nature Neuroscience* 10: 1055-1062.
27. Roy A, Krebs H, Patterson S, Judkins T, Khanna I, et al. (2007) Measurement of human ankle stiffness using the anklebot. *IEEE 10th International Conference on Rehabilitation Robotics*. pp. 356-363.
28. Browning R, Modica J, Kram R, Goswami A (2007) The effects of adding mass to the legs on the energetics and biomechanics of walking. *Medicine and Science in Sports and Exercise* 39: 515-525.
29. Royer T, Martin P (2005) Manipulations of leg mass and moment of inertia: Effects on energy cost of walking. *Medicine and Science in Sports and Exercise* 37: 649-656.
30. Birn-Jeffery A, Daley M (2012) Birds achieve high robustness in uneven terrain through active control of landing conditions. *Journal of Experimental Biology* 215: 2117-2127.
31. van Hedel H, Biedermann A, Erni T, Dietz V (2002) Obstacle avoidance during human walking: transfer of motor skill from one leg to the other. *Journal of Physiology-London* 543: 709-717.
32. Farley C, Houdijk H, Van Strien C, Louie M (1998) Mechanism of leg stiffness adjustment for hopping on surfaces of different stiffnesses. *Journal of Applied Physiology* 85: 1044-1055.
33. Kerdok A, Biewener A, McMahon T, Weyand P, Herr H (2002) Energetics and mechanics of human running on surfaces of different stiffnesses. *Journal of Applied Physiology* 92: 469-478.
34. Shamaei K, Dollar A (2011) On the mechanics of the knee during the stance phase of the gait. *Proceedings of IEEE International Conference on Rehabilitation Robotics (ICORR)*. Zurich, Switzerland.

35. Shamaei K, Cenciarini M, Dollar A (2011) On the mechanics of the ankle in the stance phase of the gait. *Proceedings of the IEEE Annual International Conference of Engineering in Medicine and Biology Society (EMBC)*. Boston, USA. pp. 8135-8140.
36. Shamaei K, Cenciarini M, Adams A, Gregorczyk K, Schiffman J, et al. (2014) Design and Evaluation of a Quasi-Passive Knee Exoskeleton for Investigation of Motor Adaptation in Lower Extremity Joints. *Biomedical Engineering, IEEE Transactions on PP*: 1-1.
37. Shamaei K, Napolitano PC, Dollar AM (2014) Design and Functional Evaluation of a Quasi-Passive Compliant Stance Control Knee-Ankle-Foot Orthosis. *Neural Systems and Rehabilitation Engineering, IEEE Transactions on* 22: 258-268.
38. Wiggin M, Sawicki G, Collins S (2011) An exoskeleton using controlled energy storage and release to aid ankle propulsion. *Proceedings of IEEE International Conference on Rehabilitation Robotics (ICORR)*. Zurich, Switzerland.
39. Lenzi T, Carrozza M, Agrawal S (2013) Powered hip exoskeletons can reduce the user's hip and ankle muscle activations during walking. *IEEE Transactions on Neural Systems and Rehabilitation Engineering*.
40. Colombo G, Joerg M, Schreier R, Dietz V (2000) Treadmill training of paraplegic patients using a robotic orthosis. *Journal of Rehabilitation Research and Development* 37: 693-700.
41. Veneman J, Kruidhof R, Hekman E, Ekkelenkamp R, Van Asseldonk E, et al. (2007) Design and evaluation of the LOPES exoskeleton robot for interactive gait rehabilitation. *IEEE Transactions on Neural Systems and Rehabilitation Engineering* 15: 379-386.
42. Irby S, Bernhardt K, Kaufman K (2005) Gait of stance control orthosis users: The dynamic knee brace system. *Prosthetics and Orthotics International* 29: 269-282.
43. Zacharias B, Kannenberg A (2012) Clinical benefits of stance control orthosis systems: An analysis of the scientific literature. *JPO: Journal of Prosthetics and Orthotics* 24: 2-7.
44. Blanchette A, Lambert S, Richards C, Bouyer L (2011) Walking while resisting a perturbation: Effects on ankle dorsiflexor activation during swing and potential for rehabilitation. *Gait & Posture* 34: 358-363.
45. Iida H, Yamamuro T (1987) Kinetic-analysis of the center of gravity of the human-body in normal and pathological gaits. *Journal of Biomechanics* 20: 987-995.

46. Crowe A, Schiereck P, Deboer R, Keessen W (1995) Characterization of human gait by means of body center-of-mass oscillations derived from ground reaction forces. *IEEE Transactions on Biomedical Engineering* 42: 293-303.
47. Orendurff M, Segal A, Klute G, Berge J, Rohr E, et al. (2004) The effect of walking speed on center of mass displacement. *Journal of Rehabilitation Research and Development* 41: 829-834.
48. Donelan J, Kram R, Kuo A (2002) Simultaneous positive and negative external mechanical work in human walking. *Journal of Biomechanics* 35: 117-124.
49. Tucker C, Ramirez J, Krebs D, Riley P (1998) Center of gravity dynamic stability in normal and vestibulopathic gait. *Gait & Posture* 8: 117-123.
50. Gregg R, Bretl T, Spong M (2010) A control theoretic approach to robot-assisted locomotor therapy. *49th IEEE Conference on Decision and Control (CDC)*: 1679-1686.
51. Shamaei K, Sawicki G, Dollar A (2013) Estimation of quasi-stiffness of the human knee in the stance phase of walking. *PLoS ONE* 8: e59993.
52. Perry J (1992) *Gait Analysis : Normal and Pathological Function*. Thorofare, NJ: SLACK. 524 p. p.
53. Rose J, Gamble J (2006) *Human Walking*. Philadelphia, PA: Williams & Wilkins.
54. Winter D (1991) *The Biomechanics and Motor Control of Human Gait : Normal, Elderly and Pathological*. Waterloo, Ont.: University of Waterloo Press. 143 p.
55. Mochon S, McMahon T (1980) Ballistic walking - an improved model. *Mathematical Biosciences* 52: 241-260.
56. Davis R, DeLuca P (1996) Gait characterization via dynamic joint stiffness. *Gait & Posture* 4: 224-231.
57. Stefanyshyn D, Nigg B (1998) Dynamic angular stiffness of the ankle joint during running and sprinting. *Journal of Applied Biomechanics* 14: 292-299.
58. Crenna P, Frigo C (2011) Dynamics of the ankle joint analyzed through moment-angle loops during human walking: gender and age effects. *Human Movement Science* 30: 1185-1198.

59. Frigo C, Crenna P, Jensen L (1996) Moment-angle relationship at lower limb joints during human walking at different velocities. *Journal of Electromyography and Kinesiology* 6: 177-190.
60. Lark S, Buckley J, Bennett S, Jones D, Sargeant A (2003) Joint torques and dynamic joint stiffness in elderly and young men during stepping down. *Clinical Biomechanics* 18: 848-855.
61. Shamaei K, Sawicki G, Dollar A (2013) Estimation of quasi-stiffness and propulsive work of the human ankle in the stance phase of walking. *PLoS ONE* 8: e59935.
62. Shamaei K, Sawicki GS, Dollar AM (2013) Estimation of quasi-stiffness of the human hip in the stance phase of walking. *PLoS ONE* 8: e81841.
63. Rouse E, Gregg R, Hargrove L, Sensinger J (2013) The difference between stiffness and quasi-stiffness in the context of biomechanical modeling. *IEEE Transactions on Biomedical Engineering* 60: 562-568.
64. Geyer H, Seyfarth A, Blickhan R (2006) Compliant leg behaviour explains basic dynamics of walking and running. *Proceedings of the Royal Society B-Biological Sciences* 273: 2861-2867.
65. Gunther M, Blickhan R (2002) Joint stiffness of the ankle and the knee in running. *Journal of Biomechanics* 35: 1459-1474.
66. Weiss P, Kearney R, Hunter I (1986) Position dependence of ankle joint dynamics: 1. passive mechanics. *Journal of Biomechanics* 19: 727-735.
67. Kearney R, Stein R, Parameswaran L (1997) Identification of intrinsic and reflex contributions to human ankle stiffness dynamics. *IEEE Transactions on Biomedical Engineering* 44: 493-504.
68. Smidt G (1973) Biomechanical analysis of knee flexion and extension. *Journal of Biomechanics* 6: 79-92.
69. Biewener A, Gillis G (1999) Dynamics of muscle function during locomotion: Accommodating variable conditions. *Journal of Experimental Biology* 202: 3387-3396.
70. Dean J, Kuo A (2011) Energetic costs of producing muscle work and force in a cyclical human bouncing task. *Journal of Applied Physiology* 110: 873-880.

71. Farahat W, Herr H (2010) Optimal Workloop Energetics of Muscle-Actuated Systems: An Impedance Matching View. *PLoS Computational Biology* 6.
72. Kram R, Taylor C (1990) Energetics of running - a new perspective. *Nature* 346: 265-267.
73. Taylor C, Heglund N, McMahon T, Looney T (1980) Energetic cost of generating muscular force during running - a comparison of large and small animals. *Journal of Experimental Biology* 86: 9-18.
74. Kram R (2000) Muscular Force or Work: What Determines the Metabolic Energy Cost of Running? *Exercise and Sport Sciences Reviews* 28: 138-144.
75. Griffin T, Roberts T, Kram R (2003) Metabolic cost of generating muscular force in human walking: insights from load-carrying and speed experiments. *Journal of Applied Physiology* 95: 172-183.
76. Grabowski A, Farley C, Kram R (2005) Independent metabolic costs of supporting body weight and accelerating body mass during walking. *Journal of Applied Physiology* 98: 579-583.
77. Tatarliev G (2011) Design of a knee simulator for testing orthoses under unlimited gait cycles. Yale University: Yale university.
78. McClay I, Manal K (1999) Three-dimensional kinetic analysis of running: significance of secondary planes of motion. *Medicine and Science in Sports and Exercise* 31: 1629-1637.
79. Benjamini Y, Hochberg Y (1995) Controlling the false discovery rate - a practical and powerful approach to multiple testing. *Journal of the Royal Statistical Society Series B-Methodological* 57: 289-300.
80. Brockway J (1987) Derivation of formulas used to calculate energy-expenditure in man. *Human Nutrition-Clinical Nutrition* 41C: 463-471.
81. Gard S, Childress D (1999) The influence of stance-phase knee flexion on the vertical displacement of the trunk during normal walking. *Archives of Physical Medicine and Rehabilitation* 80: 26-32.
82. Gard S, Childress D (2001) What determines the vertical displacement of the body during normal walking? *Journal of Prosthetics and Orthotics* 13: 64-67.

83. Minetti A (2001) Invariant aspects of human locomotion in different gravitational environments. *Acta Astronautica* 49: 191-198.

Chapter 5

Design and Functional Evaluation of a Compliant Stance Control Knee-Ankle-Foot Orthosis

5.1 Introduction

Thousands of patients suffer from knee instability as a result of impaired quadriceps following injury, stroke, post-polio, multiple sclerosis, spinal cord injury (SCI), patellofemoral pain syndrome, osteoarthritis, and others [1-5]. Traditionally, the affected knee is supported during walking using a Knee-Ankle-Foot Orthosis (KAFO), comprising a rigid thermoplastic cast formed around the impaired leg, as described in [7]. Traditional KAFOs lock the knee throughout gait, and therefore require compensatory, unnatural, and metabolically expensive movements including circumducting on the braced leg, vaulting on the contralateral leg, swing phase hip elevation, and lateral sway in the upper body [8-12]. Those problems have led to a high rate (more than 60%) of abandonment of KAFOs [13-15].

Stance Control KAFOs (SCKAFOs) have recently been commercialized and used clinically for patients with paresis and paralysis in the lower limb muscles [4,8-11,13,15-30]. Unlike traditional KAFOs, SCKAFOs lock the knee only during the stance phase and allow for free rotation during the swing phase. This improvement can lead to many medical benefits, including increased walking speed, knee range of motion, stride, step lengths, user satisfaction, reduced energy expenditure and gait asymmetry, as well as kinematic benefits to both affected and unaffected legs, when compared with regular KAFOs [8-10,21,24]. However, rigid locking of the knee joint during stance phase in current SCKAFOs hinders the shock absorbing flexion of the knee (as outlined in [31,32]), and can potentially cause increased metabolic cost, user pain and discomfort and limited gait speed. To overcome these issues, SCKAFOs can implement

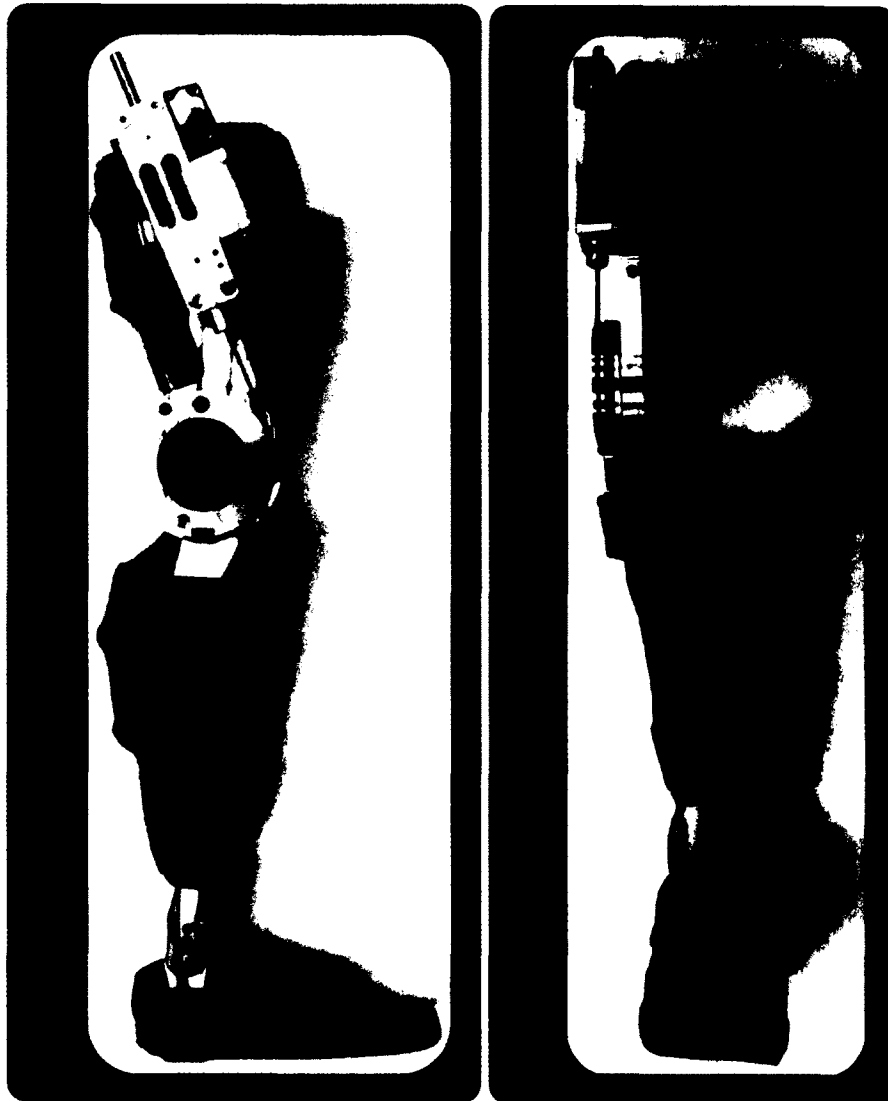


Figure 5-1. Quasi-passive compliant stance control orthosis lateral view without a shoe and frontal view with a shoe.

compliant support (instead of rigid locking) in the stance phase to replicate the damping function of the knee during stance [33]. Previous research on the moment-angle performance of the knee reveals that this joint behaves close to a linear torsional spring in the stance phase at the preferred gait speed; a spring whose torsional stiffness significantly varies depending on the subject's body size and gait speed [33-36]. Accordingly, we hypothesize that *SCKAFOs can replicate the biological spring-like function of the knee by implementing an accurately sized linear torsional spring during the stance phase and allowing for free knee motion during the swing phase of gait.*

Researchers started investigating the use of elastic components in the design of orthoses and prostheses decades ago [37-39]. In early orthotic devices, the compliant components remained attached throughout the movement cycle. More recent research tried to incorporate compliance in the design of prostheses [40,41] and ankle orthoses [42-45]. Researchers have also designed underactuated exoskeletons that implement a spring in parallel with the knee in the stance phase of gait [35,36,46]. However, these compliant devices provide a small percentage of the necessary knee quasi-stiffness (up to ~20%) and are mostly designed to assist able-bodied subjects.

This chapter presents the mechanical design and functional (i.e. non-clinical) evaluation of a quasi-passive compliant stance control orthosis (CSCO) that implements an interchangeable linear spring in parallel with an impaired knee joint to compliantly support it during the stance phase, then allows the leg to freely swing to initiate the next step, as shown in Fig. 5-1.

5.2 Device Design

5.2.1 Moment-Angle Behavior of Knee

Fig. 5-2-top schematically depicts the lower extremity limbs in a gait cycle, and Fig. 5-2-bottom shows a typical moment-angle cycle for an unimpaired knee during walking on level ground, with the corresponding gait instants labeled. The stance phase of walking is composed of a weight acceptance phase (first ~40%, as depicted in Fig. 5-2 *a* to *c*) and a stance termination phase (~40-63%, as shown in Fig. 5-2 *c* to *d*) [6,33,47,48]. During the weight acceptance phase,

the knee undergoes substantial loads to support the weight of the superior limbs; therefore, it is highly prone to collapse without proper function of the musculature system or external assistance during this phase. As Fig. 5-2 shows and previous research suggests, the knee behaves close to a linear torsional spring in the weight-acceptance phase (particularly at the preferred gait speed). This spring stiffness is defined as *the slope of a linear fit to the moment-angle graph of the knee in this phase* [33,34]. In our previous studies, we found that the knee quasi-stiffness in the weight acceptance phase can significantly vary depending on the user's body size and gait conditions demonstrating values up to $\sim 750 \text{ N.m.rad}^{-1}$ for healthy adults during level ground walking [33,34]. The knee exhibits substantially smaller quasi-stiffness and moment during the terminal stance phase and remains nearly silent during the swing phase of the gait, [33,47,49]; implying a less eminent need for external stabilization.

In our previous work, we investigated the linear moment-angle behavior of the lower extremity joints [34,50,51]. Particularly, we studied the effect of body size and gait speed on the knee moment-angle performance of subjects with gait speed of 1.01 m.s^{-1} to 2.63 m.s^{-1} , body height of 1.43 m to 1.86 m , and body weight of 56.0 kg to 94.0 kg [33,34]. We showed that the human knee exhibits a stance excursion of 6 to 30 deg , quasi-stiffness of 80 to 750 N.m.rad^{-1} , and moment of 45 to 105 N.m when walking on level ground [33]. We also showed that the angle of initiation of the weight acceptance phase (the angle at which the knee moment is zero) ranges from 6 to 32 deg and significantly varies depending on the weight carriage and gait speed [33]. The weight acceptance phase spans $\sim 40\%$ of the gait which, depending on the gait speed and duration of the gait cycle, corresponds to a period of ~ 400 to 500 ms assuming a cycle duration of ~ 1 to 1.25 sec .

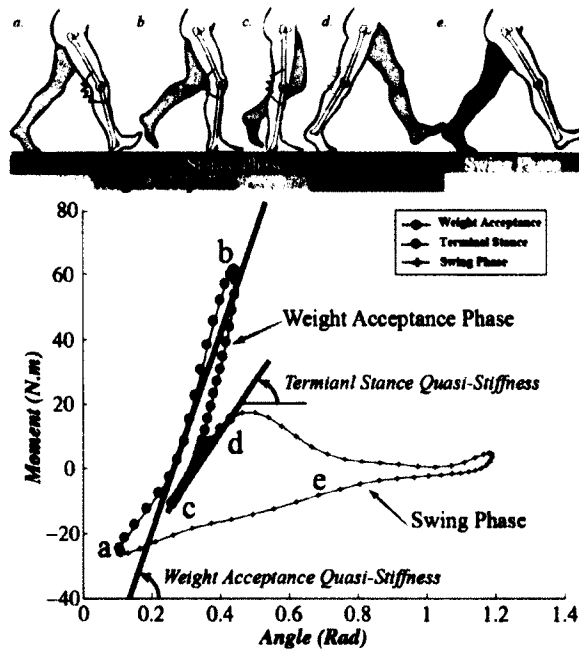


Figure 5-2. Top: Schematic of lower extremity limbs during a gait cycle (schematic graphics adapted from [6]). The knee behaves close to a torsional spring in the weight acceptance phase of the gait as indicated. Bottom: The moment-angle graph for the knee of a subject walking at 1.25 m.s^{-1} (data from [33]). The slope of the linear fit to the graph in the weight acceptance phase is termed as the knee quasi-stiffness in this phase. The knee function can be replaced by a linear torsional spring with spring constant equal to the knee quasi-stiffness.

5.2.2 Design Objectives

In order to approximate the linear moment-angle behavior of the knee, a compliant orthotic knee joint should engage a linear torsional spring (sized based on the body stature and gait conditions [33,34]) in parallel with the knee at the onset of the stance phase and disengage it at the end of the weight acceptance phase to allow for free motion during the rest of gait, as inspired by the natural function of the human knee joint. Considering the biological performance of the human knee explained in the previous chapters and extensive consultation we received from orthotists, we envision the following functional and safety requirements for the CSCO:

- a. The knee joint stiffness of CSCO in stance should be sizable/selectable for a specific user depending on stature and gait conditions.
- b. The CSCO should be capable of accommodating torsional stiffness of 80 to 750 N.m.rad^{-1} and maximum moment of up to 105 N.m .
- c. We define the angular resolution of engagement as the smallest difference between the angles at which the orthosis can engage the spring. The CSCO should demonstrate high angular resolution (we target $\sim 1 \text{ deg}$) to be able to capture the knee motion in stance.
- d. Adjustable angle of engagement/disengagement to capture the variable angle of initiation and termination of the weight acceptance phase, which ranges from 6 to 32 deg as observed for humans at different gait speeds and weight carriage conditions, as well as stair ascent/descent.
- e. We define engagement/disengagement latency as the temporal duration between the electronic signal to the CSCO and corresponding engagement/disengagement of the spring. Theoretically the mechanism should exhibit instantaneous engagement/disengagement (researchers suggest 1% of the gait cycle corresponding to $\sim 10 \text{ ms}$ [18]) to be responsive at the onset and end of the weight acceptance phase.
- f. The CSCO should demonstrate a joint excursion of 6 to 30 deg in the stance phase to capture the range of knee excursion observed for the humans.

g. We define reliability as the percentage of cycles wherein the mechanism successfully engages/disengages the spring at the intended time. To avoid causing patients to fall and stumble, the CSCO should demonstrate *100%* reliability of engagement/disengagement.

h. We define endurance as the number of the operation cycles that the orthosis can undergo before any mechanical or electrical failure occurs. We target *500,000* operation cycles, which is the number of operation cycles that the CSCO would experience in a 6 month period (as suggested by other researchers [18]).

i. The device should always allow the knee to extend so that the leg can quickly obtain an upright posture upon stumble and initiate a stable stance phase.

j. The device weight should be comparable to or lighter than available commercial SCKAFOs (we target *~3 kg*, which is the weight of SensorWalk from OttoBock).

k. We define the electric current demand as the average current the orthosis mechanism requires. The device should be capable of functioning for a whole day and require only a small battery. We envision an electric current demand of *300 mAh* for the device so that it can function throughout a day using a battery with a capacity of *2500 mAh*.

l. The CSCO should be capable of disengagement of a loaded spring to avoid causing wearers to stumble. This is particularly important when the user initiates the swing phase while the spring is still loaded. In this case, the CSCO should be able to disengage the spring; otherwise the knee would lock on the user and prevent foot clearance with the ground.

m. The engagement/disengagement control algorithm should not require the user to move to a particular kinematic configuration. Configuration-dependent engagement/disengagement can result in falling if the patient fails to move to the required configuration for engagement/disengagement; hence, it can heavily affect the performance of a stance control orthosis. The abovementioned design objectives for the CSCO are summarized in Table 5-1. Since the CSCO is intended to be used for daily life activities, noise generation and cosmetic appearance should be appealing and favorably comparable with commercially available devices.

5.2.3 Description of the Quasi-Passive Compliant Stance Control Orthosis

The CSCO is composed of a compliant stance control module (CSCM) integrated into a regular KAFO (fabricated by OttoBock Co.) that lacks a lateral knee joint, as shown in Fig. 5-1 and detailed in Fig. 5-3. The CSCM includes a uniaxial joint setup, which functions as the lateral joint of the CSCO, and a compliance control module (CCM) that exhibits two levels of stiffness through engagement/disengagement of a support spring, shown in Fig. 5-3. The lateral joint of the CSCO is primarily composed of a thigh chassis and a shank chassis as well as a pulley and additional structural components, as shown in Fig. 5-3. The CCM is assembled on the thigh and the pulley on the shank chassis. The CCM harnesses the shank chassis through a tendon attached to and wrapped around the pulley. The pulley rotates along with the knee joint, which, in turn, pulls the shaft of the CCM and compresses the return spring (and support spring, provided it is engaged). This transforms the linear stiffness of the CCM that is observed at the shaft to a torsional stiffness around the knee joint.

5.2.4 Compliance Control Module

The compliance control module (CCM) is responsible for engaging and disengaging the support spring in parallel with the knee joint. The components of this module include a shaft, friction lever, bearing block, support spring, return spring, shock absorber, and engagement mechanism, as detailed in Fig. 5-3. The CCM exploits friction-based latching to engage the support spring in the stance phase, and disengage it during the rest of gait. Friction-based latching has been utilized for prosthetic applications [52] as well as clamping purposes [53]. Here, the CCM uses a motor to drive a worm-gear set that, in combination with a spring-loaded push-button, brings a friction lever either in contact with the shaft to latch the bearing block to the shaft, or away from the shaft to unlatch the bearing block and allow for free motion of the shaft

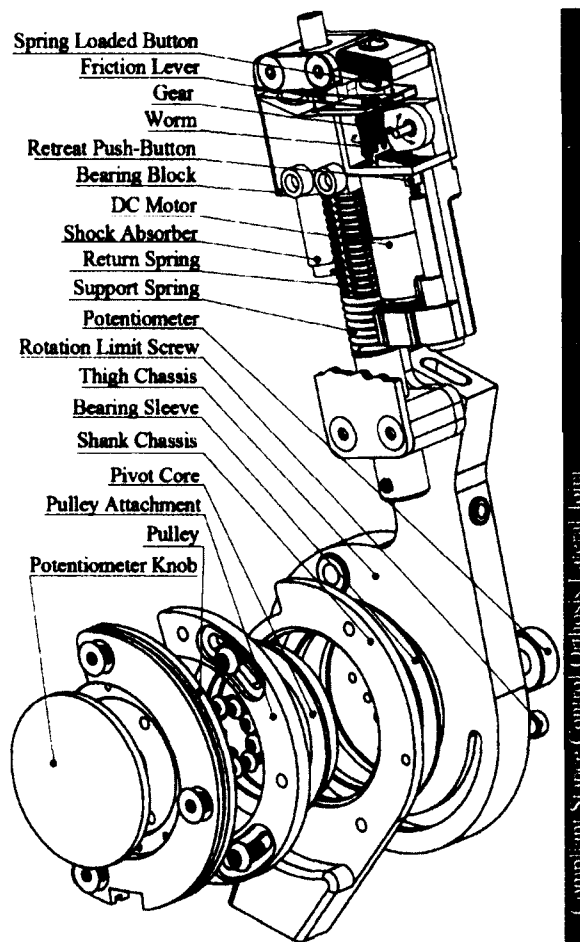


Figure 5-3. The compliant stance control module is mainly composed of the compliance control module (CCM) and the lateral joint of the stance control orthosis. The CCM is mounted on the thigh chassis and harnesses the shank chassis using a tendon that is wrapped around the pulley. The CCM engages the support spring during the weight acceptance phase (or the entire stance phase, depending on the user's gait requirements) to stabilize an affected knee, and disengages it during the rest of the gait to allow for free progression of the limb.

inside the bearing block. The engagement mechanism also includes a spring-loaded and a retreat push-button to provide the CSCO controller with feedback on the position of the friction lever. The sequence of steps for engagement and disengagement of the support spring is detailed here:

Engagement of the Support Spring: To engage the support spring, the worm-gear should spin counterclockwise to move the gear away from the friction lever and clear behind it. This movement terminates when the gear presses the retreat button, which sends a feedback signal to the controller to stop the motor, as shown in Fig. 5-4-top. The spring-loaded push-button presses the friction lever against the shaft to bring them in contact at the two points, as highlighted in Fig. 5-4-top. This introduces a small friction force on the friction lever at the contact points, which is transferred to the bearing block through the friction lever. The interaction force between the bearing block and the friction lever induces higher normal forces between the friction lever and the shaft, constituting a latching grip between the bearing block, shaft, and friction lever. As such, the bearing block moves along with the shaft and compresses the support spring. Since shaft movement always compresses the return spring, any distal force on the shaft (as a result of knee flexion, shown by an arrow on the shaft in Fig. 5-4-top) compresses both the return and support springs. Consequently, the CCM exhibits the summation of the stiffnesses of both springs along the shaft axis. A proximal force on the shaft (mainly applied by the return spring during knee extension) relaxes the friction forces on the friction lever at the contact points and releases the latching grip. Therefore, a latch only occurs in the flexion direction, and remains if the support spring is engaged and loaded to maintain the latching friction forces.

Disengagement of the Support Spring: To disengage the support spring, the worm should spin clockwise to move the gear towards the friction lever. The gear touches the friction lever and releases its latch with the shaft and moves until it presses the spring-loaded push-button after which a feedback signal is sent to the controller to stop the motor. One should notice that the forces applied on the lever by the gear and spring-loaded button generate a moment-couple that anchors the friction lever on the bearing block. Upon disengagement, the shaft freely slides inside

the bearing block and friction lever without any force being transferred to the support spring. Accordingly, a distal force on the shaft only compresses the return spring. To allow free rotation in the swing phase, a relatively slack return spring should be chosen in order to only return the shaft to its original location after the swing phase without applying a considerable moment to the knee. The CCM also includes a shock absorber to dissipate any remaining energy, in case the support spring disengages while it is loaded.

5.2.5 Control Algorithm

The controller employs a finite state machine to engage and disengage the support spring. The controller identifies the gait phase by means of an instrumented shoe insole. We evaluated two types of foot sensors: a. A foot sensor with linear placement of force sensitive resistors from OttoBock, and b. A foot sensor with ergonomic placement of integrated conductive polymers from B & L Engineering, as shown in Fig. 5-5. We observed similar performance for the CSCO using both foot sensors, and we utilize the OttoBock insole for our device. The function of the CSCO is schematically depicted in Fig. 5-6-top. Fig. 5-6-middle approximately outlines the knee angular velocity, foot contact with the ground, and the status of the friction lever. Fig. 5-6-bottom shows the knee angle profile for a subject walking at 1.25 m.s^{-1} on level ground and the period during which the support spring is intended to be engaged and loaded. Fig. 5-7 describes the finite state machine that is implemented to control the CCM for walking on level ground. The states include:

a. Weight Acceptance (WA): Either the heel sensor is on or both heel and toe sensors are on. The controller engages the support spring.

b. Terminal Stance (TS): Any of the toe sensors are on and the heel is off. If the user can maintain stability during this phase, the CCM can disengage the support spring; otherwise, the support spring can remain engaged. The ability of the user to maintain stability can be evaluated by an orthotist/physician and programmed into the device.

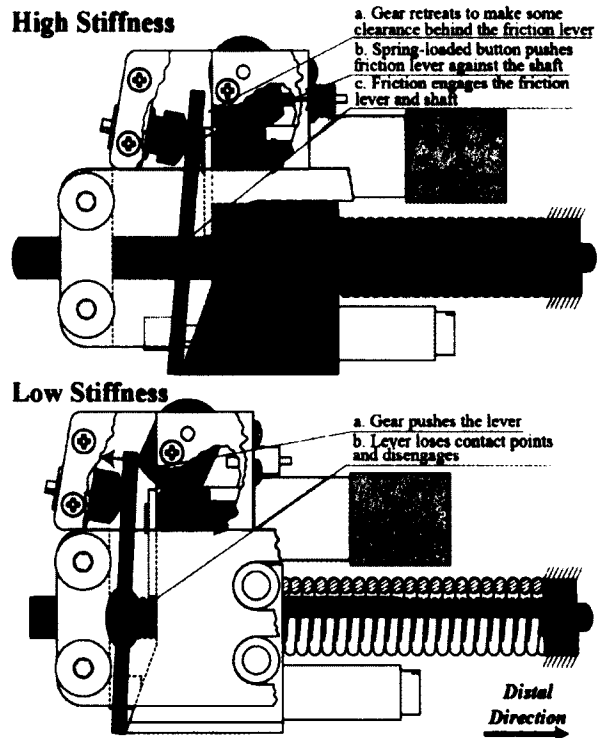


Figure 5-4. Top: *Engagement of the support spring.* When the friction lever is engaged, flexion of the knee compresses both the return and support springs of the compliance control module, Bottom: *Disengagement of the support spring.* When the friction lever is disengaged, flexion of the knee only compresses the return spring (which is mainly incorporated to return the shaft in the extension period). Only those parts of the compliance control module that are involved in each mode are colored

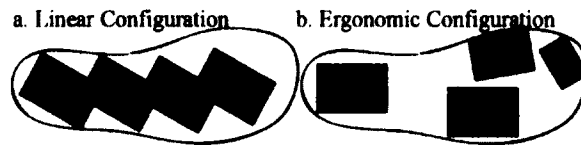


Figure 5-5. The configuration of heel and toe sensors in the instrumented shoe insoles, Left: Linear Configuration of force sensitive resistors (from OttoBock), and Right: Ergonomic Configuration of integrated conductive polymers (from B & L Engineering). Both insoles resulted in relatively similar performance for level ground and treadmill walking.

c. Swing (SW): The toe and heel sensors are off. The controller monitors the knee velocity direction during the swing phase to identify the flexion and extension period of the knee excursion in the swing phase. The controller disengages the support spring during the flexion period of the swing phase and engages it during the extension period, as a precautionary measure against the mechanism's latching latency. Although the friction lever is engaged during the extension period of the swing phase, the support spring is loaded because the engagement mechanism only initiates a latch in the flexion direction, as discussed in Section 5.2.4.

We initially employed a Microcontroller MPC5534 from Freescale Semiconductor Co. (MPC5534EVBE) to implement the finite state machine for two CSCOs (left and right orthoses), which was replaced by a custom-made controller that fits inside the thigh compartment of the CSCM. The controller measures the knee angle using a rotary potentiometer (Model 357, Vishay Co.) that is integrated inside the orthosis pulley, and the knee velocity is obtained by differentiating the potentiometer signal. The controller identifies the status of the friction lever using the signals received from the push-buttons incorporated in the CCM. More specifically, the signal from the spring-loaded push-button indicates if the friction lever is disengaged, while the signal from the retreat push-button indicates if the friction lever is engaged. A serial-to-Bluetooth adapter (Wireless RS232, Willies Computer Software Co.) establishes wireless transfer of data to a host LabView module implemented on a computer for data collection. We used a dual H-Bridge from Solarobotics Co. to drive a Faulhaber 2024 DC Motor that we used in the design of the CCM. A battery pack with capacity of *2500 mAh* powers the controller, orthosis and the wireless connection systems.

5.2.6 Design Analyses and Characterization

Moment-Angle Relationship: As discussed in Section 5.2.3, the CSCO tendon is wrapped around and anchored to the pulley that is mounted on the shank chassis. When the knee flexes, the return spring (and support spring if engaged) will compress and apply a moment on the pulley, as schematically shown in Fig. 5-8-top. This moment can be calculated as:

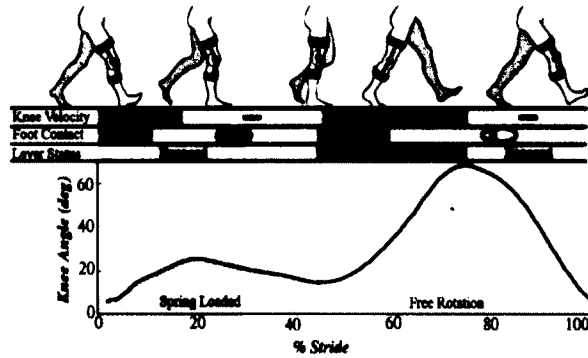
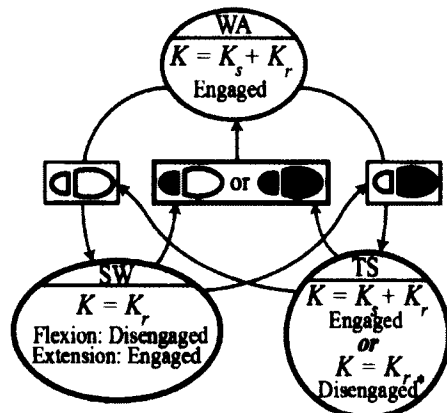


Figure 5-6. Top: The device engages a spring in the weight acceptance phase of the gait (and potentially the terminal stance depending on the needs of the user), Middle: The statuses of the knee motion, heel and toe contact with the ground, and engagement of the friction lever, Bottom: The knee angle profile for a healthy subject walking with the gait speed of 1.25 m.s^{-1} (data from [33]).



* Engagement depending on the user's impairment level

Figure 5-7. The finite state machine used to control the stiffness of the compliance stance control module for level ground walking. The finite state machine includes three states: WA: Weight Acceptance, TS: Terminal Stance, and SW: Swing Phase. The transition between the state occurs when the status of foot contact with the ground changes. Each circle shows the stiffness of the compliance control module and status of the friction lever engagement.

$$M = K_L \cdot \Delta L \cdot R \quad (5-1)$$

where, R is the radius of the pulley and K_L is the linear stiffness of the CCM observed at the shaft. Also, a knee flexion of $\Delta\varphi$ results in a shaft movement of ΔL . Thus, the stiffness of an imaginary linear torsional spring K_φ that can replace the transformed stiffness CCM around the knee would be:

$$K_\varphi = K_L \cdot \Delta L \cdot R / \Delta\varphi \quad (5-2)$$

And since $\Delta L = R\Delta\varphi$, we conclude:

$$K_\varphi = K_L \cdot R^2 \quad (5-3)$$

K_L is the stiffness of the return spring when the friction lever is disengaged and the summation of the stiffness of both springs when the support spring is engaged:

$$K_L = \begin{cases} K_r + K_s & \text{engaged} \\ K_r & \text{disengaged} \end{cases} \quad (5-4)$$

Combining equation (5-3) and (5-4) gives us:

$$K_\varphi = \begin{cases} (K_r + K_s) \cdot R^2 & \text{engaged} \\ K_r \cdot R^2 & \text{disengaged} \end{cases} \quad (5-5)$$

This suggests the following equation for the assistive moment observed at the knee joint:

$$M = \begin{cases} K_r \cdot R^2 \cdot \varphi + K_s \cdot R^2 \cdot (\varphi - \varphi_0) & \text{engaged} \\ K_r \cdot R^2 \cdot \varphi & \text{disengaged} \end{cases} \quad (5-6)$$

Here, φ_0 is the angle at which the support spring is engaged. Fig. 5-8-left shows the theoretical moment-angle performance of the CSCO.

Sizing the Support Spring: An informed selection of the support spring can help the device implement a natural amount of compliance and minimize the compensatory movements of the body. Section 5.2.1 explains that the knee's function can be replaced by a torsional spring with a stiffness equal to the knee quasi-stiffness in the stance phase. In our previous works, we showed that a subject's knee and ankle quasi-stiffnesses significantly depend on body size and gait conditions [33,54]. Current prosthetic design approaches usually employ the joint quasi-stiffness of healthy subjects with average weight and height, which requires substantial effort and time to

conduct a gait lab study for each target user size, and additional tuning for the specific patient [41,55,56]. Alternatively, we proposed a series of statistical models that can estimate the quasi-stiffnesses of the knee and ankle joints in the stance phase of gait relatively closely [34,50]. Table 5-2 lists the most general and simplified forms of the statistical models that estimate the knee quasi-stiffness in the weight acceptance phase. The most general model tends to provide a closer estimation of the knee quasi-stiffness for a wide range of gait speed (1.01 ms^{-1} to 2.63 ms^{-1}), weight (67.7 kg to 94.0 kg), height (1.43 m to 1.86 m), and knee excursion (6 deg to 28 deg), whereas the stature-based model estimates the knee quasi-stiffness only at the preferred gait speed and trades accuracy for simplicity by approximating the knee excursion and gait speed. Here, we exploit these statistical models to size the support spring of the device for users with complete impairment. For other users, the support spring stiffness can be a function of the level of impairment of the knee joint.

Friction Lever Dimensions: Fig. 5-9 shows the free body diagram of the friction lever. We assume that an initial moment around the point of contact between the lever and bearing block b (e.g. caused by the weight of the lever and the spring-loaded push-button) brings the friction lever in contact with the shaft at two points p and q . The interaction force between the lever and bearing block F_b , which is identical to the shaft force F , induces friction forces between the lever and shaft, F_p and F_q . Therefore, the normal friction forces are proportionate to the moment-arm around the center of the shaft r . Here, we derive a relationship between r , and the friction lever thickness t and diameter D under which the friction forces cause a latching grip between the shaft and friction lever.

The friction lever is stationary in the direction perpendicular to the shaft, therefore:

$$\Sigma F_x = 0 \tag{5-7}$$

where, F_x denotes any force applied on the friction lever along the x -axis. The normal contact forces at p and q (i.e. F_p^n and F_q^n) cause the tangential friction forces F_p^t and F_q^t on the friction lever. Expanding equation (5-7) concludes:

$$F_p^n = F_q^n \quad (5-8)$$

which in turn implies that the friction forces are equal:

$$F_p^t = F_q^t \quad (5-9)$$

Since the lever is stationary around b , the summation of moments applied on the lever should be zero around this point:

$$\Sigma M_b = 0 \quad (5-10)$$

where, M_b stands for any moment applied on the friction lever around an axis passing through b and perpendicular to the plane of movement. Expanding equation (5-10) and including equation (5-9) gives us:

$$F_p^n(D \cdot \sin \theta + t \cdot \cos \theta) - F_p^t(2r) = 0 \quad (5-11)$$

where D is the diameter of the hole of the friction lever, t is the thickness of the friction lever, and θ is the tilt angle of the friction lever with respect to the x -axis. In order for the friction lever to engage with the shaft, the friction forces should remain lower than the maximum friction force:

$$F_p^t \leq F_p^n \cdot \mu \quad (5-12)$$

where μ is the coefficient of friction between the shaft and lever. Applying equation (5-11) in (5-12) concludes:

$$r \geq \frac{D \cdot \sin \theta + t \cdot \cos \theta}{2\mu} \quad (5-13)$$

For small tilt angles (i.e. $\theta \sim 0$), equation (5-13) can be simplified to:

$$r \geq \frac{t}{2\mu} \quad (5-14)$$

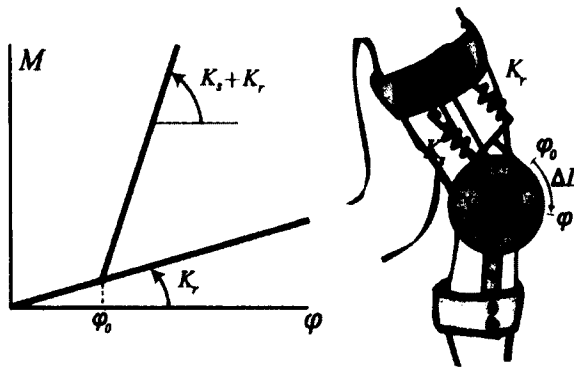


Figure 5-8. Top: The schematic configuration of the return and support spring. The output stiffness of the compliance control module is the summation of the spring constants of both springs if the support spring is engaged, and only the spring constant of the return spring otherwise. The springs apply a force on the pulley with radius R . The effect of the linear return stiffness K_r and support stiffness K_s is experienced as an imaginary torsional stiffness around the center of the pulley with the torsional stiffness K_ϕ .

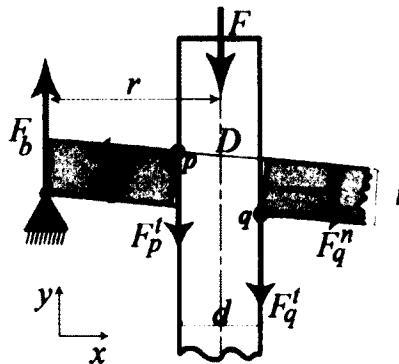


Figure 5-9. Free body diagram of the friction lever under the interaction with the shaft and bearing block. The interaction force from the bearing block F_b generates normal forces between the friction lever and the shaft F_p^n and F_q^n ; inducing tangential friction forces F_p^t and F_q^t . If the moment arm r is long enough, the latching occurs and the shaft, friction lever, and bearing block lock together.

Moreover, the maximum normal stress (σ_{max}) imposed by the interaction forces between the friction lever and shaft should not exceed the material's yield strength (σ_Y):

$$|\sigma_{max}| \leq \frac{\sigma_Y}{S} \quad (5-15)$$

Here, S is a safety factor. The maximum normal stress occurs at the outer surface of the friction lever between points b and p :

$$\sigma_{max} = \frac{3 F r}{w t^2} + \frac{F}{w t} \sqrt{9\left(\frac{r}{t}\right)^2 + 1} \quad (5-16)$$

where, w is the width of the friction lever. Combining equations (5-15) and (5-16) concludes:

$$\frac{3r}{t} + \sqrt{\left(\frac{3r}{t}\right)^2 + 1} \leq \frac{3 w t R \sigma_Y}{M_{Knee} S} \quad (5-17)$$

where M_{Knee} is the maximum knee moment that the device experiences. We have employed a steel shaft and friction lever with case hardness of Rockwell C60-C64, that theoretically exhibits a lubricated static coefficient of friction of 0.15 and yield strength of ~ 670 MPa. The shaft diameter is 9.525 mm ($3/8$ in) and the lever thickness 3.175 mm ($1/8$ in). Considering a safety factor of 1.5 and M_{Knee} of 110 N.m, the bearing block contact point should be 20 mm away from the center of the shaft.

5.3 Mechanical and Functional Evaluation

We conducted four tests to evaluate/measure the reliability, latency and endurance of the CSCO, and also the kinematic performance of three healthy volunteers and one patient participant using the CSCO, including a comparison to a commercial SCKAFO (Sensor Walk by Otto Bock).

Preclinical Static Loading: We measured the moment-angle performance of the device and the maximum moment that the device can hold. We mounted the CSCM on a test bench and applied a series of moments under three levels of stiffness and three angles of engagement. For each condition, we recorded the flexion angle at which the CSCM was stabilized. Fig. 5-10

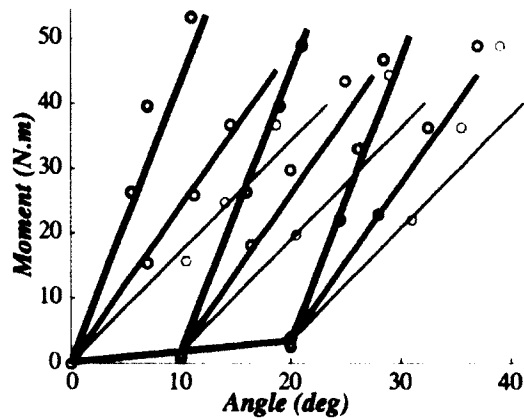


Figure 5-10. Moment-angle characterization of the compliant stance control module using three different support springs: 239 N.m.rad^{-1} shown by black, 127 N.m.rad^{-1} shown by dark gray, and 89 N.m.rad^{-1} shown by light gray, and three different angle of engagement: 0 , 10 , and 20 deg . Experimental data are shown with circles and the theoretical data with solid lines. The stiffness of the return spring is 2 N.m.rad^{-1} .

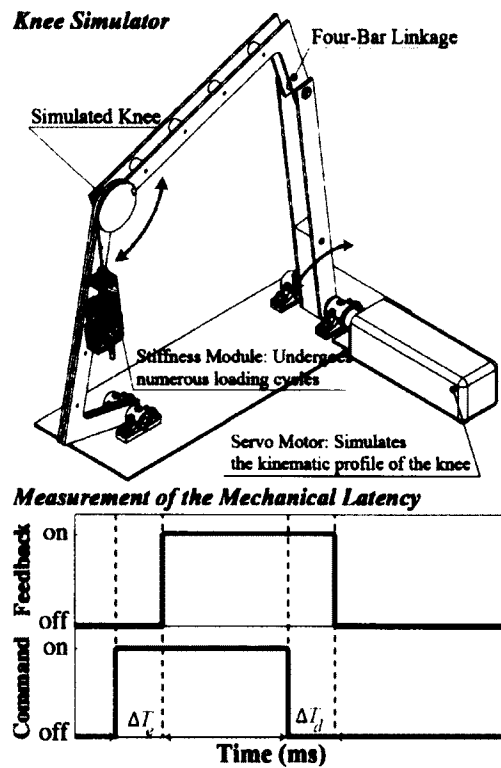


Figure 5-11. Top: Knee simulator used to evaluate the mechanical function of the compliance control module and to measure the spring engagement/disengagement latency. The simulator is primarily a four-bar linkage mechanism driven by a servo motor. The compliance control module is mounted on the device and undergoes numerous working cycles. Bottom: The simulator controller sends an engagement command signal to the compliance control module and receives the feedback from the pushbuttons embedded in the module. The time differences between these signals indicate the mechanism engagement/disengagement latency.

shows the results of the experiment wherein the device employed a return spring with linear stiffness of 0.8 N.mm^{-1} (equivalent to 2 N.m.rad^{-1}), and support springs with linear stiffnesses of: a. 92 N.mm^{-1} (equivalent to 239 N.m.rad^{-1}), b. 42 N.mm^{-1} (equivalent to 127 N.m.rad^{-1}), and c. 34 N.mm^{-1} (equivalent to 89 N.m.rad^{-1}). The moment-angle data for conditions a, b, and c are shown with black, dark gray, and light gray, respectively. The experimental data are shown with circles and the theoretical data suggested by equation (5-6) with solid lines. Fig. 5-10 shows that equation (5-6) closely explains the moment-angle performance of the CSCM, especially at the low knee flexion values usually observed in walking. As dictated by the design objectives, we also applied moments of up to 110 N.m on the CSCM and found it able to tolerate them and hold its latch. The CSCM also functioned properly when the support spring was replaced with a solid cylinder (i.e. “rigid” joint).

Preclinical Dynamic Loading: We fabricated a mechanical knee simulator in order to evaluate the reliability and measure the latency of the CCM, as schematically shown in Fig. 5-11-top. The test machine consists of a four-bar linkage actuated by a large 3-phase servomotor and servo controller (SGMAV-10A3A61 from Yaskawa and SGDV120AE from Omron Companies) [34,57]. The servomotor follows the kinematic profile of the joint for which the module is being designed (here, the knee joint angle profile, taken from normative subject data [47]). The controller also sends a digital signal to the CCM to engage the support spring during the simulated stance phase and disengage during the rest of the gait, as shown in Fig. 5-11-bottom. The setup also records the feedback signals from the push-buttons embedded in the CCM to identify when the engagement/disengagement actually occurs. As discussed earlier, the mechanical system of the CCM imposes latency on the engagement/disengagement. The engagement latency (ΔT_e) and disengagement latency (ΔT_d) were estimated by measuring the time period between the command and feedback signals. We fabricated a prototype of the CCM and tested it on the knee joint simulator as schematically shown in Fig. 5-11-top. The prototype successfully underwent $\sim 30,000$ gait cycles (with maximum moment of 60 Nm/rad) without any

failure in the mechanical components and engagement. The average latencies for both engagement and disengagement were also measured using the test machine and reported to be ~ 30 ms.

Preliminary Healthy Human Subjects Tests: We conducted a preliminary test on three healthy volunteers according to experimental protocols approved by the Institutional Review Board of Yale University. Table 5-3 includes the demographic data of the volunteers as well as the preferred gait speeds of the trials. We compared the inter-subject mean kinematic profiles of the hip, knee, and ankle of the volunteers under compliant support provided by the CSCO with the rigid support provided by a SensorWalk commercial SCKAFO (OttoBock), which is likely the most advanced commercialized stance control orthosis. This device contains an electromechanical clutch at the knee that engages to lock the knee joint during the stance phase (sensed through an insole-based sensor), and releases the knee during swing.

The experiment included three conditions each consisting of 10 minutes of walking at the preferred gait speed according to the feedback obtained from the volunteers: a. Control Condition (CC), b. Rigid Support (RS), and c. Compliant Support (CS). All conditions involved the device on the right leg of the volunteers, with no device on the left leg. The control condition consisted of the volunteers walking with a carbon-fiber jointed KAFO (i.e. free-swinging “pin” joint) without an active control module (the stance control modules of the SensorWalk and CSCO were assembled on the same KAFO, custom fit to the volunteers by a professional orthotist and fabricated by Otto Bock). The rigid support condition consisted of the volunteers walking with the SensorWalk device. For the compliant support condition, we replaced the stance control module of the SensorWalk with the CSCM. The equivalent support spring and return spring stiffnesses of the CSCM were chosen to be 240 N.m.rad^{-1} and 2 N.m.rad^{-1} , respectively. To measure the joint angles, we placed a potentiometer at the knee and ankle of the devices and an instrumented orthopaedic goniometer (a potentiometer integrated in a goniometer from Elite

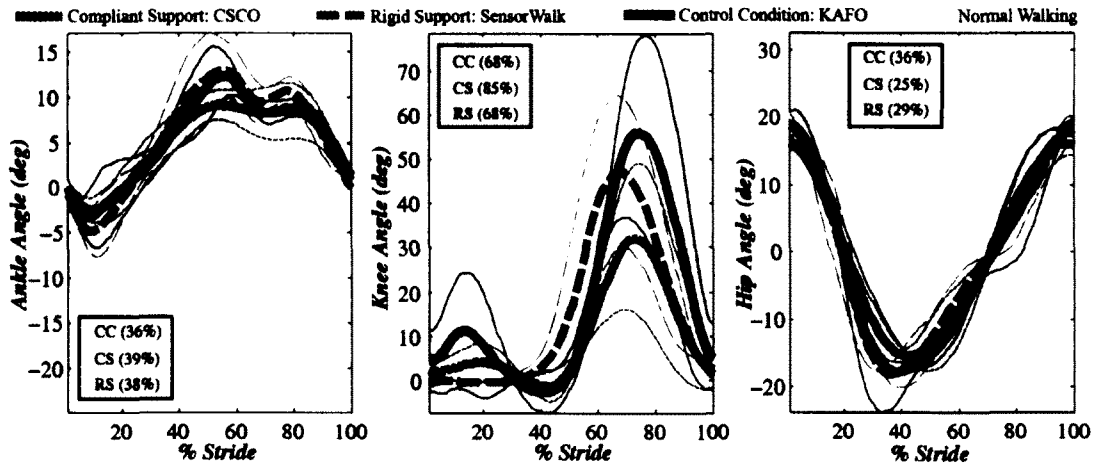


Figure 5-12. Inter-subject mean angle profiles of the ankle, knee, and hip joints for three healthy volunteers walking at the preferred gait speed on a treadmill. Compliant Support (CS): Volunteers walking with the CSCO with support spring stiffness of $240 N.m.rad^{-1}$, shown by black. Rigid Support (RS): Volunteers walking with SensorWalk representing current stance control orthosis, shown by dark gray, and Control Condition (CC): Volunteers walking with the KAFO of SensorWalk/CSCO, shown by light gray. The figure also includes the normative angle profiles observed in average humans in normal walking [33, 56]. The thin lines show one standard deviation above and below the graphs.



Figure 5-13. High-speed image captures of the compliant stance control orthosis in a gait cycle of a healthy subject walking on a treadmill. The device compliantly supports the knee during the weight acceptance phase and liberates it during the rest of the gait.

Medical Instruments) at the hip joint of the volunteers. Fig. 5-12 illustrates the graphs of the inter-subject mean angles of hip, knee, and ankle by thicker traces as well as the lower and upper boundaries defined by the standard deviations with thinner traces. In this figure, black represents the results achieved by the CSCO, dark gray by the SensorWalk, and light gray by the jointed passive KAFO. The right heel strikes identified the beginning of the gait cycles. To give a sense of the repeatability of the traces over the entire gait period, the coefficients of variability (CV, described in [47]) of the mean profiles are also reported on each graph.

In order to compare the two Stance-Control Orthosis conditions (CSCO and SensorWalk), we calculated the common variance of correlation (R^2) and f-test p-value (p) between the joint angles when walking with those devices and when walking with the passive, jointed KAFO (control condition). We found R^2 values of 98%, 70%, and 98% for the ankle, knee, and hip angles, respectively, when walking with the SensorWalk, and R^2 values of 97%, 97%, and 98% when walking with the CSCO compared to walking with the KAFO as the baseline (as suggested by other researchers [58]), with $p < 0.0001$ for all profiles. Considering those values, the performance of our CSCO is closer to the control condition than the Sensor Walk, and especially so for the knee joint. These similarities and differences can also be qualitatively seen in the traces in Fig. 5-12.

As additional measures, we reported the preferred gait speed of the volunteers across all conditions. We found an average preferred speed of $\sim 0.93 \text{ ms}^{-1}$ for the control and compliant support conditions, and $\sim 0.83 \text{ ms}^{-1}$ for the rigid support condition, as reported in Table 5-3. A sequence of high-speed image captures of the treadmill gait of one of the volunteers is also shown in Fig. 5-13.

TABLE 5-1. Target and Realized Values for the Design Parameters

Design Parameter	Target	Realized
Spring Interchangeability	Yes	Yes
Joint Excursion in Stance (deg)	[6 to 30]	[0, 40]
Angular Resolution (deg)	1	<1
Engagement Latency (ms)	10	30
Maximum Moment (N.m)	105	110
Torsional Stiffness (N.m.rad ⁻¹)	[80 to 750]	~∞
Angle of Engagement (deg)	[0, 32]	[0, 60]
Weight (kg)	3	3
Endurance	500,000	>140,000
Electric Current Demand (mAh)	300	50
Reliability	100%	100%
Knee Extension Allowance	Always	Always
Disengagement under Load	Yes	Yes
Configuration-Independent Engagement	Yes	Yes

TABLE 5-2. Models to Size the Support Spring of the Compliant Stance Control Orthosis

Model	$K_s \left(\frac{Nm}{rad} \right)$	$V \left(\frac{m}{s} \right)$	$H \text{ (m)}$	$W \text{ (kg)}$	$\phi \text{ (}^\circ\text{)}$
General Form	$K_s = \frac{69.8 VHW - 112.8 VW - 73.6 WH + 192.0 W - 4458}{\phi - (1.37 - 0.52 V)WH + 264}$	[1.01, 2.63]	[1.43, 1.86]	[67.7, 94.0]	[6, 28]
Stature-Based†	$K_s = 5.21 W \sqrt{H^3} - 7.50 W \sqrt{H} - 5.83 WH + 11.64 W - 6$	$1.097\sqrt{H}$	[1.43, 1.86]	[67.7, 94.0]	16.5

K_s : Stiffness of Support Spring V : Gait Speed H : User's Height

ϕ : Knee Excursion in the Weight Acceptance Phase W : User's Weight

† To obtain the stature-based models, the general-form models are simplified for the approximated optimal gait speed of $V = 1.097\sqrt{H}$, and average knee excursion of $\phi = 16.5^\circ$ [33].

TABLE 5-3. Demographic Data of the Participants and Trials Information

No	Gender	Weight (kg)	Height (cm)	CC Speed (%)	CS Speed (%)	RS Speed (%)	Stiffness (Nm/rad)
1	M	71	178	1.00	1.00	1.00	240
2	M	70	170	0.90	0.90	0.75	240
3	M	74	169	0.90	0.90	0.80	240
	Mean	73	172	0.93	0.93	0.85	240
	SD	2.6	4	0.06	0.06	0.13	0

Preliminary Clinical Tests: We conducted a preliminary clinical test on a volunteer with unilateral right knee and ankle full impairment secondary to spina-bifida, as shown in Fig. 5-14 and according to experimental protocols approved by the Providence VA Medical Center (PVAMC) and Human Investigation Committee of Yale University. The subject weight was 68 kg and height 1.68 m . We compared the intra-subject mean kinematic profiles of the trunk, hip, knee, and ankle as well as the EMG activities of five muscles including Erector Spinalis (ES), Gluteus Maximus (GM), Hamstrings (Ham), Vastus Lateralis (VL), and Vastus Medialis (VM). The experimental conditions included the volunteer walking with the CSCO, SensorWalk, and his own locked KAFO at the preferred gait speed of $\sim 0.67\text{ m/s}$ with the aid of a pair of crutches.

All conditions involved the device on the right leg of the volunteers, with no device on the left leg. The baseline condition consisted of the volunteer walking with his own KAFO, which was a locked knee joint KAFO. The stance control modules of the SensorWalk and CSCO were assembled on a KAFO that was custom fitted to the volunteer by a professional orthotist. The equivalent support spring and return spring stiffnesses of the CSCM were chosen to be 240 N.m.rad^{-1} and 2 N.m.rad^{-1} , respectively [34]. Our collaborators at PVAMC led the efforts in screening, and training and data collection sessions in the gait laboratory located at PVAMC with a 3D motion capture system (Qualysis Oqus, Gothenburg, Sweden) for data collection and Visual3D (C-Motion) for data analysis, as detailed elsewhere [59]. The EMG signals were rectified, filtered (i.e. signal spikes that were higher than three standard deviation of the EMG signal during walking were replaced with “0”), enveloped (i.e. moving RMS using 51 frame window), and normalized to maximum EMG value during walking. The subject participated in 5 training sessions for each device that included walking with each device for ~ 1 hour prior to the data collection session.

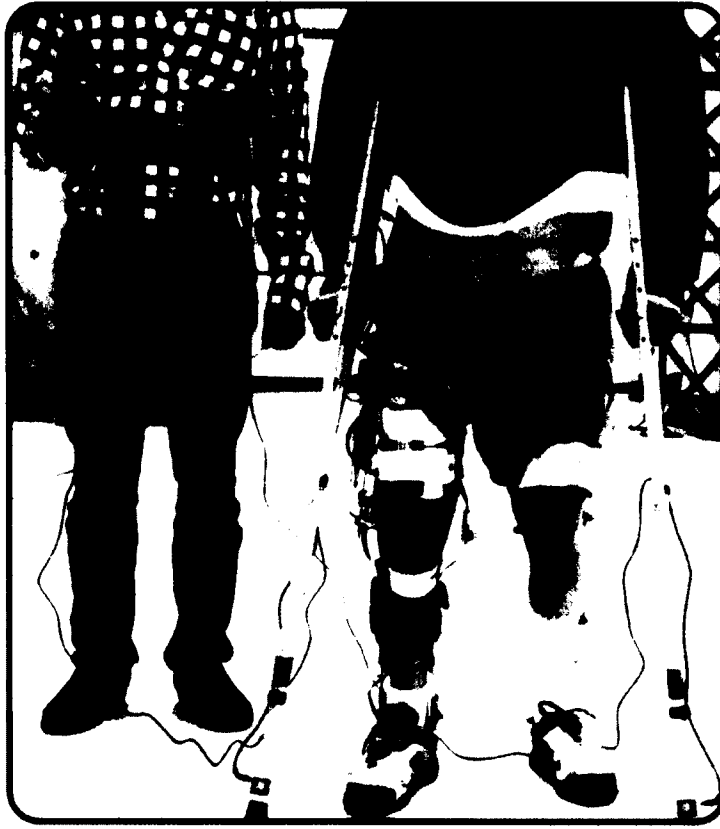


Figure 5-14. The preclinical experiments included a volunteer with impaired knee and ankle secondary to spina bifida, and across three conditions consisting of walking with the CSCO, SensorWalk, and the KAFO that the subject used for the daily life activities.

We analyzed 3-4 trials of walking with each device. Fig. 5-15 shows the graphs of the intra-subject mean angles of hip, knee, and ankle by thicker traces as well as the lower and upper boundaries defined by 1 standard deviation with thinner traces. Fig. 5-16 includes the trunk angles for the three conditions. In Fig. 5-15 and 16, the first to third columns include the graphs of the sagittal, frontal, and transverse planes, respectively. Fig. 5-17 includes the EMG signals of the muscles for the three conditions. In Fig. 5-15 to 17, black represents the results achieved by the KAFO, dark gray by the SensorWalk, and light gray by the CSCO. The right heel strikes identified the beginning of the gait cycles. One should notice that the results of this preliminary clinical test are only intended to provide initial insight and we do not intend to draw any statistical conclusion using the data presented here.

The angle profiles of Fig. 5-15 show that both CSCO and SensorWalk resulted in higher range of motion and more natural patterns for the ankle and knee joints in the sagittal plane when compared to walking with the KAFO. It is also observed that the subject showed substantially higher undesirable/unnatural knee rotations in the transverse plane. Compared with the KAFO, the CSCO and SensorWalk resulted in higher transverse rotations for the hip in the transverse plane. The CSCO resulted in smaller knee flexion in the swing phase for the subject when compared with SensorWalk.

The trunk angle profiles of Fig. 5-16 show that the subject walked with SensorWalk with a trunk that was more anteriorly inclined and longitudinally rotated when compared with walking with the CSCO. The trunk had most upright posture and least frontal movement when walking the CSCO. The EMG signals of Fig. 5-17 show that the VL muscle had substantially lower activity in the swing phase when walking with the CSCO and SensorWalk and compared with KAFO. The muscles in average had minimal activity in the initial stance phase for walking with the CSCO. We do not observe a difference in the activities of the GM and Ham muscles across conditions.

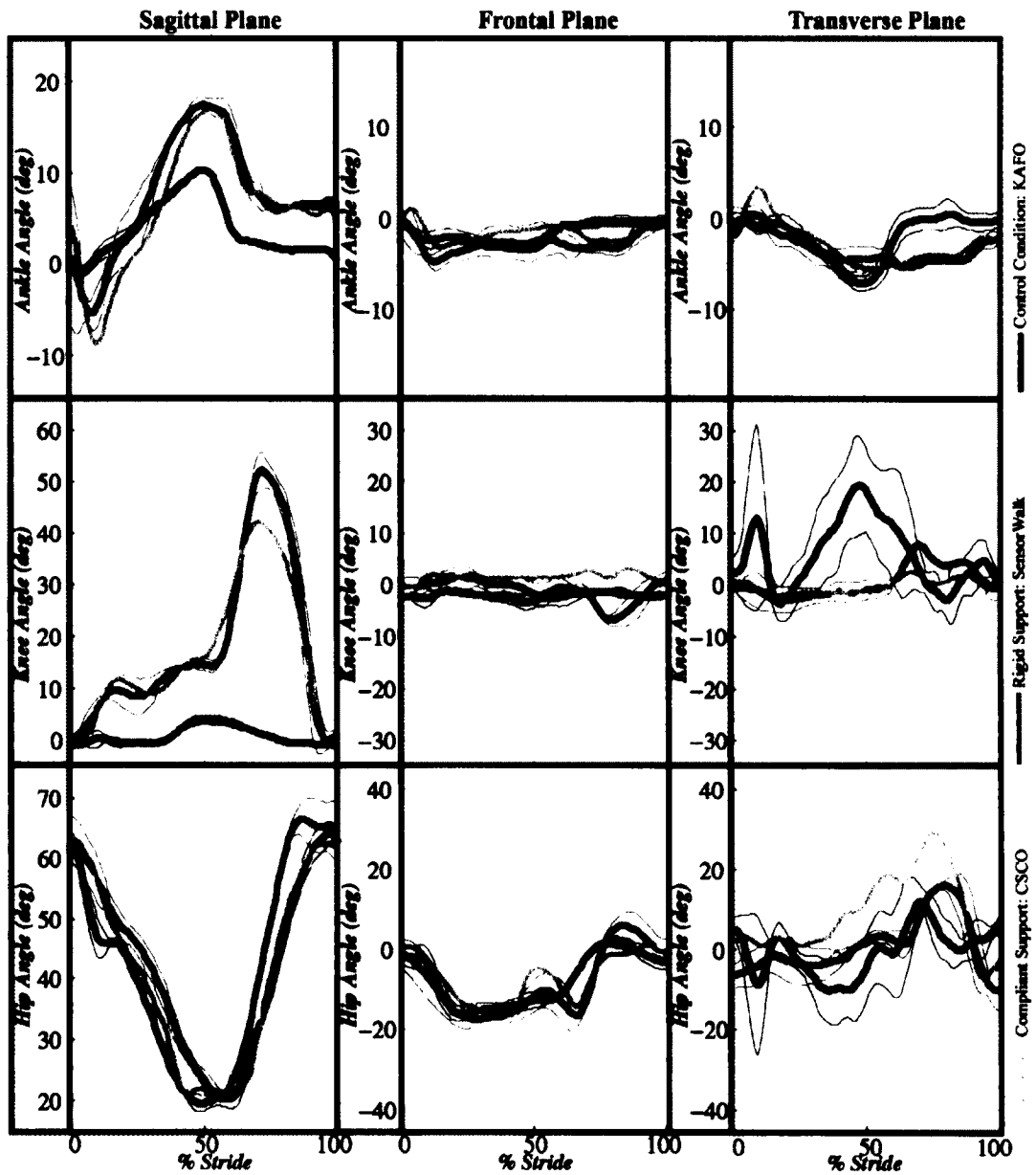


Figure 5-15. Intra-subject mean angle profiles of the lower extremity joints across the conditions. The columns include the profiles of the joints in sagittal, frontal, and transverse planes.

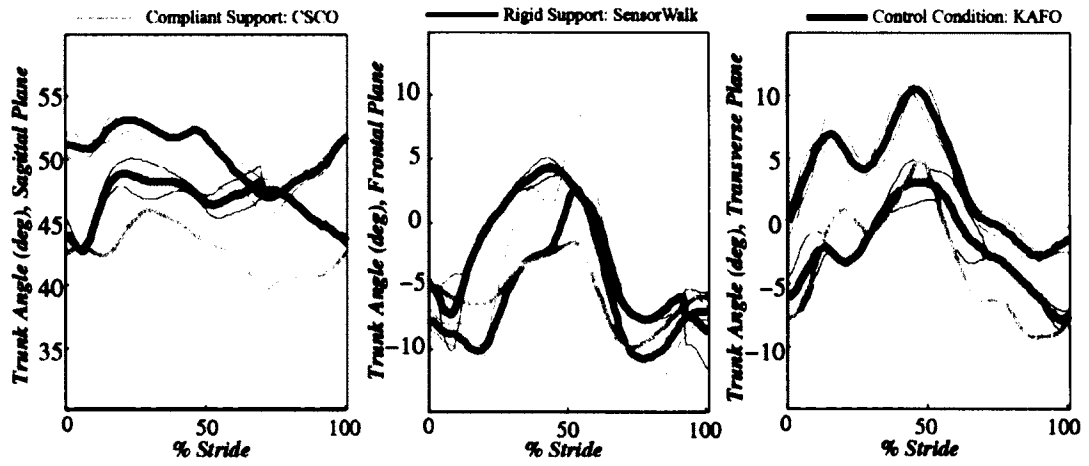


Figure 5-16. Intra-subject mean angle profiles of the trunk across the conditions. The columns include the profiles of the joints in sagittal, frontal, and transverse planes.

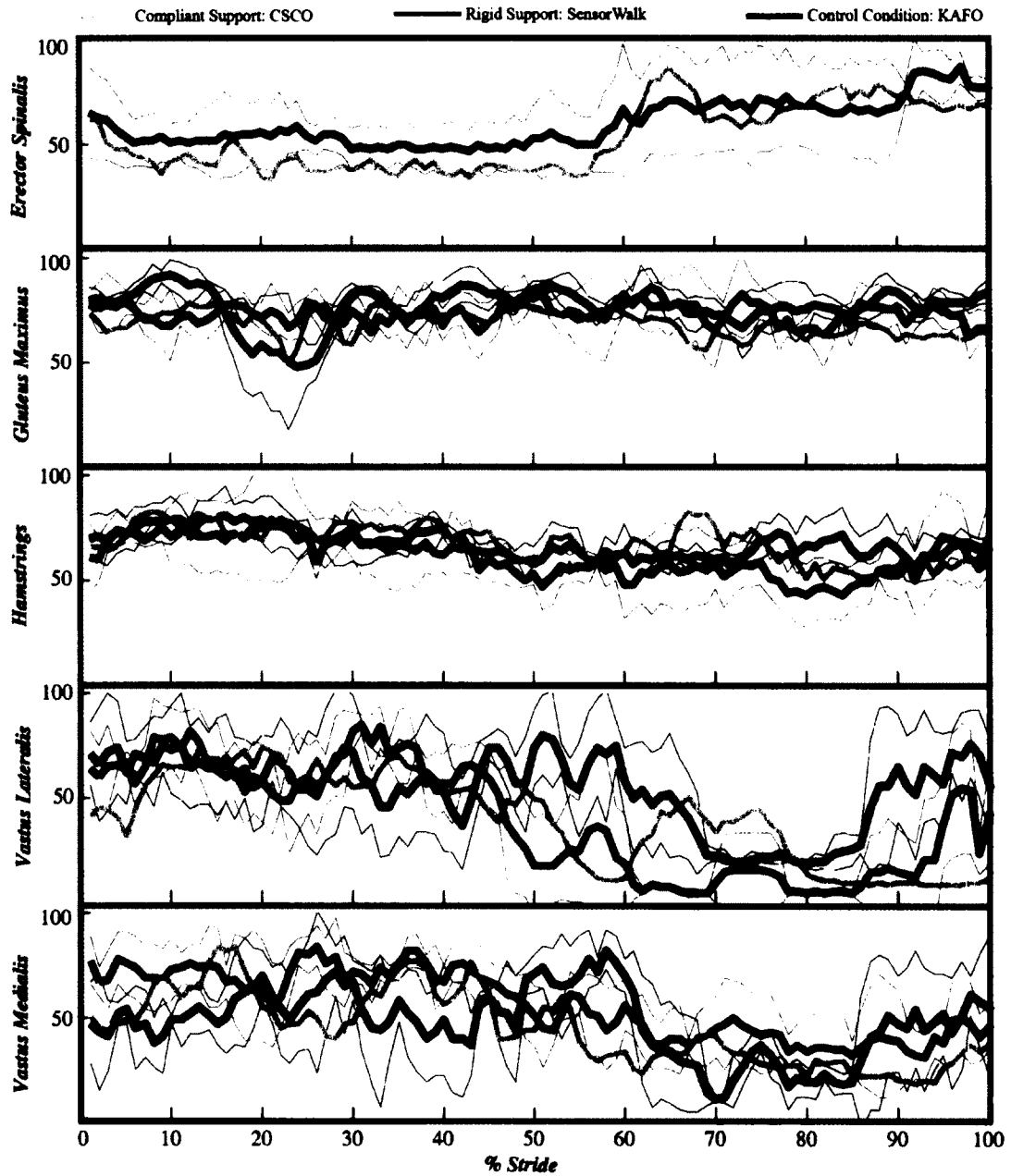


Figure 5-17. Intra-subject mean EMG signals for five target muscles across the conditions. The signals are normalized with respect to the maximum signal value in walking and explained in (%) of the maximum value.

The EMG data for ES muscle were not recorded for walking with the KAFO. We observe that the ES muscle showed lower level of activity during the initial stance phase of walking with the CSCO when compared with walking with SensorWalk.

5.4 Conclusions and Future Work

In this chapter, we presented the mechanical design and functional evaluation of a quasi-passive compliant stance control orthosis (CSCO) that can compliantly support the impaired or weak knee joint of a patient suffering from musculoskeletal disorders when walking on level ground. Inspired by the natural behavior of healthy human knees, the CSCO implements a spring in parallel with the knee joint to fully/partially replace the function of quadriceps in the stance phase, and liberates the knee joint in the swing phase to allow for free progression of the leg to initiate the next step. We further discussed the control algorithm developed to identify the gait phase and determine the engagement/disengagement of the orthosis support spring.

We conducted four experiments to ensure that the CSCO demonstrates proper reliability, latency, and durability, and also to ensure that the CSCO does not substantially affect gait kinematics. In the first set of tests, we applied static moments on the compliant stance control module (CSCM) of the CSCO and observed that the moment-angle behavior of the CSCM validates the theoretical characterization of the device. In the second set of tests, we evaluated the reliability, latency, and endurance of the CSCO on a testing machine over more than *30,000* working cycles. In the third set of tests, we conducted a preliminary human subjects test on three healthy volunteers using the CSCO, SensorWalk, and a control condition using the KAFO of the CSCO/SensorWalk. We found that the kinematic patterns of the volunteers remained relatively invariant during walking with the CSCO and relatively variant with SensorWalk, in comparison to those of the volunteers during walking with the KAFO as the baseline. Finally, we conducted a preliminary clinical test for a patient with unilateral below-knee impairment and found evidence

that the CSCO can help restore the natural gait kinematics and obtain lower muscle activation level during gait.

The design of the CSCO is based on the hypothesis that compliant support can be beneficial to subjects with an unimpaired hip and an impaired knee. Although our preliminary experiments show that the CSCO could provide biomechanical benefits to healthy subjects, statistical inference about the hypothesis requires substantial experiments including healthy and impaired subjects. Particularly, the experiments should include patients with neuromuscular deficits in order to determine to what extent compliant stance control can stabilize a fully/partially impaired knee. We have designed the CSCO for the same population targeted by current stance control orthoses. However, the CSCO should be tested on subjects with a variety of neuromuscular impairments to identify the population for whom the CSCO is most beneficial.

There are a number of follow-on directions from the described work that can be addressed in the future. First and foremost, the device will be tested on impaired volunteers in order to examine the performance in its intended use scenario. We would examine whether the device can help enable higher gait speed, longer walking distance/period, and lower energy expenditure compared with current SCKAFOs in a human subjects experiment on a series of impaired subjects (currently ongoing by the study researchers and clinical collaborators). In addition to further testing, a few aspects of the design of the CSCO can be improved, including more sophisticated heat treatment of the friction lever to improve the endurance of the CSCM, as well as making the device smaller and lighter by reducing the performance range during stance, which is currently oversized in terms of both range of motion (current ~ 40 deg reduced to ~ 20 deg observed in normal human walking) and knee torque (currently capable of 110 N.m, able to be reduced to around 50 N.m [47]).

REFERENCES

1. Robert W, Leslie M (1987) A physiologic rationale for orthotic prescription in paraplegia. *Clinical Prosthetics and Orthotics* 11: 66-73.
2. Hurley E (2006) Use of KAFOs for patients with cerebral vascular accident, traumatic brain injury, and spinal cord injury. *Journal of Prosthetics and Orthotics* 18: 199-201.
3. Taylor M (2006) KAFOs for patients with neuromuscular deficiencies. *Journal of Prosthetics & Orthotics* 18: 202-203.
4. Earl J, Piazza S, Hertel J (2004) The protonics knee brace unloads the quadriceps muscles in healthy subjects. *Journal of Athletic Training* 39: 44-49.
5. Slemenda C, Brandt K, Heilman D, Mazzuca S, Braunstein E, et al. (1997) Quadriceps weakness and osteoarthritis of the knee. *Annals of Internal Medicine* 127: 97-104.
6. Rose J, Gamble J (2006) *Human Walking*. Philadelphia, PA: Williams & Wilkins.
7. Redford J, Basmajian J, Trautman P (1995) *Orthotics: Clinical Practice and Rehabilitation Technology*. New York: Churchill Livingstone. 337 p. p.
8. Irby S, Bernhardt K, Kaufman K (2005) Gait of stance control orthosis users: The dynamic knee brace system. *Prosthetics and Orthotics International* 29: 269-282.
9. Irby S, Bernhardt K, Kaufman K (2007) Gait changes over time in stance control orthosis users. *Prosthetics and Orthotics International* 31: 353-361.
10. Zacharias B, Kannenberg A (2012) Clinical benefits of stance control orthosis systems: An analysis of the scientific literature. *JPO: Journal of Prosthetics and Orthotics* 24: 2-7.
11. Yakimovich T, Lemaire E, Kofman J (2009) Engineering design review of stance-control knee-ankle-foot orthoses. *Journal of Rehabilitation Research and Development* 46: 257-267.
12. Waters R, Campbell J, Thomas L, Hugos L, Davis P (1982) Energy costs of walking in lower-extremity plaster casts. *Journal of Bone and Joint Surgery-American* 64: 896-899.

13. Hwang S, Kang S, Cho K, Kim Y (2008) Biomechanical effect of electromechanical knee-ankle-foot-orthosis on knee joint control in patients with poliomyelitis. *Medical & Biological Engineering & Computing* 46: 541-549.
14. Phillips B, Zhao H (1993) Predictors of assistive technology abandonment. *Assistive Technology* 5: 36-45.
15. Kaufman K, Irby S, Mathewson J, Wirta R, Sutherland D (1996) Energy-efficient knee-ankle-foot orthosis: A case study. *JPO: Journal of Prosthetics and Orthotics* 8: 79-85.
16. Rasmussen A, Smith K, Damiano D (2007) Biomechanical evaluation of the combination of bilateral stance-control knee-ankle-foot orthoses and a reciprocating gait orthosis in an adult with a spinal cord injury. *JPO: Journal of Prosthetics and Orthotics* 19: 42-47.
17. Yakimovich T, Lemaire E, Kofman J (2006) Preliminary kinematic evaluation of a new stance-control knee-ankle-foot orthosis. *Clinical Biomechanics* 21: 1081-1089.
18. Yakimovich T, Kofman J, Lemaire E (2006) Design and evaluation of a stance-control knee-ankle-foot orthosis knee joint. *IEEE Transactions on Neural Systems and Rehabilitation Engineering* 14: 361-369.
19. Davis P, Bach T, Pereira D (2010) The effect of stance control orthoses on gait characteristics and energy expenditure in knee-ankle-foot orthosis users. *Prosthetics and Orthotics International* 34: 206-215.
20. Cullell A, Moreno J, Rocon E, Forner-Cordero A, Pons J (2009) Biologically based design of an actuator system for a knee-ankle-foot orthosis. *Mechanism and Machine Theory* 44: 860-872.
21. McMillan A, Kendrick K, Michael J, Aronson J, Horton G (2004) Preliminary evidence for effectiveness of a stance control orthosis. *JPO: Journal of Prosthetics and Orthotics* 16: 6-13.
22. Lemaire E, Goudreau L, Yakimovich T, Kofman J (2009) Angular-velocity control approach for stance-control orthoses. *IEEE Transactions on Neural Systems and Rehabilitation Engineering* 17: 497-503.
23. Bernhardt K, Irby S, Kaufman K (2006) Consumer opinions of a stance control knee orthosis. *Prosthetics and Orthotics International* 30: 246-256.

24. Zissimopoulos A, Fatone S, Gard S (2007) Biomechanical and energetic effects of a stance-control orthotic knee joint. *Journal of Rehabilitation Research and Development* 44: 503-513.
25. Dollar A, Herr H (2008) Lower extremity exoskeletons and active orthoses: challenges and state-of-the-art. *IEEE Transactions on Robotics* 24: 144-158.
26. Stein R, Hayday F, Chong S, Thompson A, Rolf R, et al. (2005) Speed and efficiency in walking and wheeling with novel stimulation and bracing systems after spinal cord injury: A case study. *Neuromodulation* 8: 264-271.
27. Font-Llagunes J, Pàmies-Vilà R, Alonso J, Lúgrís U (2011) Simulation and design of an active orthosis for an incomplete spinal cord injured subject. *Procedia IUTAM* 2: 68-81.
28. Tokuhara Y, Kameyama O, Kubota T, Matsuura M, Ogawa R (2000) Biomechanical study of gait using an intelligent brace. *Journal of Orthopaedic Science* 5: 342-348.
29. Arazpour M, Chitsazan A, Ahmadi Bani M, Rouhi G, Tabatabai F, et al. (2013) The effect of a knee ankle foot orthosis incorporating an active knee mechanism on gait of a person with poliomyelitis. *Prosthetics and Orthotics International*.
30. Lemaire E, Samadi R, Goudreau L, Kofman J (2013) Mechanical and biomechanical analysis of a linear piston design for angular-velocity-based orthotic control. *Journal of Rehabilitation Research and Development* 50: 43.
31. Gard S, Childress D (2001) What determines the vertical displacement of the body during normal walking? *Journal of Prosthetics and Orthotics* 13: 64-67.
32. Ratcliffe R, Holt K (1997) Low frequency shock absorption in human walking. *Gait & Posture* 5: 93-100.
33. Shamaei K, Dollar A (2011) On the mechanics of the knee during the stance phase of the gait. *Proceedings of IEEE International Conference on Rehabilitation Robotics (ICORR)*. Zurich, Switzerland.
34. Shamaei K, Sawicki G, Dollar A (2013) Estimation of quasi-stiffness of the human knee in the stance phase of walking. *PLoS ONE* 8: e59993.
35. Cherry M, Choi D, Deng K, Kota S, Ferris D (2006) Design and fabrication of an elastic knee orthosis: preliminary results. *Proceedings of IDETC/CIE ASME 2006 International*

Design Engineering Technical Conferences & Computers and Information in Engineering Conference. Philadelphia, USA.

36. Walsh C, Endo K, Herr H (2007) A quasi-passive leg exoskeleton for load-carrying augmentation. *International Journal of Humanoid Robotics* 4: 487-506.
37. Glancy J (1976) Elastic-materials as a source of external power in orthotics - preliminary-report. *Orthotics and Prosthetics* 30: 13-21.
38. Allard P, Duhaime M, Thiry P, Drouin G (1981) Use of gait simulation in the evaluation of a spring-loaded knee-joint orthosis for duchenne muscular-dystrophy patients. *Medical & Biological Engineering & Computing* 19: 165-170.
39. Fisher L, Judge G (1985) Bouncy knee - a stance phase flex-extend knee unit. *Prosthetics and Orthotics International* 9: 129-136.
40. Marks L, Michael J (2001) Science, medicine, and the future - Artificial limbs. *British Medical Journal* 323: 732-735.
41. Martinez-Vilialpando E, Herr H (2009) Agonist-antagonist active knee prosthesis: A preliminary Study in level-ground walking. *Journal of Rehabilitation Research and Development* 46: 361-373.
42. Farris D, Sawicki G (2012) Linking the mechanics and energetics of hopping with elastic ankle exoskeletons. *J Appl Physiol* 113: 1862-1872.
43. Ferris D, Bohra Z, Lukos J, Kinnaird C (2006) Neuromechanical adaptation to hopping with an elastic ankle-foot orthosis. *Journal of Applied Physiology* 100: 163-170.
44. Wiggan M, Sawicki G, Collins S (2011) An exoskeleton using controlled energy storage and release to aid ankle propulsion. *Proceedings of IEEE International Conference on Rehabilitation Robotics (ICORR)*. Zurich, Switzerland.
45. Bregman D, van der Krogt M, de Groot V, Harlaar J, Wisse M, et al. (2011) The effect of ankle foot orthosis stiffness on the energy cost of walking: A simulation study. *Clinical Biomechanics* 26: 955-961.
46. Elliott G, Sawicki G, Marecki A, Herr H (2013) The biomechanics and energetics of human running using an elastic knee exoskeleton. *Proceedings of IEEE Conference on Rehabilitation Robotics (ICORR)*. Seattle, USA.

47. Winter D (1991) *The Biomechanics and Motor Control of Human Gait : Normal, Elderly and Pathological*. Waterloo, Ont.: University of Waterloo Press. 143 p.
48. Perry J (1992) *Gait Analysis : Normal and Pathological Function*. Thorofare, NJ: SLACK. 524 p. p.
49. Mochon S, McMahon T (1980) Ballistic walking - an improved model. *Mathematical Biosciences* 52: 241-260.
50. Shamaei K, Sawicki G, Dollar A (2013) Estimation of quasi-stiffness and propulsive work of the human ankle in the stance phase of walking. *PLoS ONE* 8: e59935.
51. Shamaei K, Sawicki GS, Dollar AM (2013) Estimation of quasi-stiffness of the human hip in the stance phase of walking. *PLoS ONE* 8: e81841.
52. Collins S, Kuo A (2010) Recycling energy to restore impaired ankle function during human walking. *Plos One* 5.
53. Sorensen J, Nebr L (1991) Quick action bar clamp. USA.
54. Shamaei K, Cenciarini M, Dollar A (2011) On the mechanics of the ankle in the stance phase of the gait. *Proceedings of the IEEE Annual International Conference of Engineering in Medicine and Biology Society (EMBC)*. Boston, USA. pp. 8135-8140.
55. Markowitz J, Krishnaswamy P, Eilenberg M, Endo K, Barnhart C, et al. (2011) Speed adaptation in a powered transtibial prosthesis controlled with a neuromuscular model. *Philosophical Transactions of the Royal Society B-Biological Sciences* 366: 1621-1631.
56. Sup F, Bohara A, Goldfarb M (2008) Design and control of a powered transfemoral prosthesis. *International Journal of Robotics Research* 27: 263-273.
57. Tatarliev G (2011) Design of a knee simulator for testing orthoses under unlimited gait cycles. Yale University: Yale university.
58. Kao P, Lewis C, Ferris D (2010) Invariant ankle moment patterns when walking with and without a robotic ankle exoskeleton. *Journal of Biomechanics* 43: 203-209.
59. Grabowski A, D'Andrea S (2013) Effects of a powered ankle-foot prosthesis on kinetic loading of the unaffected leg during level-ground walking. *Journal of Neuroengineering and Rehabilitation* 10.

Chapter 6

Summary and Conclusions

In this dissertation, we characterized the mechanics and energetics of the impaired and unimpaired human knee joint during normal walking as well as in interaction with exoskeletal impedances during the stance phase of walking on level ground and treadmill. The dissertation starts with a preliminary investigation of the moment-angle behavior of the knee joint during normal walking, revealing that the behavior of the knee joint can be characterized by the slope of a linear fit to the moment-angle graph of this joint during the stance phase of gait. Particularly, the knee joint exhibits linear behavior during the stance phase of gait during normal walking at various gait speeds and a spring-type behavior at the preferred gait speed, which are both user-specific and gait-specific.

The user and gait specific spring-type behavior of the knee joint during the stance phase of walking led us to formulate three main hypotheses: a. The moment-angle behavior of the knee joint can be sufficiently accurately characterized using a set of measurable parameters including body size and gait speed, b. The behavior of unaffected human lower extremity joints during normal walking adapts to an externally-applied mechanical stiffness in parallel with the knee joint such that the overall kinematic and kinetic patterns remain invariant and particularly, the knee joint stiffness and moment during the stance phase adapt to an externally-applied stiffness and moment, and c. A knee orthosis can restore the natural spring-type behavior of an impaired knee joint during the stance phase, provided it implemented a spring tuned to the gait requirements of the user during the stance phase. We took three major steps to test the formulated hypotheses.

To test the first hypothesis and to characterize the moment-angle behavior of the knee joint during normal walking, a series of statistical models were developed that can relatively closely estimate the quasi-stiffnesses of the knee joint using a set of measurable parameters including

body weight and height, gait speed, and joint excursion. To develop the models, we derived generic equations for the moment of the knee joint through inverse dynamics analysis. The generic moment equation was simplified for the instance of the knee joint peak moment in the stance phase to obtain a set of parameters that can characterize the quasi-stiffnesses of this joint. Linear regression was then applied between the characterizing parameters and knee quasi-stiffnesses to establish the most general-form statistical models. These models were simplified to develop most specific models for the preferred gait speed to estimate the quasi-stiffnesses only using the body weight and height.

The statistical models of this study can be used in the design of knee orthoses/exoskeletons and prostheses, and bipedal robots aiming to replicate the moment-angle behavior of the knee joint. The models can also be used in evaluation of gait pathologies in clinical settings as well as studies of general gait biomechanics and physiology. As an example, we extensively used these models in the design of a quasi-passive knee exoskeleton and a quasi-passive compliant stance control orthosis.

The statistical models developed in this study have several limitations worth mentioning. These models were statistically developed using the empirical data of a set of healthy subjects suggesting that we anticipate an estimation error when using the models for *prediction purposes* for new subjects. Along this line, we observed moderate estimation error for the models when using them in tuning the stiffness of the exoskeleton during the experimental sessions. Therefore, the statistical models of this study should be used as a starting point in the design of orthoses and prostheses, and additional measures should be taken for further device tuning.

Ideally, development of statistical models of this study requires a more concrete experimental protocol where: a. the size of the population is determined using statistical power analysis, b. the gender and age is controlled, c. the gait regime (walking/running) is controlled, d. the gait speed is controlled, e. the gait form (treadmill/over ground) is controlled, and f. data collection procedure is consistent. Due to data collection limitations we experienced, the knee joint

statistical models were developed using two sets of empirical data collected in two different gait laboratories. The first data set included 9 subjects walking on an instrument treadmill at four assigned walking speeds; whereas, the second data set included 5 subjects walking over ground at 20 self-selected gait speeds. We anticipate that the inconsistency in the data sets might have induced nuisance effects in the coefficients of the polynomials of the models. Moreover, the statistical models of this study are meant to provide a particularly accurate estimation of the knee quasi-stiffness around the preferred gait speed. This implies that the empirical data used to establish the models should have included sufficient gait trials including walking at the preferred gait speed.

Using a lower extremity joint quasi-stiffness as a design framework has several limitations. Particularly, determination of the quasi-stiffness for a user with a certain level of impairment raises several questions namely: a. it is difficult to determine an ideal quasi-stiffness for an impaired user given it is impossible to measure the user quasi-stiffness in a gait laboratory, b. the quasi-stiffness is a function of the level of impairment which is difficult to quantify, c. implementation of the linear behavior of the knee joint using mechanical devices can be a very challenging task, and d. the behavior of a joint is a function of the user gait requiring substantial functional versatility of the device for stiffness modulation. We observed that the knee joint quasi-stiffness can be a useful parameter in the design of knee exoskeletons and orthoses that are meant to operate during walking on level ground. However, we anticipate that a similar approach for a device meant to operate in variable gait conditions could have several limitations mainly because the device requires substantial gait and user adaptability and ability to negotiate obstacles and ground stiffness/topography.

To test the second hypothesis and to study the human body interaction with exoskeletal impedances we designed a pair of quasi-passive knee exoskeletons each of which implements a spring with a desired stiffness in parallel with the knee joint in the weight acceptance phase of the gait cycle where the knee behaves similarly to a linear torsional spring. Using the exoskeletons

and mass replicas of the exoskeletons in a series of experiments on healthy adults, we experimentally studied motor adaptation in lower extremity joints to externally-applied impedances in parallel with the knee joint during the weight acceptance phase of gait.

The experimental results revealed that the lower extremity joints demonstrate substantial adaptation to the parallel stiffnesses leading to invariant kinematic and kinetic patterns during walking. The exoskeleton mass did not impose notable disturbance on the moment and angle patterns but resulted in an overall higher range of moments. The exoskeleton articulation was found to impose inconsequential kinematic and kinetic constraints on the overall angle and moment patterns, implying that a simple uniaxial hinge joint can be a viable design choice for knee exoskeletons. The exoskeleton mass, articulation, and stiffness were mostly found to locally affect the knee joint moment and angle profiles around the initial and terminal stance as well as terminal swing phase.

A detailed analysis of the moment-angle of the knee joint in the weight acceptance phase of gait and in interaction with exoskeletal impedances revealed that the knee joint quasi-stiffness adapts to externally applied stiffnesses such that the overall stiffness of the complex of the knee joint and exoskeleton remains invariant; a behavior that was also observed for the knee complex moments. It was also observed that the overall moment-angle behavior of the knee complex remained linear under the assistance provided by the exoskeleton suggesting that the human body prefers to experience a linear behavior at the knee joint during the weight acceptance phase, which could be associated with higher rates of energy recovery. The exoskeleton stiffness did not have a significant effect on the mechanical work of the knee joint in the weight acceptance phase implying that the adaptation to the exoskeletal stiffnesses does not necessitate additional mechanical work.

It was found that the knee joint can fully accommodate externally-applied mechanical stiffnesses up to ~80% of the knee joint quasi-stiffness, above which the knee joint quasi-stiffness remains invariant and the hip joint angle profile starts showing significant changes. This implies

that lower extremity joints may only be able to accommodate monoarticular assistive schemes to a certain level before biarticular consequences appear. However, the biarticular consequences that we observed for the knee joint were mild and could be ignored when designing a knee exoskeleton. As a future research direction, the cross-talk between the knee and ankle joints, and the knee and hip joints can be experimentally explored using experimental exoskeletal devices. Future research could also center on development of biarticular assistance paradigms using exoskeletons that span multiple lower extremity joints.

We also found that the noise imposed by motion artifacts, power source of an instrumented treadmill, and actuation and electronics of an exoskeleton can obscure recording of the EMG activities of muscles. As precautionary steps we found that the EMG data collection should take place on level ground instead of a treadmill, all wired communication between the exoskeleton and the data recording computer should be disconnected, the location of the EMG sensors should be farthest from the exoskeleton electronics and actuators, and the location of EMG sensors should be checked prior to the data collection.

The exoskeletons were meant to ideally disengage the springs exactly at the end of the weight acceptance phase. In practice, we had two options to achieve this: a. To use the signal from the foot sensor and disengage the spring when the foot is flat, and b. To tune the exoskeleton for each subject to disengage the spring after a certain time through the gait cycle (e.g. at ~40% of the gait). We chose the former to be consistent among all the subjects and across the conditions, and to avoid introducing nuisance factors. However, we believe that the latter could have resulted in a smoother function for the exoskeleton. For example, we observed that the exoskeleton disengaged the spring earlier than the end of the weight acceptance phase for some subjects (i.e. the energy stored in the spring was dissipated) and later for some others (i.e. the spring hindered the terminal stance flexion/ slightly locked on the users). We believe that timing of the disengagement could have affected our results especially it could have limited the ability of the users to adapt to the exoskeleton and optimally use the exoskeleton assistance.

We designed and fabricated the quasi-passive exoskeletons merely for studying the interaction between the human limbs and exoskeletal impedances in an experimental setup. Using the exoskeleton, we found that a spring in parallel with the human knee joint in the stance phase of gait can partially replace the musculature involvement. Although the results of the study were very insightful about the behavior of the lower extremity joint in response to exoskeletal impedances, we do not envision using the current exoskeletons for daily life applications. Instead, we believe that the assistance method of current exoskeletons (i.e. a spring in parallel with the knee joint during the weight acceptance phase) can be integrated into light weight exoskeletons in addition to other assistance schemes for the other lower extremity joints, particularly the ankle joint which is involved in the body propulsion.

We found that the exoskeleton mass was the major contributor to the increase in the energy expenditure and the exoskeleton assistance only mildly reduced the metabolic cost of walking. We also know that the human body is optimally efficient in using passive biological compliance, suggesting that using passive or quasi-passive mechanical systems might be limitedly successful in improving gait energetics. Firstly, quasi-passive mechanisms can only operate under well-specified gait conditions (e.g. walking on level ground) implying that these devices show very limited adaptability. Secondly, it is very challenging to develop light-weight quasi-passive systems that could augment human body which is substantially more efficient than engineered systems. Thirdly, it is very challenging to develop quasi-passive systems with suitably high bandwidth or suitably small latency for gait applications. Therefore, we believe that quasi-passive assistive devices can hardly find a way into daily life applications. Future steps in the design of lower extremity augmenting exoskeletons can center on light-weight active devices that show suitable power/weight ratio, band-width, adaptability, and endurance.

To be consistent across the experimental conditions, we did not provide any training to the subjects who walked with the quasi-passive exoskeletons and asked to merely walk with the exoskeleton. We observed that the subjects showed different levels of ability to accommodate the

assistance provided by the device. More particularly, we found that the exoskeleton engagement timing can have a major role in allowing the users to trust the device and utilize the assistance provided by them. For example, we found that the exoskeleton locked on a number of the subjects in the terminal stance even when there was a small delay (~ 10 ms) in the disengagement of the spring, causing the subject to take more cautious steps afterwards and distrusting the exoskeletons. Therefore, we believe that the level of training provided to the users of lower extremity devices can substantially affect the performance of the device. We allowed the subjects to use the exoskeletons for ~ 1 hour prior to the data collection session. However, we recommend future experimental protocols consider additional and longer training sessions.

One of the challenges we had during the design and fabrication phase was the lack of a knee brace in the market that is adjustable for a range of user size and is sturdy enough to withstand the range of loads that an exoskeletal device provides. As a solution, we added reinforcements to a commercially available adjustable knee brace to make it sturdy enough for our application. However, we believe that the research in the field of lower extremity exoskeleton can substantially benefit from a light-weight adjustable knee brace on which assistive methods can be implemented and tested on a wide range of users.

As an improvement to current stance control orthosis, we developed a quasi-passive compliant stance control orthosis (CSCO) that provides a level of compliant support tuned to the body weight and height of a patient according to the statistical models developed in this research. Inspired by the natural spring-type behavior of unaffected knee joints, the CSCO implements a spring in parallel with the knee joint to partially replace the function of the knee muscles-tendon units in the stance phase, and liberates the knee joint in the swing phase to allow for free progression of the leg to initiate the next step.

Using a friction-based latching mechanism, the CSCO demonstrated proper reliability, latency, and durability, and satisfied all design criteria inspired by the natural behavior of the human knee joint. A preliminary human subjects test on three healthy volunteers revealed that the

kinematic patterns of the volunteers remained relatively invariant during walking with the CSCO and relatively variant with a state-of-the-art stance control orthosis, in comparison to those of the volunteers during walking with the KAFO as a baseline.

A preliminary test of the CSCO on a patient with impaired knee and ankle joints showed that the compliant support provided by a stance control orthosis can help users restore the natural function of their impaired knee joint. However, the device should be tested on many more subjects to statistically quantify the potential effects of compliant stabilization of an impaired knee joint in the stance phase. Having expressed this, our clinical tests on the impaired user revealed that designers should consider many other factors in a design process other than what biomechanical analysis explain. For example, we found that any conspicuous and noisy orthotic device can hardly satisfy users and the market.

We also found that purely mechanical orthotic devices have substantial superiority over electromechanical orthotic devices from the prospective of a user, orthotist, physician, and insurance providers. Therefore, we highly recommend that future efforts focus on smart light-weight purely mechanical mechanisms that can reliably implement assistance paradigms instead of robotic electromechanical systems. Finally, we found that current medical electronic sensors (e.g. foot sensors) demand substantial work to gain an acceptable level of reliability, versatility, and endurance which is another reason for limited success of electromechanical devices. We also observed that humans are highly versatile in using lower limb devices and providing the inputs that the control schemes of lower extremity devices require to function. Therefore, we recommend that future design efforts consider the versatility of human users and potential methods of using capabilities of humans to learn to use assistive devices.

Although we found some evidence of effectiveness of the CSCO, the improvements were perceived to be relatively mild when compared with a state-of-the-art stance control orthosis. In fact, we found that the weight of an orthosis is a major contributor to the energy expenditure and discomfort, and can obscure potential improvements that introduction of compliance or any

assistance scheme could provide. Therefore, we suggest that future design efforts center on reduction of device weight as a priority. The exoskeleton and CSCO designs employed a friction-based latching mechanism capable of satisfying almost all of the design criteria. We believe that friction-based latching mechanisms can be employed in the design of lower extremity assistive devices to realize simple variable-stiffness devices without requiring bulky actuators and power units.

The findings of this research can give insight to the design of exoskeletons/orthoses and prostheses for lower extremity joints. In terms of exoskeleton/orthosis design, replication of the moment-angle behavior of the lower extremity joints by an exoskeletal device was found to be a viable strategy to assist and unload these joints. Moreover, it was found that human lower extremity joints may accommodate exoskeletal assistance only to a certain level, above which the exoskeleton performance could lead to biarticular consequences. The findings of this research also suggest that compliant support provided by a stance control orthosis can lead to more natural gait and less compensatory movements when compared with rigid support. In terms of informing the design process, the statistical models of the current study can help tune the design parameters of orthoses and prostheses according to the body requirements of a user to result in natural gait and minimal compensatory movements.